Diplomarbeit von
Sonja Overesch

Variational Resummation of Effective Potential in ϕ^4-Theory

vorgelegt dem
Fachbereich Physik der
Freien Universität Berlin

Hauptgutachter: Prof. Dr. Hagen Kleinert

März 2007

Contents

1. Introduction

1.1. Nambu-Goldstone Theorem

Whenever we consider arbitrary field configurations in quantum statistics or statistical field theory, the minimum of the corresponding potential plays an important role. This is due to the fact that even small fluctuations show huge effects unless we are not located at the minimum of the energy. Consider, for instance, the mexican-hat potential in Figure 1.1 a

$$V(\boldsymbol{\phi}) \;=\; \frac{1}{2}\, m^2\, \boldsymbol{\phi}^2 \;+\; \frac{g}{24}\left(\boldsymbol{\phi}^2\right)^2 , \qquad m^2 \;<\; 0\,. \tag{1.1}$$

For an 1-dimensional field ($N=1$), (1.1) is also called double-well potential. It has a maximum at $\phi=0$ and an infinite set of minima $\phi_0=\sqrt{-6m^2/g}$ with modulus $\phi=|\boldsymbol{\phi}|$. Note, that it is important to distinguish between spatial dimension D and field dimension N. For a potential like (1.1), it does not make sense to perform perturbation expansions around $\phi=0$ since fluctuations drive the system to one of the minima. In classical systems, the minima are the places where the system is frozen into in the low-temperature limit $T\to 0$. For increasing temperature, the system can be described by a power series in T around the minimum, which takes the increasing thermal fluctuations into account.

Most potentials possess more than one configuration of minimal energy. These minima may be separated and of finite number as well as degenerated and continuously connected. The double-well potential, for instance, has two disjoint minima which can merely be connected by means of macroscopic fluctuations across the barrier in the middle. In two and higher field dimensions, however, the minima of the mexican hat form an uninterrupted groove, see Figure 1.1 b, whose excitations are called *Nambu-Goldstone modes*. After adding the gradient term to the potential, we define the action

$$\mathcal{A}[\boldsymbol{\phi}] \;=\; \int d^D x \left\{ \frac{1}{2}\left[\nabla\boldsymbol{\phi}(\mathbf{x})\right]^2 \;+\; V\big(\boldsymbol{\phi}(\mathbf{x})\big) \right\} . \tag{1.2}$$

The field $\boldsymbol{\phi}(\mathbf{x})$ may be divided into a background or field expectation $\boldsymbol{\Phi}(\mathbf{x})$ and local fluctuations $\boldsymbol{\delta\phi}(\mathbf{x})$. These fluctuations are sufficient to generate such long-range configurations like the Goldstone modes. Consider an $O(N)$-symmetric potential with expectation $\boldsymbol{\Phi}(\mathbf{x}) \neq \mathbf{0}$, e.g., the mexican hat for N field components. Thus, there exist $(N-1)$ transversal Goldstone modes or – in terms of particles in statistical field theory – $(N-1)$ *Goldstone bosons*.

As the potential's curvature corresponds to the effective masses of its particles, Goldstone bosons have zero mass. This matter of fact can also be derived from the effective action

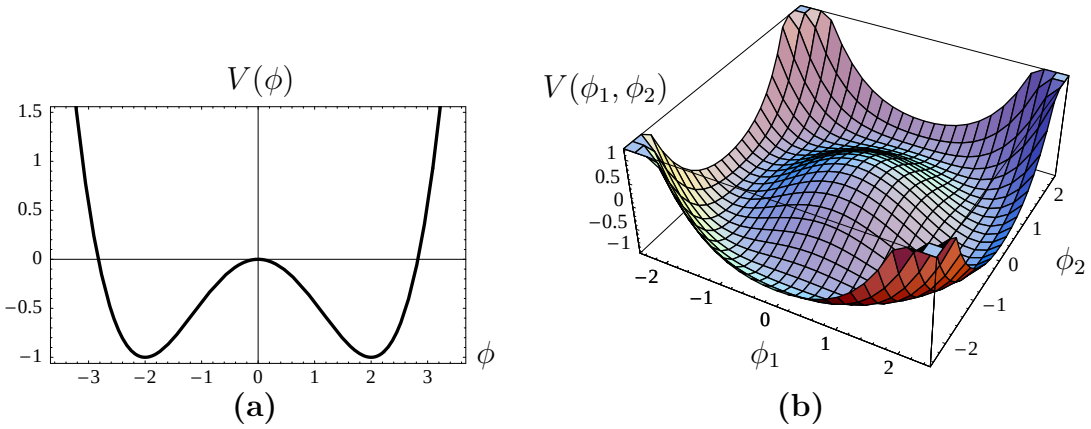

Figure 1.1.: In the case of the double-well potential **(a)**, two isolated minima at nonzero field $|\phi_0| = \sqrt{-6m^2/g}$ exist, whereas the mexican hat **(b)** for $N=2$ has a continuous rotationally symmetric groove of minima ($m^2=-1$ and $g=3/2$).

$\Gamma[\mathbf{\Phi}]$, which follows from the action (1.2) after integrating over the fluctuations. The effective action defines the two-point correlation function

$$\Gamma^{(2)}(\mathbf{x}_1, \mathbf{x}_2) \;=\; \left.\frac{\delta^2\Gamma[\Phi]}{\delta\Phi(\mathbf{x}_1)\,\delta\Phi(\mathbf{x}_2)}\right|_{\Phi(\mathbf{x})=\Phi}, \tag{1.3}$$

which sheds light on the mass of the particles by means of its inverse, i.e., the *propagator* or *correlation function* $G(\mathbf{x}_1, \mathbf{x}_2)$. In the case of non-zero field expectation, the two-point function becomes anisotropic and separates into longitudinal and transversal contributions $\Gamma_L^{(2)}(\mathbf{x}_1, \mathbf{x}_2)$ and $\Gamma_T^{(2)}(\mathbf{x}_1, \mathbf{x}_2)$, respectively. Neglecting the influence of fluctuations, the corresponding propagators read accordingly

$$G_L(\mathbf{x}_1, \mathbf{x}_2) \;=\; \frac{1}{\Gamma_L^{(2)}(\mathbf{x}_1, \mathbf{x}_2)} \;=\; \frac{1}{-\Delta + m^2 + \Phi^2\, g/2}\,\delta(\mathbf{x}_1 - \mathbf{x}_2)\,, \tag{1.4}$$

$$G_T(\mathbf{x}_1, \mathbf{x}_2) \;=\; \frac{1}{\Gamma_T^{(2)}(\mathbf{x}_1, \mathbf{x}_2)} \;=\; \frac{1}{-\Delta + m^2 + \Phi^2\, g/6}\,\delta(\mathbf{x}_1 - \mathbf{x}_2)\,. \tag{1.5}$$

At the minimum $\Phi = \phi_0$ of (1.1), they reduce to

$$G_L(\mathbf{x}_1, \mathbf{x}_2)\Big|_{\Phi=\phi_0} \;=\; \frac{1}{-\Delta - 2\,m^2}\,\delta(\mathbf{x}_1 - \mathbf{x}_2)\,, \tag{1.6}$$

$$G_T(\mathbf{x}_1, \mathbf{x}_2)\Big|_{\Phi=\phi_0} \;=\; \frac{1}{-\Delta}\,\delta(\mathbf{x}_1 - \mathbf{x}_2)\,. \tag{1.7}$$

Whereas the longitudinal part has mass $-2\,m^2$, the transversal Goldstone bosons are obviously massless. This is exactly what the *Nambu-Goldstone theorem* states [1, Ch. 3]:

> *If a quantum field theory without long-range interactions has a continuous symmetry and sufficiently negative mass, there is a nonzero field expectation and the transversal fluctuations have zero mass.*

1.2. Phase Transitions and Order Parameters

Matter can usually be found in different states of aggregation. Water, for instance, can become ice as well as water vapor, a magnetic system can be ferromagnetic or paramagnetic among others. These states of aggregation or *phases* differ in symmetry, thermodynamic, mechanical or electromechanical properties. Depending on external conditions like pressure p, temperature T or magnetic field $\mathbf{B}$, the system settles for one certain phase. If we vary these control parameters in a suitable way, the system passes over into another state. Consider, for instance, a ferromagnet in $N = 3$ dimensions. Due to thermal fluctuations, it is impossible for the electrons to be perfectly arranged at temperatures $T \neq 0$. At $T = 0$, however, we find a constant global order, called *spontaneous magnetization* $\mathbf{M}$. For small temperatures, so-called *Weiss' domains* arise inside which the elementary magnets are arranged. The transition point between normal (high-temperature) and ordered (low-temperature) phase is referred to as *critical temperature* T_c or, more generally, *critical point*. The spontaneous magnetization $\mathbf{M}$ being zero above and nonzero below T_c is suitable to describe phase transitions. In general, there exist some *order parameters* $\boldsymbol{\phi}$ which are zero in one phase and nonzero in the other. In the case of a ferromagnet, $\boldsymbol{\phi}$ is a vector of dimension $N = 3$. For a transition gas-liquid, the density difference with respect to the liquid phase may be defined to be the order parameter, thus it has the dimension $N = 1$. The local generalization of order parameters is an *order field* $\boldsymbol{\phi}(\mathbf{x})$.

With respect to the later calculations of the effective potential, the background $\boldsymbol{\Phi}$ serves as an order parameter. The anharmonic potential with a positive quadratic term describing the normal phase has its only minimum at $\boldsymbol{\phi} = \mathbf{0}$, which corresponds to field expectation $\langle\boldsymbol{\phi}\rangle = \mathbf{0}$. The mexican hat has its minima at $\boldsymbol{\phi} \neq \mathbf{0}$, i.e., nonzero field expectation. In fact, this potential describes the ordered phase: whereas the anharmonic potential is rotationally symmetric, there is a spontaneous breakdown of the symmetry when coming to the mexican hat which has one longitudinal direction and $N-1$ transversal ones. Likewise, the paramagnetic phase is rotationally symmetric, the ferromagnetic phase, however, has a preferred direction because of the spontaneous magnetization. Thus, the symmetry is reduced. This is where the name *ordered phase* comes from.

There are different kinds of phase transitions being classified in 1933 for the first time by *P. Ehrenfest* according to the partial derivatives of the thermodynamic potentials. According to Ehrenfest, a phase transition is of n^{th} order if the first (n–1) partial derivatives with respect to the natural variables are continuous, whereas at least one of the n^{th} partial derivatives is discontinuous. As a consequence, the difference between two phases decreases with increasing transition order. The so-called *Kosterlitz-Thouless phase transition* [2], occurring exclusively in two spatial dimensions, is of infinite order. In this case, Gibbs free enthalpy has the form

$$G(T) \sim \exp\left\{-\frac{K}{\sqrt{T - T_c}}\right\}. \tag{1.8}$$

All derivatives are continuous at $T = T_c$. A famous example of such a Kosterlitz-Thouless phase transition is the transition of a thin ^{4}He film from fluid to suprafluid. Typical examples

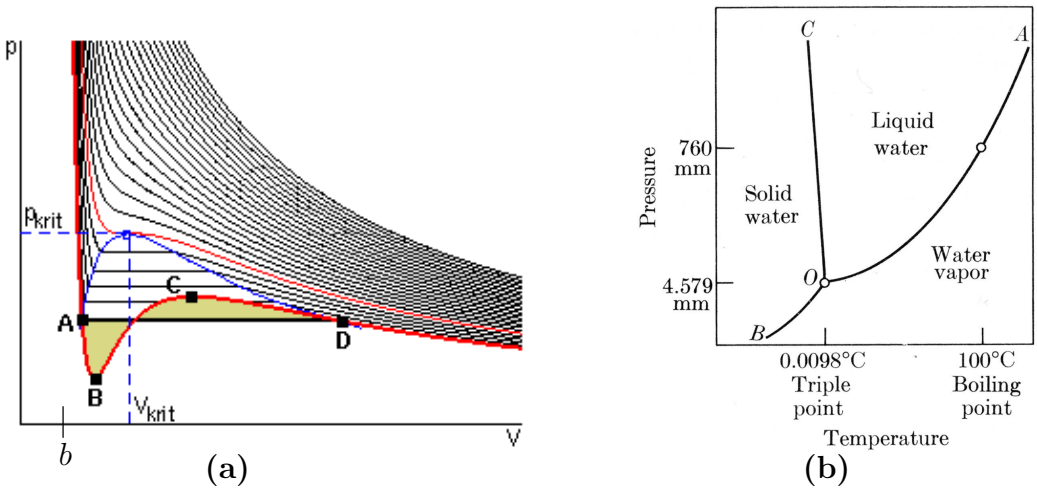

Figure 1.2.: Isothermal lines **(a)** of the Van-der-Waals gas [3]. Below a critical line, non-physical areas between B and C arise, which are replaced by Maxwell's construction as exemplified for the lower curve. In the ocher area, both gas and liquid phase exist. The vertical asymptote corresponds to the proper volume b. **(b)**: Phase diagram of water with triple point O, critical point A, vapor pressure curve $O-A$, sublimation curve $B-O$ and melting pressure curve $O-C$ [4].

of first-order transitions are melting or evaporation, whereas ferromagnetic or superconductor transitions are of second order. Nowadays, it is more common to distinguish merely between *continuous* and *discontinuous* phase transitions, stemming from the continuous or discontinuous behavior of the order parameter at the critical point. In terms of this definition, first-order phase transitions regarding Ehrenfest are discontinuous, all transitions of second and higher order are referred to as continuous.

The critical point shows an interesting phenomenon: in spite of short-range interactions, long-range fluctuations are found near the critical point, which are characterized as *critical behavior*. Completely different systems show similar critical behavior. In the case of continuous transitions, the critical behavior turns out to be classifiable by means of *critical exponents*.

1.3. Discontinuous Phase Transitions

In this section, we consider the *Van-der-Waals gas* as a typical example of discontinuous phase transitions. It is characterized by its equation of state

$$\left(p + \frac{a}{V}\right)(V - b) = k_B NT \tag{1.9}$$

with pressure p, volume V, temperature T, Boltzmann constant k_B and constants a and b that include the long-range interaction and the proper volume of the particles, respectively. Figure 1.2 a shows the isothermal lines, i.e., the pressure as a function of the volume for fixed temperature. In the case of the critical isothermal line T_c, the points B, C and the turning point between coincide. Below, the isothermal lines show non-physical regions with $\partial p/\partial V > 0$, which would make the system mechanically unstable. The actual behavior is described by *Maxwell's construction*: a horizontal line from point A to D, dividing this region into two parts with equal area, visualizes the occurring condensation, i.e., a phase transition from gas to liquid or the other way around that constitutes an area in which both phases coexist. By means of this, it is avoided that volume and pressure decrease simultaneously. The extensive variable V becomes discontinuous and since the volume corresponds to a first partial derivative of Gibbs potential G,

$$V = \left(\frac{\partial G}{\partial p}\right)_{T,N}, \tag{1.10}$$

it gives rise to the name discontinuous or, with regard to Ehrenfest, first-order phase transition. Moreover, it shows that coexistent phases are restricted to first-order transitions. Above the critical temperature, condensation is no longer possible. *Gibbs phase rule*

$$f = 2 + k - p \tag{1.11}$$

describes the relation between the number k of components, the number p of coexistent phases and the number f of degrees of freedom within an arbitrary system. Consider, for instance, the phase diagram of water in Figure 1.2 b. Water consists of $k = 1$ component, thus there are two degrees of freedom within a pure phase: temperature and pressure. Due to two degrees of freedom, a pure phase takes a two-dimensional area in the diagram. At the vapor pressure curve, both liquid water and water vapor are existent, hence we have two phases and one degree of freedom. In fact, the vapor pressure curve has a one-dimensional structure. The same holds for both the melting pressure curve and the sublimation curve. At the so-called triple point O, however, all three phases coexist and zero degrees of freedom correspond to zero dimensions, i.e., a point. Above the critical point A, a transition between liquid and gas phase is no longer possible: a fluid phase arises, which depends merely on the temperature.

1.4. Continuous Phase Transitions and Critical Exponents

In the following, we concentrate on continuous phase transitions which are of special interest. This is due to the fact that near the critical point, many physical quantities, in particular the order parameters, show an universal power-law behavior $\sim |\tau|^{\varphi}$ with φ called *critical exponent*. Here, $\tau = (T - T_c)/T_c$ denotes the reduced temperature which defines the region of critical fluctuations. A physical property F, for instance, behaves near the critical temperature like

$$F(\tau) = \begin{cases} C_1 \, |\tau|^{\varphi} & \text{if } \tau \downarrow 0\,, \\ C_2 \, |\tau|^{\varphi'} & \text{if } \tau \uparrow 0\,. \end{cases} \tag{1.12}$$

In principle, φ and φ' may be different. Experiments and a thorough analysis with renormalization group theory, however, show that both exponents are exactly the same, i.e., it makes no difference whether we approach the critical point from above or below. The critical exponent can be obtained from the data by plotting $\ln|F(\tau)|$ versus $\ln|\tau|$ and extracting the slope

$$\varphi \;=\; \lim_{\tau\to 0} \frac{\ln\bigl|F(\tau)\bigr|}{\ln|\tau|}\,. \tag{1.13}$$

In 1970, R. B. Griffith suggested that these exponents show *universality* [5]. This means that they merely depend on

- spatial dimension D,
- dimension N of order parameter,
- range of particle interaction.

Considering the range of interaction, we denote interactions to be of *short-range* if they decay with increasing distance r like $\sim r^{-(D+2+a)}$ for $a>0$. Classical theories are restricted to *long-range* interactions with $a<D/2-2$, whereas the intermediate area $D/2-2<a<0$ is most difficult to describe.

The coherence length ζ is a quantity that characterizes the range of correlations. Near the critical point, ζ dominates all microscopic length scales since it diverges like a power in $T-T_c$

$$\zeta \;=\; \zeta_0 \left(\frac{T-T_c}{T_c}\right)^{-\nu}\,, \tag{1.14}$$

with $\nu>0$ being a critical exponent. Thus, all microscopic properties become irrelevant. They merely express themselves by means of the coefficients $C_{1,2}$ in the power laws (1.12) but even the ratio of these coefficients, when approaching the critical point from above and below, is universal. The system behaves in a collective and universal way, and it is not surprising that merely global properties like dimension or symmetry have an influence on its behavior. For the complete and unique characterization of a system [6, Ch. 1], a set of critical exponents α, β, γ, δ, ν, η is introduced with, e.g.,

$$C \sim |\tau|^{-\alpha}\,, \tag{1.15}$$

$$|\mathbf{M}| \sim |\tau|^{\beta}\,, \qquad \text{for}\, T \,<\, T_c\,, \tag{1.16}$$

$$|\mathbf{M}| \sim |\mathbf{B}|^{1/\delta}\,, \qquad \text{for}\, T \,=\, T_c\,, \tag{1.17}$$

$$\chi_L(\mathbf{k}=\mathbf{0}) \;\sim |\tau|^{-\gamma}\,, \tag{1.18}$$

$$\lim_{\mathbf{k}\to 0} \mathbf{k}^2\, \chi_T(\mathbf{k}) \sim |\tau|^{\eta\nu}\,. \tag{1.19}$$

Here, C denotes the specific heat, χ the susceptibility at zero field, $\mathbf{k}$ the momentum, and $\mathbf{B}$ the magnetic field. These critical exponents are not independent of each other but are

related by *scaling relations* which were first introduced by B. Widom in 1965 [7]:

$$\alpha + \beta\,(1+\delta) \;=\; 2\,, \tag{1.20}$$
$$\gamma + \beta\,(1-\delta) \;=\; 0\,, \tag{1.21}$$
$$\nu\,(2-\eta) \;=\; \gamma\,. \tag{1.22}$$

Furthermore, additional *hyperscaling relations* exist, which include the dimension D [6, Ch. 1]. Taking all these relations into account, there remain only two independent exponents which are typically chosen to be ν and η. With the aid of critical exponents, completely different systems near phase transitions can be grouped into universal classes depending merely on symmetry properties. Regarding the dimension N of the order parameter (also denoted as dimension of spin), they classify into

- $N = 0$: polymer,
- $N = 1$: Ising model,
- $N = 2$: XY-model,
- $N = 3$: Heisenberg model,
- $N = \infty$: spherical model.

1.5. Phase Transitions and Goldstone Theorem

In order to emphasize the interconnection between phase transitions and Goldstone theorem, we consider the correlation function

$$G_{ij}(\mathbf{x},\mathbf{y}) \;=\; \big\langle \phi_i(\mathbf{x})\,\phi_j(\mathbf{y})\big\rangle\,, \tag{1.23}$$

which is the expectation value of the product of two components of the order field. Its cumulant version reads

$$G_{c,ij}(\mathbf{x},\mathbf{y}) \;=\; G_{ij}(\mathbf{x},\mathbf{y}) \;-\; \big\langle \phi_i(\mathbf{x})\big\rangle\,\big\langle \phi_j(\mathbf{y})\big\rangle\,. \tag{1.24}$$

The correlation function is particularly interesting in the ordered phase where it describes the deviations $\boldsymbol{\delta\phi}(\mathbf{x})$ of the order field from its expectation value $\boldsymbol{\Phi}$

$$\boldsymbol{\delta\phi}(\mathbf{x}) \;=\; \boldsymbol{\phi}(\mathbf{x}) \;-\; \boldsymbol{\Phi}. \tag{1.25}$$

Then, the cumulant correlation function reads

$$G_{c,ij}(\mathbf{x},\mathbf{y}) \;=\; \big\langle \delta\phi_i(\mathbf{x})\,\delta\phi_j(\mathbf{y})\big\rangle \tag{1.26}$$

and differs from (1.23) by means of the non-vanishing background function $\Phi_i\Phi_j$. For a ferromagnet, for instance, $\boldsymbol{\delta\phi}(\mathbf{x})$ corresponds to the deviations from the spontaneous magnetization $\boldsymbol{\Phi} = \mathbf{M}$. Due to the broken symmetry, the correlation function is anisotropic and

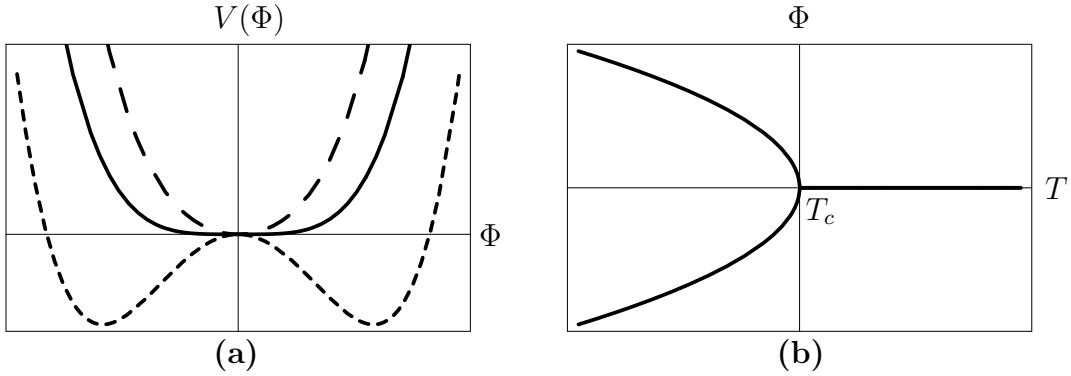

Figure 1.3.: Phase transition **(a)** from anharmonic potential $T > T_c$ (long-dashed) to double-well $T < T_c$ (short-dashed). $T = T_c$ (solid) corresponds to the transition point. **(b)**: Symmetry breakdown when coming from normal to ordered phase. The order parameter has no longer a unique value.

can be divided analogously to (1.4) and (1.5) into a longitudinal and a transversal part with respect to the order field

$$G_{ij}(\mathbf{x}, \mathbf{y}) \;=\; P^L_{ij}\, G_L(\mathbf{x}, \mathbf{y}) \;+\; P^T_{ij}\, G_T(\mathbf{x}, \mathbf{y})\,, \tag{1.27}$$

with projection operators to be defined in Chapter 7. In the case of an $O(N)$-symmetric energy functional, fluctuations in transversal directions are symmetry transformations. Thus, they do not require energy and consequently have infinite coherence length for all temperatures. In other words, they show a critical behavior not just near the critical point but everywhere. This is in accordance with the Goldstone theorem: due to the spontaneous breakdown of a continuous symmetry, long-range modes with long-range, critical behavior emerge.

1.6. Landau Theory

Physical systems are uniquely determined if the corresponding effective action is known. This is, however, not always given. In order to describe a system at least in a region near a second-order phase transition, L. D. Landau developed a theory that is specified by the critical behavior [6,19]. It implies that the thermodynamic potential $G(T, \mathbf{h}, \mathbf{\Phi})$, Gibbs free enthalpy, for instance, can be expanded into a power series in terms of the order parameter $\mathbf{\Phi}$. Since the order parameter vanishes when approaching the critical point from above as well as from below, it is obvious that such an expansion for small values of $\Phi = |\mathbf{\Phi}|$ is justified. The parameter $\mathbf{h}$ denotes the conjugated field, e.g., the magnetic field $\mathbf{H}$ for an order parameter $\mathbf{\Phi}$ being the magnetization $\mathbf{M}$. Moreover, G is supposed to depend only on the modulus of the order parameter and of its conjugated field. Assuming the symmetry $G(T, 0, \Phi) = G(T, 0, -\Phi)$ for a vanishing field $\mathbf{h}$, the power series merely consists of even powers. We truncate the series after the fourth power and assume this coefficient to be positive for stability reasons. Otherwise, the sixth power has to be taken into account. The

universal ansatz reads

$$G(T,h,\Phi) \;=\; G(T,0,0) \;+\; \frac{A}{2}\,\Phi^2 \;+\; \frac{B}{24}\,\Phi^4\,. \tag{1.28}$$

In general, the coefficients depend on the temperature. We obtain them by minimizing with respect to Φ

$$\frac{\partial\, G(T,h,\Phi)}{\partial\,\Phi} \;=\; A\Phi \;+\; \frac{B}{6}\,\Phi^3 \;\stackrel{!}{=}\; 0\,, \tag{1.29}$$

$$\frac{\partial^2\, G(T,h,\Phi)}{\partial\,\Phi^2} \;=\; A \;+\; \frac{B}{2}\,\Phi^2 \;\stackrel{!}{>}\; 0\,. \tag{1.30}$$

The first equation (1.29) has two possible solutions

$$\Phi = 0\,, \tag{1.31a}$$

$$\Phi = \pm\sqrt{-\frac{6A}{B}}\,. \tag{1.31b}$$

Consider the normal phase where $\Phi = 0$ is a solution of (1.29) anyway. Then, due to (1.30), A has to be positive. In the ordered phase, however, Φ is nonzero. Thus, (1.29) has the solution (1.31b). In accordance with (1.30), A has to be negative. To sum up, we have

$$\begin{aligned} \text{normal phase} \quad &\Rightarrow \quad A > 0\,, \\ \text{ordered phase} \quad &\Rightarrow \quad A < 0\,. \end{aligned}$$

For this reason, we state that the coefficient in front of Φ^2 must change its sign at the critical point T_c and therefore we write

$$A \;=\; a\,\big(T - T_c\big)\,, \qquad a > 0\,. \tag{1.33}$$

The change of sign of A is closely related to the spontaneous symmetry breakdown that can also be observed in connection with the anharmonic and the mexican-hat potential. We see immediately, that m^2 in (1.1) has the same property as the coefficient A in the previous example. In fact, the rotationally symmetric anharmonic potential represents the normal phase. The mexican hat is the ordered phase due to symmetry breakdown as shown in Figure 1.3 a, where the critical point has been attributed to a critical temperature T_c. Inserting (1.33) into (1.31b), we obtain the temperature dependence of the order parameter

$$\Phi(T) \;=\; \begin{cases} \pm\sqrt{-\frac{6a}{B}(T - T_c)} & T < T_c\,, \\ 0 & T > T_c\,. \end{cases} \tag{1.34}$$

Figure 1.3 b shows that the order parameter Φ is not a unique function of the temperature: approaching the critical temperature from above, two values of Φ are possible that differ in their signs, e.g., positive or negative magnetization. Local fluctuations around the critical point decide which value is adopted. *Spontaneous symmetry breakdown* denotes just the possibility of different values for the order parameter. An additional cubic term in (1.28) would change the transition to first order and would obviously not permit spontaneous symmetry breakdown. Thus, this phenomenon is reserved to second-order phase transitions.

1.7. Resummation of Effective Potential

Specializing the effective action in a constant background yields the effective potential. It is usually calculated by means of a so-called *loop expansion*. In connection with Feynman diagrams, the n^{th} order with regard to $\hbar$ consists of all 1-particle irreducible Feynman diagrams with n loops. Assuming spontaneously broken symmetry, problems arise since some approximations do not manage to reproduce the convexity of the effective potential. This problem can be solved by a Maxwell construction [9], for instance, transforming the approximated effective potential to a convex one, similarly to the construction in connection with phase diagrams in Figure 1.2 a. Another possibility is the *Cornwall-Jackiw-Tomboulis (CJT) formalism* [10] which calculates the effective potential to any given order by resumming all 1-particle irreducible diagrams.

With respect to the $O(N)$-model, two common approaches are the *Hartree approximation* and the *large-N limit*. The Hartree approximation [11] stems from many-body physics and consists of a self-consistent resummation of bubble diagrams. In the CJT formalism, all 1-particle irreducible diagrams must be calculated, which leads directly to the effective potential. The large-N approximation can be regarded as the Hartree approximation in the limit $N \to \infty$.

There are further problems concerning the effective potential. Perturbation expansions are divergent weak-coupling series and require resummation of all tadpole diagrams [12]. As we will show in detail in Chapter 8, it is impossible to optimize the renormalized but unresummed effective potential with respect to the background in order to obtain the free energy. But a resummation can be performed, for instance, by variational perturbation theory (VPT) [1, Ch. 5], transforming the divergent weak-coupling series into a convergent strong-coupling series.

In the limit of large N, the effective potential can be calculated without resummation. Consider the Wick contractions of the expectation value of a quartic term

$$\begin{aligned}\left\langle \Phi(\mathbf{x})\, \Phi^*(\mathbf{x})\, \Phi(\mathbf{x}')\, \Phi^*(\mathbf{x}') \right\rangle \;=\; & \left\langle \Phi(\mathbf{x})\Phi^*(\mathbf{x}) \right\rangle \left\langle \Phi(\mathbf{x}')\Phi^*(\mathbf{x}') \right\rangle + \left\langle \Phi(\mathbf{x})\Phi^*(\mathbf{x}') \right\rangle \left\langle \Phi(\mathbf{x}')\Phi^*(\mathbf{x}) \right\rangle \\ & + \left\langle \Phi(\mathbf{x})\Phi(\mathbf{x}') \right\rangle \left\langle \Phi^*(\mathbf{x})\Phi^*(\mathbf{x}') \right\rangle . \end{aligned} \tag{1.35}$$

The possible contractions are referred to as *Hartree*-, *Fock*-, and *Bogoliubov*-contractions. All three of them have to be taken into account. For large N, however, both Fock and Bogoliubov terms can be neglected [13, Ch. 26]:

$$\left\langle \Phi(\mathbf{x})\, \Phi^*(\mathbf{x})\, \Phi(\mathbf{x}')\, \Phi^*(\mathbf{x}') \right\rangle \overset{N\to\infty}{\sim} \left\langle \Phi(\mathbf{x})\Phi^*(\mathbf{x}) \right\rangle \left\langle \Phi(\mathbf{x}')\Phi^*(\mathbf{x}') \right\rangle . \tag{1.36}$$

The so-called *Hubbard-Stratonovich transformation* is a calculation procedure for the effective potential that merely takes the Hartree term into account. Therefore, it yields exact results in the limit $N \to \infty$. In fact, VPT can be regarded as a generalization of Hubbard-Stratonovich for all values of N [14]. This matter of fact will be worked out in this thesis.

Furthermore, renormalization becomes necessary in statistical field theory due to arising singularities. It is a well-known problem that renormalization and resummation cannot agree together in most cases [15]. The original effective potential is, of course, renormalizable, but performing renormalization after resummation leads to renormalization constants that are no longer independent of the medium [16], for instance. Merely for $T=0$ this sequence succeeds. In the CJT-formalism, the full bilocal propagator has to be renormalized after resummation. This turns out to be impossible. A procedure that consists of cut-off renormalization prior to resummation has been developed by J. Lenaghan and D. Rischke in 2000 [15]. However, the Hartree approximation requires vanishing cut-off Λ. This matter of fact does not agree with the $O(N)$ model which becomes trivial in the limit $\Lambda \to \infty$ and requires at least a finite value of Λ. The large-N approximation is also valid for non-vanishing cut-off.

With regard to all bosonic systems, the Goldstone theorem has to be preserved [17,18]. Whereas it is satisfied all along the large-N limit, it cannot be respected for all temperatures in the Hartree approximation [15]. If we perform resummation first, the renormalization leads to massive Goldstone bosons [15]. In 1997, H. Kleinert proposed VPT as an improvement of the Hartree approximation that preserves the Goldstone theorem [14]. A further advantage of variational resummation are the achieved exponentially fast convergent series [6, Ch. 19]. In this thesis, we renormalize the effective potential in ϕ^4-theory, resum it by means of VPT and show afterwards that all Goldstone bosons still have zero mass. By doing so, we give up self-consistency since we include the field expectation Φ into the effective action. This procedure is exactly the reason why the Goldstone theorem is preserved. VPT is a non-perturbative resummation that conserves symmetry, thus it does not violate the Goldstone theorem either. Note that in contrast to the CJT-formalism, we renormalize a local quantity as shown in detail in Chapter 6. Furthermore, we verify that the phase transition remains continuous and analyze in what extend the point of transition is affected by quantum fluctuations.

1.8. Outline of the Thesis

The ϕ^4-potential (1.1) describes a multifunctional and illuminating physical system. Depending on the sign of m^2, it implies both anharmonic and mexican-hat potential which turn into each other by means of a continuous phase transition. Due to the mathematically closely related shape, the potential (1.1) enables us to study two completely different systems. For this reason, we have chosen it to be the central system we consider.

This thesis is composed of two parts. The first one is entitled **Quantum Statistics**. Admittedly, we are mainly interested in statistical field theory, but minima of the potential being shifted from zero in the ordered phase impact the original variational procedure [1, Ch. 5] with regard to the substituted quantity. In order to check the variational procedure, we consider quantum mechanics first before going to statistical field theory. In **Chapter 2**, we derive the loop expansion of the effective potential within quantum statistics, where we consider, in particular, the low-temperature limit which leads to the corresponding quantum mechanical results. We remain in arbitrary dimension D up to the second loop order, which gives rise to longitudinal and transversal frequencies describing the symmetry breakdown

in the ordered phase. The third loop order is disproportionately more tedious to calculate. Therefore, we confine ourselves to determining it merely for $D=1$ dimension. In **Chapter 3**, we proceed to VPT and apply it to the effective potential. With the help of the second and third loop order in $D=1$ dimension, we study the convergence with respect to the increasing order. The so-called *sunset term* in the second loop order is preferably neglected [1, Ch. 5] since it complicates matters. Therefore, we check its effect on the variational results in order to investigate whether this simplification is justified. In $D=2$ dimensions, longitudinal and transversal frequencies enable us to introduce a second variational parameter and to investigate its influence on the accuracy. Finally, we consider the convergence with increasing dimension D. This limit can be regarded as the analogy of the large-N limit in statistical field theory in which the ϕ^4- theory is exactly solvable. On this account, we expect and obtain, indeed, improving VPT results in quantum mechanics.

In the second part, we concentrate on **Statistical Field Theory**. The methods for deriving the effective potential of (1.1) are adopted from quantum statistics. In **Chapter 4**, we concentrate on $N=1$ real field and calculate the first two loop orders of the effective potential. Here, we encounter singularities and have to renormalize the effective potential. The complete regularization and renormalization procedure is presented in **Chapter 5**. Calculating the self-energy represents an alternative approach to renormalization, which is therefore worked out in **Chapter 6**. In order to obtain longitudinal and transversal masses analogously to the frequencies in quantum statistics, we extend our calculations to N real fields in **Chapter 7**. The actual variational procedure in statistical field theory is succinctly treated in **Chapter 8** in order to assure ourselves that VPT is, indeed, applicable. Due to the renormalization invariance, it is impossible to assess the achieved accuracy. Therefore, we focus our attention to check the requirements we have proposed for the theory: by means of Landau expansion, we verify that VPT preserves the character of a continuous phase transition. Moreover, we confirm that the Goldstone theorem is still preserved. In the large-N limit, the Hubbard-Stratonovich transformation enables us to calculate the effective potential without resummation. With this, we establish VPT as a generalization of the Hubbard-Stratonovich transformation to all values of N.

Part I.

Quantum Statistics

2. Effective Potential

In this chapter, we derive the effective potential in quantum mechanics for a rotationally symmetric potential. We deduce the effective potential from the partition function in quantum statistics by means of the background method in order to obtain an expansion in powers of $\hbar$. This expansion is closely related to Feynman diagrams: the n^{th} order corresponds to all 1-particle irreducible vacuum diagrams with n loops. Diagrams and analytic expressions can be converted into each other with the aid of Feynman rules. However, we are primarily interested in quantum mechanics which follows from the low-temperature limit $T \to 0$ in quantum statistics. In order to avoid confusion, we change the notation of the mass into a capital letter M throughout this part.

2.1. Partition Function

Consider a quantum mechanical particle propagating from space-time point $(\mathbf{x}_a\,, t_a)$ to $(\mathbf{x}_b\,, t_b)$. The probability of this transition is equal to the absolute square of the time evolution amplitude

$$\big(\mathbf{x}_b, t_b \,\big|\, \mathbf{x}_a, t_a\big) \;:=\; \big\langle \mathbf{x}_b \,\big|\, \hat{U}(t_b, t_a) \,\big|\, \mathbf{x}_a \big\rangle\,, \tag{2.1}$$

with $\hat{U}(t_b, t_a)$ being the time evolution operator with respect to the Hamiltonian $\hat{H}$

$$\hat{U}(t_b, t_a) \;:=\; e^{-\imath\, \hat{H}(t_b - t_a)/\hbar}\,. \tag{2.2}$$

In the path integral formalism, propagation is described by interference of all possible paths the particle can walk along, i.e., all paths with initial point $\mathbf{x}_a$ and final point $\mathbf{x}_b$ [19,20]. This can be expressed by adding up all these paths with a phase factor, yielding the path integral

$$\big(\mathbf{x}_b, t_b \,\big|\, \mathbf{x}_a, t_a\big) \;=\; \int_{\mathbf{x}(t_a)=\mathbf{x}_a}^{\mathbf{x}(t_b)=\mathbf{x}_b} \mathcal{D}\mathbf{x}\; e^{\imath\, \mathcal{A}[\mathbf{x}]/\hbar}\,. \tag{2.3}$$

Here, we defined the classical action of a particle with mass M in a potential $V(\mathbf{x})$ by

$$\mathcal{A}[\mathbf{x}] \;=\; \int_{t_a}^{t_b} dt\, \left[\frac{M}{2}\,\dot{\mathbf{x}}^2(t) - V\big(\mathbf{x}(t)\big)\right]. \tag{2.4}$$

Let E_n be the eigenvalues of $\hat{H}$ belonging to the orthonormal eigenstates $|\psi_n\rangle$. Thus, we have the eigenvalue equation

$$\hat{H}\,|\psi_n\rangle \;=\; E_n\,|\psi_n\rangle\,. \tag{2.5}$$

In that case, we define the canonical partition function $\mathcal{Z}$ as a sum over all Boltzmann factors

$$\mathcal{Z} \;=\; \sum_n \mathrm{e}^{-E_n/k_BT} \;=\; \mathrm{Tr}\,\left(e^{-\hat{H}/k_BT}\right) \tag{2.6}$$

with the temperature T and the Boltzmann constant k_B. In the last step of (2.6), we used that for an arbitrary operator

$$\hat{O}\,|\psi_n\rangle \;=\; O_n\,|\psi_n\rangle\,, \tag{2.7}$$

the trace is defined by

$$\mathrm{Tr}\,\hat{O} \;:=\; \sum_n \big\langle \psi_n \,|\, \hat{O} \,|\, \psi_n \big\rangle\,. \tag{2.8}$$

The outstanding similarity between the Boltzmann factor $e^{-\hat{H}/k_BT}$ and the quantum mechanical time evolution operator (2.2) gives rise to the substitution

$$t_b - t_a \;\leftrightarrow\; \frac{-\imath\,\hbar}{k_BT} \;\equiv\; -\imath\,\hbar\beta\,, \tag{2.9}$$

through which Boltzmann factor and time evolution operator turn into each other. This so-called *Wick rotation* (2.9) connects the real-time evolution of a quantum mechanical system with its equilibrium thermodynamics. Performing the Wick rotation for the classical action (2.4) and defining the imaginary-time

$$\tau \;:=\; \imath\,t\,, \tag{2.10}$$

we obtain the imaginary time action

$$\mathcal{A}[\mathbf{x}] \;=\; \int_0^{\hbar\beta} d\tau \left[\, \frac{M}{2}\,\dot{\mathbf{x}}^2(\tau) + V\big(\mathbf{x}(\tau)\big) \right]. \tag{2.11}$$

Applying (2.8) in space representation, the partition function (2.6) reads

$$\mathcal{Z} \;=\; \int d^Dx\, \big\langle \mathbf{x} \big|\, e^{-\beta\hat{H}}\, \big|\mathbf{x}\big\rangle \;=\; \int d^Dx\, \big\langle \mathbf{x} \big|\, e^{-\imath\hat{H}(-\imath\hbar\beta)/\hbar}\, \big|\mathbf{x}\big\rangle\,. \tag{2.12}$$

Obviously, the matrix element in (2.12) is the analytic continuation of the real time evolution amplitude with the help of Wick rotation

$$\big(\mathbf{x}_b, \hbar\beta \,\big|\, \mathbf{x}_a, 0\big) \;=\; \big(\mathbf{x}_b, t_b \,\big|\, \mathbf{x}_a, t_a\,\big)\,\Big|_{t_a=0}^{t_b=-\imath\hbar\beta}\,. \tag{2.13}$$

Therefore, we write the partition function (2.12) as an ordinary integral over the imaginary time evolution amplitude where initial and final space point coincide:

$$\mathcal{Z} \;=\; \int d^Dx\, \big(\mathbf{x}, \hbar\beta \,\big|\, \mathbf{x}, 0\big)\,. \tag{2.14}$$

It can be transferred to path integral formalism by summing over all periodic paths $\mathbf{x}(\hbar\beta) = \mathbf{x}(0)$. Analogously to the time evolution amplitude (2.3) in real time, we have now [21]

$$\mathcal{Z} \;=\; \int d^D x' \int_{\mathbf{x}(0)=\mathbf{x}'}^{\mathbf{x}(\hbar\beta)=\mathbf{x}'} \mathcal{D}\mathbf{x}\, e^{-\mathcal{A}[\mathbf{x}]/\hbar} \;\equiv\; \oint \mathcal{D}\mathbf{x}\, e^{-\mathcal{A}[\mathbf{x}]/\hbar}\,, \tag{2.15}$$

with the imaginary time action $\mathcal{A}[\mathbf{x}]$ defined in (2.11). Finally, the free energy $\mathcal{F}$ follows from (2.15) by means of

$$\mathcal{F} \;:=\; -\frac{1}{\beta} \ln \mathcal{Z}\,. \tag{2.16}$$

2.2. Definition of Effective Action and Effective Potential

Within quantum statistics, the so-called *correlation functions* play an important role. They are defined to be the expectation values of products of different positions of the path $\mathbf{x}(\tau)$. In order to calculate these expectation values, it is convenient to introduce an additional external current $\mathbf{j}(\tau)$ into the action, which disturbs the system

$$\mathcal{A}[\mathbf{x},\mathbf{j}] \;:=\; \mathcal{A}[\mathbf{x}] - \int_0^{\hbar\beta} d\tau\, \mathbf{j}(\tau)\, \mathbf{x}(\tau)\,. \tag{2.17}$$

Defining the generating functional

$$\mathcal{Z}\,[\,\mathbf{j}\,] \;:=\; \oint \mathcal{D}\mathbf{x}\, e^{-\mathcal{A}[\mathbf{x},\mathbf{j}]/\hbar}\,, \tag{2.18}$$

we obtain the expectation value of the path with the help of functional derivatives with respect to the current as we will see in the following. For vanishing current, $\mathbf{j}(\tau) \equiv \mathbf{0}$, (2.18) turns into the partition function (2.15)

$$\mathcal{Z}\,[\,\mathbf{j}\,]\,\Big|_{\mathbf{j}\,\equiv\,\mathbf{0}} \equiv \mathcal{Z}\,. \tag{2.19}$$

In the same way, also the free energy (2.16) becomes a generating functional of $\mathbf{j}(\tau)$

$$\mathcal{F}[\,\mathbf{j}\,] \;=\; -\frac{1}{\beta} \ln \mathcal{Z}\,[\,\mathbf{j}\,]\,, \tag{2.20}$$

which yields just the free energy (2.16) for vanishing current

$$\mathcal{F}\,[\,\mathbf{j}\,]\,\Big|_{\mathbf{j}\,\equiv\,\mathbf{0}} \equiv \mathcal{F}\,. \tag{2.21}$$

With regard to (2.17) and (2.18), the first functional derivative of the energy functional (2.20) corresponds, except for the prefactor, to the expectation value $\mathbf{X}(\tau)$ of the path $\mathbf{x}(\tau)$

$$\frac{\delta\,\mathcal{F}[\,\mathbf{j}\,]}{\delta\, j_i(\tau)} \;=\; -\frac{1}{\hbar\beta\,\mathcal{Z}[\,\mathbf{j}\,]} \oint \mathcal{D}\mathbf{x}\, e^{-\mathcal{A}[\mathbf{x},\mathbf{j}]/\hbar}\, x_i(\tau) \;=:\; -\frac{1}{\hbar\beta}\, X_i(\tau)\,. \tag{2.22}$$

The current can hence be written as a functional of the background by inverting (2.22) formally

$$\mathbf{j}(\tau) \;=\; \mathbf{j}[\mathbf{X}](\tau)\,. \tag{2.23}$$

The effective action $\Gamma[\mathbf{X}]$ is defined to be the Legendre transform of the free energy with respect to the external current

$$\Gamma[\mathbf{X}] \;:=\; \hbar\beta\,\mathcal{F}[\mathbf{j}[\mathbf{X}]] + \int_0^{\hbar\beta} d\tau\;\mathbf{j}[\mathbf{X}](\tau)\;\mathbf{X}(\tau)\,. \tag{2.24}$$

If we wish to calculate only the effective potential rather than the effective action, it is sufficient to consider a time-independent current $\mathbf{j}$. Thus, the action (2.17) becomes a function of $\mathbf{j}$

$$\mathcal{A}[\mathbf{x}]\,(\mathbf{j}) \;:=\; \mathcal{A}[\mathbf{x}] \;-\; \mathbf{j}\int_0^{\hbar\beta} d\tau\,\mathbf{x}(\tau)\,, \tag{2.25}$$

and both generating functionals (2.18) and (2.20) reduce to generating functions. Moreover, the functional derivative (2.22) is now a partial derivative

$$\frac{\partial\,\mathcal{F}(\mathbf{j})}{\partial\,j_i} \;=\; -\,\frac{1}{\hbar\beta\,\mathcal{Z}(\mathbf{j})}\oint\mathcal{D}\mathbf{x}\,e^{-\mathcal{A}[\mathbf{x}](\mathbf{j})/\hbar}\int_0^{\hbar\beta} d\tau\,x_i(\tau) \;=:\; -\,X_i\,. \tag{2.26}$$

Inverting (2.26) formally, we obtain the current $\mathbf{j}$ as a function of the path average $\mathbf{X}$

$$\mathbf{j} \;=\; \mathbf{j}(\mathbf{X})\,. \tag{2.27}$$

Analogously to the effective action, the effective potential $V_{\text{eff}}(\mathbf{X})$ is defined to be the Legendre transform of the free energy with respect to the external current:

$$V_{\text{eff}}\,(\mathbf{X}) \;:=\; \mathcal{F}(\mathbf{j}(\mathbf{X})) + \mathbf{j}(\mathbf{X})\,\mathbf{X}\,. \tag{2.28}$$

The effective action $\Gamma[\mathbf{X}]$ and the effective potential $V_{\text{eff}}(\mathbf{X})$ are related according to

$$V_{\text{eff}}(\mathbf{X}) \;=\; \frac{1}{\hbar\beta}\,\Gamma[\mathbf{X}]\Big|_{\mathbf{X}(\tau)=\mathbf{X}}\,. \tag{2.29}$$

Due to (2.21), the effective potential (2.28) is equal to the free energy for vanishing current $\mathbf{j}(\mathbf{X})\equiv 0$

$$V_{\text{eff}}(\mathbf{X})\,\Big|_{\mathbf{j}\equiv 0} \equiv \mathcal{F}. \tag{2.30}$$

On the other hand, extremizing the effective potential (2.28) yields with regard to (2.26)

$$\frac{\partial\,V_{\text{eff}}(\mathbf{X})}{\partial\,X_i} \;=\; j_i(\mathbf{X}) \;\stackrel{!}{=}\; 0\,. \tag{2.31}$$

Thus, a vanishing current corresponds to the extremized effective potential. In other words, we obtain the free energy (2.30) by extremizing the effective potential. Moreover, we know that according to

$$\mathcal{F} \;=\; E \;-\; T\,S\,, \tag{2.32}$$

the free energy is the same as the ground-state energy in the low-temperature limit $T\to 0$, which means, with regard to (2.9), $\beta\to\infty$.

2.3. Saddle Point Approximation

The effective potential $V_{\text{eff}}(\mathbf{X})$ is defined to be the Legendre transform of the free energy with respect to the external current $\mathbf{j}$ and can be calculated from the partition function. This is typically be done by applying the so-called *saddle point approximation* which is suitable for the low-temperature limit $\beta \to \infty$. It is an alternative to the *background method* which we apply in the following sections. In order to appreciate this method and its advantages, we shortly present the idea of the saddle point approximation as it is given, for instance, in Ref. [21]. Moreover, we will refer to the saddle point approximation in Chapter 8: the large-N limit can be regarded as the analogy of the saddle point approximation in the statistical field theory.

To simplify matters, we consider the case of classical statistics in $D = 1$ dimension instead of the path integral formalism. The main difference is that the former path $\mathbf{x}(\tau)$ becomes then a time-independent space coordinate x. As a consequence, the path integrals reduce to ordinary integrals and the partition function of a particle with mass M in a potential $V(x)$ reads

$$\mathcal{Z} \;=\; \int_{-\infty}^{\infty} \frac{dx}{\lambda}\, e^{-\beta V(x)} \tag{2.33}$$

with the thermal de Broglie-wavelength

$$\lambda \;=\; \sqrt{\frac{2\pi\hbar^2\beta}{M}}\,. \tag{2.34}$$

Now we add an external current j to the potential analogously to (2.25), leading to the generating function

$$\mathcal{Z}(j) \;:=\; \int_{-\infty}^{\infty} \frac{dx}{\lambda}\, e^{-\beta V(x,j)}\,. \tag{2.35}$$

In the low-temperature limit $\beta \to \infty$, the minimum of $V(x,j) := V(x) - jx$ yields the crucial contribution in the integral (2.35). The corresponding x-value of this minimum is called *saddle point* x_0 and can be determined by

$$\left.\frac{\partial\, V(x,j)}{\partial\, x}\right|_{x\,=\,x_0} = 0\,. \tag{2.36}$$

We introduce a new variable δx describing the deviations from the saddle point

$$x \;=\; x_0 \,+\, \delta x\,, \tag{2.37}$$

and perform a Taylor expansion of the potential $V(x,j)$ around x_0 :

$$V(x,j) \;=\; V(x_0,j) \,+\, \frac{1}{2}\,V^{(2)}(x_0)\,\delta x^2 \,+\, \frac{1}{6}\,V^{(3)}(x_0)\,\delta x^3 \,+\, \cdots\,. \tag{2.38}$$

The current j is linearly coupled to the potential. For this reason, the derivatives of second and higher order of the potential do not explicitly depend on j any more. The first derivative vanishes due to (2.36). Inserting (2.38) into the partition function (2.35) and expanding the resulting exponential function leads to

$$\begin{aligned}\mathcal{Z}(j) &= e^{-\beta V(x_0,j)} \int_{-\infty}^{\infty} \frac{d\,\delta x}{\lambda} \exp\left\{-\frac{\beta}{2} V^{(2)}(x_0)\,\delta x^2\right\} \left\{1 - \frac{\beta}{6} V^{(3)}(x_0)\,\delta x^3 \right. \\ &\left. - \frac{\beta}{24} V^{(4)}(x_0)\,\delta x^4 + \frac{\beta^2}{72} \left[V^{(3)}(x_0)\right]^2 \delta x^6 + \cdots\right\}. \end{aligned} \tag{2.39}$$

Due to the Gaussian exponential function, all integrals with odd powers of δx vanish. The remaining integrals are solved according to

$$\int_{-\infty}^{\infty} dx\, x^{2n}\, e^{-Ax^2/2} = \sqrt{\frac{2\,\pi}{A}}\, \frac{(2n-1)!!}{A^n}. \tag{2.40}$$

Up to the second order with respect to β^{-1}, the partition function (2.39) reads

$$\mathcal{Z}(j) = \frac{e^{-\beta V(x_0,j)}}{\hbar\,\beta\,\sqrt{V^{(2)}(x_0)\,/\,M}} \left\{1 - \frac{V^{(4)}(x_0)}{8\,\beta\,\left[V^{(2)}(x_0)\right]^2} + \frac{5\,\left[V^{(3)}(x_0)\right]^2}{24\,\beta\,\left[V^{(2)}(x_0)\right]^3} + \cdots\right\}. \tag{2.41}$$

The free energy follows by expanding the logarithm of (2.41) up to the first order:

$$\mathcal{F}(j) = V(x_0) - x_0 j + \frac{1}{\beta} \ln\left(\hbar\beta\sqrt{\frac{V^{(2)}(x_0)}{M}}\right) + \frac{1}{\beta^2}\left\{\frac{V^{(4)}(x_0)}{8\left[V^{(2)}(x_0)\right]^2} - \frac{5\left[V^{(3)}(x_0)\right]^2}{24\left[V^{(2)}(x_0)\right]^3} + \cdots\right\}. \tag{2.42}$$

Now, we have to express the saddle point in terms of the path average X that follows from the free energy analogously to (2.22) by means of

$$X(j) = -\frac{\partial\,\mathcal{F}(j)}{\partial\, j}. \tag{2.43}$$

Thus, we derive an expression for $X = X(x_0)$ and invert it afterwards. To this end, we insert (2.42) into (2.43), yielding

$$X(x_0) = \frac{\partial\, x_0}{\partial\, j}\left[j - V^{(1)}(x_0)\right] + x_0 - \frac{V^{(3)}(x_0)}{2\,\beta\,V^{(2)}(x_0)}\,\frac{\partial\, x_0}{\partial\, j} + \cdots. \tag{2.44}$$

Because of x_0 being the saddle point according to (2.36), we know that $V^{(1)}(x_0) = j$. Furthermore, it follows that

$$\frac{\partial\, V^{(1)}(x_0)}{\partial\, j} = 1 \qquad \Leftrightarrow \qquad \frac{\partial\, x_0}{\partial\, j} = \frac{1}{V^{(2)}(x_0)}. \tag{2.45}$$

Inserting $V^{(1)}(x_0)$ and (2.45) into (2.44) leads to

$$X(x_0) = x_0 - \frac{V^{(3)}(x_0)}{2\,\beta\,\left[V^{(2)}(x_0)\right]^2} + \cdots. \tag{2.46}$$

After inverting (2.46), we insert $x_0 = x_0(X)$ into the free energy (2.42). Finally, the Legendre transform analogously to (2.28) yields the desired effective potential

$$V_{\text{eff}}(X) = V(X) + \frac{1}{\beta}\ln\left(\hbar\beta\sqrt{\frac{V^{(2)}(X)}{M}}\right) + \frac{1}{\beta^2}\left\{\frac{V^{(4)}(X)}{8\left[V^{(2)}(X)\right]^2} - \frac{\left[V^{(3)}(X)\right]^2}{12\left[V^{(2)}(X)\right]^3} + \cdots\right\}. \tag{2.47}$$

2.4. Background Method

As we have seen in the previous section, it can be tedious to calculate the effective potential via the saddle point approximation. The so-called *background method* proves to be a more efficient approximation. Within this theory, there is no need to introduce an artificial current and the effective potential can be calculated in other ways than performing the Legendre transform. In the following, we present the background method for the D-dimensional path integral (2.15).

The background method [22–24] was first introduced by B. De Witt in 1965. It consists of dividing the path $\mathbf{x}(\tau)$ into a background $\mathbf{X}(\tau)$ and fluctuations $\boldsymbol{\delta}\mathbf{x}(\tau)$

$$\mathbf{x}(\tau) \;=\; \mathbf{X}(\tau) \;+\; \boldsymbol{\delta}\mathbf{x}(\tau)\,. \tag{2.48}$$

This ansatz can be compared to those in the saddle point approximation (2.37). More precisely, the saddle point corresponds to the leading order of the background which is just the field expectation (2.46). For the purpose of calculating the effective potential, it is sufficient to consider a time-independent background $\mathbf{X}(\tau)\equiv\mathbf{X}$. We insert the ansatz (2.48) for a constant background into an arbitrary potential $V(\mathbf{x})$ and perform a Taylor expansion around the background. For reasons of simplicity, we denote the partial derivatives by

$$\frac{\partial^n V(\mathbf{X})}{\partial X_i\,\partial X_j\,\cdots\,\partial X_m} \;=:\; V_{ij\cdots m}(\mathbf{X})\,. \tag{2.49}$$

In this formalism, the Taylor expansion of the potential reads

$$\begin{aligned} V(\mathbf{X}+\boldsymbol{\delta x}) \;&=\; V(\mathbf{X}) \;+\; V_i(\mathbf{X})\,\delta x_i(\tau) \;+\; \frac{1}{2}\,V_{ij}(\mathbf{X})\,\delta x_i(\tau)\,\delta x_j(\tau) \\ &\quad+\frac{1}{6}\,V_{ijk}(\mathbf{X})\,\delta x_i(\tau)\,\delta x_j(\tau)\,\delta x_k(\tau) \\ &\quad+\frac{1}{24}\,V_{ijkl}(\mathbf{X})\,\delta x_i(\tau)\,\delta x_j(\tau)\,\delta x_k(\tau)\,\delta x_l(\tau) \;+\; \cdots\,. \end{aligned} \tag{2.50}$$

For reasons of clarity, we use Einstein's sum convention, i.e., adding up all indices that occur repeatedly. Now we insert the Taylor expansion (2.50) into the imaginary-time action (2.11), yielding

$$\begin{aligned} \mathcal{A}[\mathbf{X}+\boldsymbol{\delta x}] =\; &\hbar\,\beta\,V(\mathbf{X}) \;+\; \int_0^{\hbar\beta} d\tau \Bigg\{ \frac{1}{2}\,\delta x_i(\tau)\Big[-M\,\partial_\tau^2 + V_{ij}(\mathbf{X})\Big]\delta x_j(\tau) \\ &+\frac{1}{6}\,V_{ijk}(\mathbf{X})\,\delta x_i(\tau)\,\delta x_j(\tau)\,\delta x_k(\tau) \;+\; \frac{1}{24}\,V_{ijkl}(\mathbf{X})\,\delta x_i(\tau)\,\delta x_j(\tau)\,\delta x_k(\tau)\,\delta x_l(\tau) \;+\; \cdots \Bigg\} \\ \equiv\;\; &\mathcal{A}^{(\mathrm{cl})}(\mathbf{X}) + \mathcal{A}^{(\mathrm{fluc})}[\mathbf{X} \;+\; \boldsymbol{\delta x}] \end{aligned} \tag{2.51}$$

with the classical action $\mathcal{A}^{(\mathrm{cl})}(\mathbf{X})$ and the fluctuation part $\mathcal{A}^{(\mathrm{fluc})}[\mathbf{X}+\boldsymbol{\delta x}]$. Note that we have vanishing terms linear in the fluctuations $\boldsymbol{\delta x}(\tau)$. A detailed proof is given in Ref. [1, Ch. 3] where a functional integro-differential equation for the effective action is solved order by

order in $\hbar$. Analogously to the action (2.51), the partition function (2.15) in the background formalism has a decomposition into classical and fluctuation part

$$\begin{aligned} \mathcal{Z}(\mathbf{X}) &= e^{-\mathcal{A}^{(\mathrm{cl})}(\mathbf{X})/\hbar} \oint \mathcal{D}\boldsymbol{\delta x}\; e^{-\mathcal{A}^{(\mathrm{fluc})}[\mathbf{X}+\boldsymbol{\delta x}]/\hbar} \\ &\equiv \mathcal{Z}^{(\mathrm{cl})}(\mathbf{X})\, \mathcal{Z}^{(\mathrm{fluc})}(\mathbf{X})\,. \end{aligned} \tag{2.52}$$

For reasons of brevity, we define

$$\tilde{\mathcal{A}}[\mathbf{X}+\boldsymbol{\delta}\mathbf{x}] := \int_0^{\hbar\beta} d\tau \frac{1}{2}\,\delta x_i(\tau)\Big[-M\,\partial_\tau^2 + V_{ij}(\mathbf{X})\Big]\delta x_j(\tau)\,. \tag{2.53}$$

We calculate the fluctuation part of the partition function (2.52) by expanding the exponential function with third and higher powers of the fluctuations in accordance with (2.51) and obtain

$$\begin{aligned} \mathcal{Z}^{(\mathrm{fluc})}(\mathbf{X}) &= \oint \mathcal{D}\boldsymbol{\delta x}\; e^{-\tilde{\mathcal{A}}[\mathbf{X}+\boldsymbol{\delta}\mathbf{x}]/\hbar}\Bigg[1 - \frac{V_{ijk}(\mathbf{X})}{6\,\hbar}\int_0^{\hbar\beta} d\tau\;\delta x_i(\tau)\,\delta x_j(\tau)\,\delta x_k(\tau) \\ &- \frac{V_{ijkl}(\mathbf{X})}{24\,\hbar}\int_0^{\hbar\beta} d\tau\;\delta x_i(\tau)\,\delta x_j(\tau)\,\delta x_k(\tau)\,\delta x_l(\tau) \;+\; \frac{V_{ijk}(\mathbf{X})\,V_{lmn}(\mathbf{X})}{72\,\hbar^2} \\ &\times \int_0^{\hbar\beta} d\tau_1 \int_0^{\hbar\beta} d\tau_2\;\delta x_i(\tau_1)\,\delta x_j(\tau_1)\,\delta x_k(\tau_1)\delta x_l(\tau_2)\,\delta x_m(\tau_2)\,\delta x_n(\tau_2) \;+\; \cdots\Bigg]\,. \end{aligned} \tag{2.54}$$

Now we define the expectation values by means of

$$\langle \bullet \rangle := \frac{1}{\mathcal{Z}^{(1)}(\mathbf{X})} \oint \mathcal{D}\boldsymbol{\delta x}\; \bullet\; e^{-\tilde{\mathcal{A}}[\mathbf{X}+\boldsymbol{\delta}\mathbf{x}]/\hbar} \tag{2.55}$$

with the first-order partition function

$$\mathcal{Z}^{(1)}(\mathbf{X}) = \oint \mathcal{D}\boldsymbol{\delta x}\; e^{-\tilde{\mathcal{A}}[\mathbf{X}+\boldsymbol{\delta}\mathbf{x}]/\hbar}\,. \tag{2.56}$$

Due to the symmetry, expectation values with odd powers vanish, so (2.54) reduces to

$$\begin{aligned} \mathcal{Z}^{(\mathrm{fluc})}(\mathbf{X}) &= \mathcal{Z}^{(1)}(\mathbf{X})\Bigg[1 - \frac{V_{ijkl}(\mathbf{X})}{24\,\hbar}\int_0^{\hbar\beta} d\tau\;\big\langle \delta x_i(\tau)\,\delta x_j(\tau)\,\delta x_k(\tau)\,\delta x_l(\tau)\big\rangle \\ &+ \frac{V_{ijk}(\mathbf{X})\,V_{lmn}(\mathbf{X})}{72\,\hbar^2}\int_0^{\hbar\beta} d\tau_1 \int_0^{\hbar\beta} d\tau_2\;\big\langle \delta x_i(\tau_1)\,\delta x_j(\tau_1)\,\delta x_k(\tau_1)\delta x_l(\tau_2)\,\delta x_m(\tau_2)\,\delta x_n(\tau_2)\big\rangle + \cdots\Bigg]\,. \end{aligned} \tag{2.57}$$

In accordance with (2.20) and (2.30), we conclude that the effective potential and the partition function are related by

$$V_{\mathrm{eff}}(\mathbf{X}) = -\frac{1}{\beta}\ln \mathcal{Z}(\mathbf{X})\,. \tag{2.58}$$

Inserting (2.51), (2.52), and (2.57) into (2.58) and expanding the logarithm, we obtain the effective potential

$$\begin{aligned} V_{\text{eff}}(\mathbf{X}) \;&=\; V(\mathbf{X}) \;-\; \frac{1}{\beta}\ln \mathcal{Z}^{(1)}(\mathbf{X}) \;+\; \frac{V_{ijkl}(\mathbf{X})}{24\,\hbar\,\beta}\int_0^{\hbar\beta} d\tau\,\left\langle \delta x_i(\tau)\,\delta x_j(\tau)\,\delta x_k(\tau)\,\delta x_l(\tau)\right\rangle \\ &- \frac{V_{ijk}(\mathbf{X})\,V_{lmn}(\mathbf{X})}{72\,\hbar^2\,\beta}\int_0^{\hbar\beta} d\tau_1\int_0^{\hbar\beta} d\tau_2\,\left\langle \delta x_i(\tau_1)\,\delta x_j(\tau_1)\,\delta x_k(\tau_1)\delta x_l(\tau_2)\,\delta x_m(\tau_2)\,\delta x_n(\tau_2)\right\rangle \;+\cdots \\ &\equiv V(\mathbf{X}) \;+\; V_{\text{eff}}^{(1)}(\mathbf{X}) \;+\; V_{\text{eff}}^{(\text{int})}(\mathbf{X})\,. \end{aligned} \tag{2.59}$$

All contractions of the fluctuations are included in the interaction part $V_{\text{eff}}^{(\text{int})}(\mathbf{X})$.

2.5. Effective Potential in First Loop Order

In accordance with (2.59), the first-order term $V_{\text{eff}}^{(1)}(\mathbf{X})$ of the effective potential reads explicitly

$$V_{\text{eff}}^{(1)}(\mathbf{X}) \;=\; -\,\frac{1}{\beta}\ln \mathcal{Z}^{(1)}(\mathbf{X})\,, \tag{2.60}$$

with the first-order partition function defined by (2.53) and (2.56). For further calculations, we denote the operator in the integral of (2.53) by

$$\hat{O}_{ij}(\tau) \;:=\; M\left[-\,\partial_\tau^2 \;+\; \frac{1}{M}\,V_{ij}(\mathbf{X})\right]. \tag{2.61}$$

The so-called *integral kernel* $G_{ij}^{-1}(\tau_1,\tau_2)$ is defined by

$$G_{ij}^{-1}(\tau_1,\tau_2) \;:=\; \hat{O}_{ij}(\tau_1)\,\delta(\tau_1-\tau_2)\,. \tag{2.62}$$

With regard to (2.53), (2.56), and (2.62), the first-order term of the partition function can hence be written as

$$\mathcal{Z}^{(1)}(\mathbf{X}) \;=\; \oint \mathcal{D}\boldsymbol{\delta x}\,\exp\!\left\{-\,\frac{1}{2\,\hbar}\int_0^{\hbar\beta} d\tau_1\int_0^{\hbar\beta} d\tau_2\;\delta x_i(\tau_1)\;G_{ij}^{-1}(\tau_1,\tau_2)\;\delta x_i(\tau_2)\right\}. \tag{2.63}$$

This is just a Gaussian path integral: let A be a D-dimensional self-adjoint matrix with positive determinant $\det A>0$. Then, we obtain

$$\int_{-\infty}^{\infty} d^D x\; e^{-\mathbf{x}^T A\mathbf{x}/2} \;=\; \frac{(2\pi)^{D/2}}{\sqrt{\det A}}\,. \tag{2.64}$$

The Gaussian path integral in (2.63) can be regarded as a functional generalization of (2.64)

$$\oint \mathcal{D}\boldsymbol{\delta}\mathbf{x}\,\exp\!\left\{-\frac{1}{2\hbar}\int_0^{\hbar\beta} d\tau_1\int_0^{\hbar\beta} d\tau_2\;\delta x_i(\tau_1)\;G_{ij}^{-1}\,(\tau_1,\tau_2)\;\;\delta x_j(\tau_2)\right\} \;=\; \frac{1}{\sqrt{\det G^{-1}}}\,. \tag{2.65}$$

We write the square root in (2.65) as

$$\frac{1}{\sqrt{\det G^{-1}}} \;=\; \exp\left(-\frac{1}{2}\mathrm{Tr}\ln G^{-1}\right)\,, \tag{2.66}$$

with trace log being the sum of the logarithms of the integral kernel's eigenvalues λ

$$\mathrm{Tr}\ln G^{-1} \;:=\; \sum_{\lambda} \ln\lambda\,. \tag{2.67}$$

We obtain them by solving the corresponding eigenvalue problem

$$\int_0^{\hbar\beta} d\tau_2\, G^{-1}_{ij}(\tau_1,\tau_2)\,\delta x_j(\tau_2) \;=\; M\,\lambda\,\delta x_i(\tau_1) \tag{2.68}$$

for periodic eigenstates $\delta x_i(0)=\delta x_i(\hbar\beta)$. Now we specialize our formalism in a rotationally symmetric potential $V(\mathbf{x})=V(x)$. In arbitrary dimension D, we can define one longitudinal and $D-1$ transversal directions with respect to the background $\mathbf{X}$. To this end, we introduce the longitudinal and transversal projection operators

$$P^L_{ij} \;:=\; \frac{X_i\,X_j}{X^2} \qquad \text{and} \qquad P^T_{ij} \;:=\; \delta_{ij} \;-\; P^L_{ij}\,. \tag{2.69}$$

They have the following properties:

$$P^L_{ij}\,X_j \;=\; X_i\,, \qquad P^T_{ij}\,X_j \;=\; 0\,, \tag{2.70}$$

$$P^L_{ij}\,P^L_{ij} \;=\; 1\,, \qquad P^T_{ij}\,P^T_{ij} \;=\; D-1\,, \tag{2.71}$$

$$P^L_{ij}\,P^L_{jk} \;=\; P^L_{ik}\,, \qquad P^T_{ij}\,P^T_{jk} \;=\; P^T_{ik}\,, \tag{2.72}$$

$$P^L_{ij}\,P^T_{jk} \;=\; P^T_{ij}\,P^L_{jk} \;=\; 0\,, \qquad P^L_{ij} \;+\; P^T_{ij} \;=\; \delta_{ij}\,. \tag{2.73}$$

In terms of the projection operators, the second derivative of the rotationally symmetric potential $V(X)$ reads

$$V_{ij}(X) \;=\; V''(X)\,P^L_{ij} \;+\; \frac{V'(X)}{X}P^T_{ij}\,, \tag{2.74}$$

where $V'(X)$ and $V''(X)$ denote the first and the second derivative with respect to the modulus $X=|\mathbf{X}|$, respectively. Now we turn our attention back to the eigenvalue problem (2.68). First, the eigenstates $\delta x_i(\tau)$ are decomposed into functions $v_i^{(n)}(\tau)$ according to the longitudinal ($n=1$) and transversal ($n=2,...,D$) directions. Second, we decompose them with respect to the Matsubara frequencies

$$\omega_m \;=\; \frac{2\pi}{\hbar\beta}\,m\,, \qquad m\in\mathbb{Z}\,, \tag{2.75}$$

since we are looking for periodic eigenstates. Due to the delta-function in (2.62), the eigenvalue problem (2.68) amounts to solving

$$\hat{O}_{ij}(\tau)\, v_j^{(m,n)}(\tau) \;=\; M\,\lambda^{(m)}\, v_i^{(m,n)}(\tau)\,, \qquad n \;=\; 1,2,...,D\,, \tag{2.76}$$

with the periodic eigenfunctions $\mathbf{v}^{(m,n)}(\hbar\beta)=\mathbf{v}^{(m,n)}(0)$. For the longitudinal eigenfunctions, we choose the ansatz

$$v_j^{(m,1)}(\tau) \;=\; X_j\, e^{-\imath\omega_m\tau} \tag{2.77}$$

with the background X_j. Inserting (2.77) into (2.76), the corresponding eigenvalues turn out to be

$$\lambda_L^{(m)} \;=\; \omega_m^2 + \frac{1}{M}\, V''(X)\,. \tag{2.78}$$

For the transversal eigenfunctions $n=2,...,D$, we choose

$$v_j^{(m,n)}(\tau) \;=\; Y_j^{(n)}\, e^{-\imath\omega_m\tau}\,, \tag{2.79}$$

with $Y_j^{(n)}$ being perpendicular to the background X_j and among each other: $X_jY_j^{(n)}=0$ and $Y_j^{(n)}Y_j^{(n')}=0$ for $n\neq n'$. Due to the symmetry, the transversal eigenvalues do not depend on n and are therefore $(D-1)$-fold degenerated

$$\lambda_T^{(m)} \;=\; \omega_m^2 + \frac{1}{M}\,\frac{V'(X)}{X}\,. \tag{2.80}$$

With regard to the occurring Matsubara frequencies, it is suggestive to define the longitudinal and transversal X-dependent frequencies

$$\omega_L^2\,(X) \;:=\; \frac{1}{M}\, V''(X)\,, \qquad \omega_T^2\,(X) \;:=\; \frac{1}{M}\,\frac{V'(X)}{X}\,. \tag{2.81}$$

Thus, the eigenvalues (2.78) and (2.80) read

$$\lambda_L^{(m)} \;=\; \omega_m^2 \;+\; \omega_L^2\,(X)\,, \qquad \lambda_T^{(m)} \;=\; \omega_m^2 \;+\; \omega_T^2\,(X)\,. \tag{2.82}$$

In terms of the projection operators (2.69) and the frequencies (2.81), the integral kernel (2.62) has the decomposition

$$G_{ij}^{-1}(\tau_1,\tau_2) \;= M\Big\{ P_{ij}^L\big[-\partial_\tau^2+\omega_L^2(X)\big] + P_{ij}^T\big[-\partial_\tau^2+\omega_T^2\,(X)\big]\Big\}\,\delta(\tau_2-\tau_1)\,. \tag{2.83}$$

Applying (2.62), (2.66), and (2.82), we identify the trace-log term (2.67) with

$$\mathrm{Tr}\ln G^{-1} \;=\; \sum_{m=-\infty}^{\infty}\Big[\ln\lambda_L^{(m)} + (D-1)\ln\lambda_T^{(m)}\Big]\,. \tag{2.84}$$

In order to evaluate this Matsubara sum, we recall the one-dimensional harmonic oscillator partition function (B.34) and find

$$\frac{1}{2}\,\mathrm{Tr}\ln G_\omega^{-1} \;=\; -\ln\mathcal{Z}_\omega \;=\; \ln\left(2\sinh\frac{\hbar\beta\omega}{2}\right)\,, \tag{2.85}$$

which reduces in the low-temperature limit to

$$\frac{1}{2}\,\mathrm{Tr}\ln G_\omega^{-1} \;\longrightarrow\; \frac{\hbar\,\beta\,\omega}{2} \quad \text{for } \beta\to\infty\,. \tag{2.86}$$

It remains to substitute the longitudinal and transversal frequencies $\omega\to\omega_{L,T}$ in accordance with (2.81), and we obtain the first-order effective potential (2.60) in the low-temperature limit:

$$V_{\text{eff}}^{(1)}(X) \;=\; \frac{\hbar\,\omega_L(X)}{2} + (D-1)\,\frac{\hbar\,\omega_T(X)}{2}\,. \tag{2.87}$$

2.6. Calculation of Propagator

For all calculations in second and higher orders, we require the so-called *propagator* $G_{ij}(\tau_a,\tau_b)$ which we therefore calculate in this section. It is defined to be the inverse of the integral kernel $G_{ij}^{-1}(\tau_a,\tau_b)$ in (2.62)

$$\int_0^{\hbar\beta} d\tau_2\, G_{ij}^{-1}(\tau_1,\tau_2)\, G_{jk}(\tau_2,\tau_3) \;=\; \hbar\,\delta_{ik}\,\delta(\tau_1-\tau_3)\,. \tag{2.88}$$

The Matsubara decomposition of the integral kernel (2.83) reads

$$G_{ij}^{-1}(\tau_1,\tau_2) \;=\; \sum_{m=-\infty}^{\infty} G_{ij}^{-1(m)}\, e^{-\imath\omega_m(\tau_1-\tau_2)}\,. \tag{2.89}$$

As usual, the Fourier coefficients follow from inverse Fourier transform:

$$G_{ij}^{-1(m)} \;=\; \frac{1}{\hbar\beta}\int_0^{\hbar\beta} d\tau\; G_{ij}^{-1}(\tau,0)\, e^{\imath\omega_m\tau}\,. \tag{2.90}$$

By applying the decomposition (2.83) of the integral kernel into longitudinal and transversal parts, we obtain a similar expression for the Fourier coefficients (2.90), namely

$$G_{ij}^{-1(m)} \;=\; \frac{M}{\hbar\beta}\Big\{P_{ij}^L\left[\omega_m^2+\omega_L^2\,(X)\right] + P_{ij}^T\left[\omega_m^2+\omega_T^2\,(X)\right]\Big\}\,. \tag{2.91}$$

Furthermore, we write both the propagator and the $\delta-$function in Matsubara decomposition

$$G_{ij}(\tau_1,\tau_2) \;=\; \sum_{m'=-\infty}^{\infty} G_{ij}^{(m')}\, e^{-\imath\omega_{m'}(\tau_1-\tau_2)} \tag{2.92}$$

and

$$\delta(\tau_1-\tau_3) \;=\; \frac{1}{\hbar\,\beta}\sum_{m=-\infty}^{\infty} e^{-\imath\omega_m(\tau_1-\tau_3)}\,. \tag{2.93}$$

In order to calculate the Fourier coefficients of the propagator, we insert (2.89), (2.92), and (2.93) into the integral identity (2.88), which leads to

$$\sum_{m,m'=-\infty}^{\infty} G_{ij}^{-1(m)}\, \mathrm{G}_{jk}^{(m')}\, \mathrm{e}^{-\imath(\omega_m \tau_1 - \omega_{m'}\tau_3)} \int_0^{\hbar\beta} d\tau_2\, \mathrm{e}^{-\imath\tau_2(\omega_{m'}-\omega_m)} \;=\; \frac{1}{\beta}\,\delta_{ik} \sum_{m=-\infty}^{\infty} \mathrm{e}^{-\imath\omega_m(\tau_1-\tau_3)}\,. \quad (2.94)$$

When we perform the τ_2-integration, we obtain a Kronecker symbol $\delta_{m,m'}$ that cancels one sum on the left-hand side of (2.94) and the equation reduces to

$$\hbar\beta \sum_{m=-\infty}^{\infty} G_{ij}^{-1(m)}\, G_{jk}^{(m)}\, \mathrm{e}^{-\imath\omega_m(\tau_1-\tau_3)} \;=\; \frac{1}{\beta}\,\delta_{ik} \sum_{m=-\infty}^{\infty} \mathrm{e}^{-\imath\omega_m(\tau_1-\tau_3)}\,. \quad (2.95)$$

We merely have to compare the coefficients and obtain immediately

$$G_{ij}^{-1(m)}\, G_{jk}^{(m)} \;=\; \frac{1}{\hbar\,\beta^2}\,\delta_{ik}\,. \quad (2.96)$$

Because of the orthonormality (2.73) of the projection operators, it is possible to decompose also the propagator $G_{ij}^{(m)}$ into a longitudinal and transversal part analogously to (2.83) and (2.91)

$$G_{jk}^{(m)} \;=\; P_{jk}^{L}\, G_{L}^{(m)} + P_{jk}^{T}\, G_{T}^{(m)}\,. \quad (2.97)$$

Now we insert the decompositions (2.91) and (2.97) of the integral kernel and the propagator into (2.96). With respect to (2.72) and (2.73), we find

$$P_{ik}^{L}\left[\omega_m^2 + \omega_L^2\,(X)\right] G_{L}^{(m)} + P_{ik}^{T}\left[\omega_m^2 + \omega_T^2\,(X)\right] G_{T}^{(m)} \;=\; \frac{1}{M\beta}\left[\,P_{ik}^{L} + P_{ik}^{T}\,\right]\,. \quad (2.98)$$

Thus, we identify the longitudinal and transversal Matsubara coefficients of the propagator with

$$G_{L}^{(m)} \;=\; \frac{1}{M\,\beta}\,\frac{1}{\omega_m^2 + \omega_L^2\,(X)}\,, \qquad G_{T}^{(m)} \;=\; \frac{1}{M\,\beta}\,\frac{1}{\omega_m^2 + \omega_T^2\,(X)}\,. \quad (2.99)$$

The complete Fourier coefficient follows after inserting (2.99) into (2.97)

$$G_{jk}^{(m)} \;=\; \frac{1}{M\,\beta}\left[\,P_{jk}^{L}\,\frac{1}{\omega_m^2 + \omega_L^2\,(X)} \;+\; P_{jk}^{T}\,\frac{1}{\omega_m^2 + \omega_T^2\,(X)}\,\right]\,. \quad (2.100)$$

Finally, we insert (2.100) into the Matsubara series (2.92) and obtain the propagator

$$\begin{aligned} G_{ij}(\tau_1,\tau_2) \;&=\; \frac{1}{M\,\beta} \sum_{m=-\infty}^{\infty} \left[\,P_{ij}^{L}\,\frac{1}{\omega_m^2 + \omega_L^2\,(X)} \;+\; P_{ij}^{T}\,\frac{1}{\omega_m^2 + \omega_T^2\,(X)}\,\right] e^{-\imath\omega_m(\tau_1-\tau_2)} \\ &:=\; P_{ij}^{L}\,G_L(\tau_1,\tau_2) \;+\; P_{ij}^{T}\,G_T(\tau_1,\tau_2)\,. \end{aligned} \quad (2.101)$$

The general result of the propagators (2.101) has been calculated in Appendix B, the result for the low-temperature limit $T \to 0$ can be found in (B.32). We just have to replace the frequencies $\omega \to \omega_{L,T}(x)$ in accordance with (2.81), yielding

$$G_L(\tau_1,\tau_2) \;=\; \frac{\hbar}{2\,M\,\omega_L\,(X)}\,e^{-\omega_L|\tau_1-\tau_2|}\,, \quad G_T(\tau_1,\tau_2) \;=\; \frac{\hbar}{2\,M\,\omega_T\,(X)}\,e^{-\omega_T|\tau_1-\tau_2|}\,. \quad (2.102)$$

By taking the low-temperature limit, the results pass from quantum statistics into quantum mechanics.

2.7. Effective Potential in Second Loop Order

Now we come back to the interaction part of the effective potential defined in (2.59). The propagator calculated in the previous section corresponds to the expectation value

$$G_{ij}(\tau_1,\tau_2) \;=\; \big\langle \delta x_i(\tau_1)\delta x_j(\tau_2)\big\rangle\,. \tag{2.103}$$

Therefore, we reduce the expectation values of higher powers in (2.59) to propagators by applying Wick contractions

$$\big\langle \delta x_i(\tau)\,\delta x_j(\tau)\,\delta x_k(\tau)\,\delta x_l(\tau)\big\rangle \;=\; 3\,G_{ij}(\tau,\tau)\,G_{kl}(\tau,\tau)\,, \tag{2.104}$$

$$\begin{aligned}\big\langle \delta x_i(\tau_1)\,\delta x_j(\tau_1)\,\delta x_k(\tau_1)\,\delta x_l(\tau_2)\,\delta x_m(\tau_2)\,\delta x_n(\tau_2)\big\rangle \;=\; & 6\,G_{il}(\tau_1,\tau_2)\,G_{jm}(\tau_1,\tau_2)\,G_{kn}(\tau_1,\tau_2)\\ & +9\,G_{ij}(\tau_1,\tau_1)\,G_{kl}(\tau_1,\tau_2)\,G_{mn}(\tau_2,\tau_2)\,.\end{aligned} \tag{2.105}$$

Here, we benefit from the fact that most contractions coincide due to the same time arguments. The second term in (2.105) can be omitted as it would lead to a one-particle reducible Feynman diagram. With regard to (2.104) and (2.105), the interaction part $V_{\rm eff}^{(\rm int)}(\mathbf{X})$ in (2.59) can be written as

$$\begin{aligned}V_{\rm eff}^{(\rm int)}(\mathbf{X}) \;=\; & \frac{V_{ijkl}(\mathbf{X})}{8\,\hbar\,\beta}\int_0^{\hbar\beta} d\tau\; G_{ij}(\tau,\tau)\,G_{kl}(\tau,\tau)\\ & -\frac{V_{ijk}(\mathbf{X})\,V_{lmn}(\mathbf{X})}{12\,\hbar^2\,\beta}\int_0^{\hbar\beta}d\tau_1\int_0^{\hbar\beta}d\tau_2\; G_{il}(\tau_1,\tau_2)\,G_{jm}(\tau_1,\tau_2)\,G_{kn}(\tau_1,\tau_2)\;+\;\cdots\,.\end{aligned} \tag{2.106}$$

There exists a so-called *loop expansion* of the interaction part

$$V_{\rm eff}^{(\rm int)}(\mathbf{X}) \;=\; -\,\frac{1}{\beta}\sum_{l=2}^{\infty} V_{\rm eff}^{(l)}(\mathbf{X})\,. \tag{2.107}$$

The name is due to the fact that all interaction terms of the effective potential can be described by Feynman loop diagrams. The term $V_{\rm eff}^{(l)}(\mathbf{X})$ consists of all one-particle irreducible vacuum diagrams with l loops. A diagram is called irreducible if it does not break into two pieces when cutting one line, vacuum diagram means that all lines start and end in vertices. The summation in (2.107) starts with $l=2$ loops, the zero- and first-order terms correspond to the potential itself and the trace-log term, respectively. There exists an immediate connection between diagrams and mathematical formalism. Lines and vertices and integrals and propagators can be transferred into each other by applying the so-called *Feynman rules*. Therefore, we present them for a rotationally symmetric potential of a constant background $\mathbf{X}$ in D dimensions:

(1) All vertices and their outgoing lines are denoted arbitrarily with indices.

(2) A propagator $G_{ij}(\tau_a,\tau_b)$ corresponds to a line connecting the lines i and j of the vertices a and b, respectively:

$$a\;\overset{\;i\quad j\;}{\text{———}}\;b \;\;\equiv\;\; G_{ij}(\tau_a,\tau_b)\,. \tag{2.108}$$

(3) A vertex a with n outgoing lines represents the τ-integral

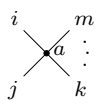

$$\equiv \; -\frac{1}{\hbar}\, V_{ij\cdots m}(\mathbf{X}) \int_0^{\hbar\beta} d\tau_a \tag{2.109}$$

over the propagators connected with vertex a. Here, we applied the notation (2.49).

In order to calculate the loop expansion (2.107) of the effective potential, we have to evaluate the associated Feynman integrals for each order. There exists also a Feynman diagram for the first-order term, which we add in this place

$$\mathrm{Tr}\ln G^{-1} \;=\; \text{  } \,. \tag{2.110}$$

In second loop order, there exist two Feynman diagrams

$$V_{\text{eff}}^{(2)} \;=\; \frac{1}{8} \;\text{ 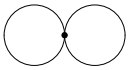 }\; + \frac{1}{12} \;\text{  }\,. \tag{2.111}$$

More precisely and with regard to the Feynman rules (2.108) and (2.109), we identify the diagrams with

$$\text{ 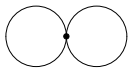 } \;=\; -\frac{1}{\hbar}\, V_{ijkl}(\mathbf{X}) \int_0^{\hbar\beta} d\tau\; G_{ij}(\tau,\tau)\, G_{kl}(\tau,\tau) \tag{2.112}$$

and

$$\text{  } \;=\; \frac{1}{\hbar^2}\, V_{ijk}(\mathbf{X})\, V_{lmn}(\mathbf{X}) \int_0^{\hbar\beta} d\tau_1 \int_0^{\hbar\beta} d\tau_2\; G_{il}(\tau_1,\tau_2)\, G_{jm}(\tau_1,\tau_2)\, G_{kn}(\tau_1,\tau_2)\,. \tag{2.113}$$

The diagram (2.112) is called *direct diagram*, (2.113) is referred to as *sunset diagram*. In order to calculate these diagrams, we have to determine the occurring higher derivatives of the potential first

$$V_{ijk}(\mathbf{X}) \;=\; P_{ijk}^{L}\, V'''(X) \;+\; P_{ijk}^{T} \left[\, \frac{V''(X)}{X} \;-\; \frac{V'(X)}{X^2} \,\right] \tag{2.114}$$

and

$$V_{ijkl}(\mathbf{X}) \;=\; P_{ijkl}^{L}\, V^{(4)}(X) \;+\; P_{ijkl}^{T}\, \frac{V'''(X)}{X} \;+\; P_{ijkl}^{E} \left[\, \frac{V''(X)}{X^2} \;-\; \frac{V'(X)}{X^3} \,\right]. \tag{2.115}$$

Here, we have introduced projection operators of third order order

$$P_{ijk}^{L} \;=\; \frac{X_i\, X_j\, X_k}{X^3}\,, \tag{2.116}$$

$$P_{ijk}^{T} \;=\; \delta_{ij}\, \frac{X_k}{X} + \delta_{jk}\, \frac{X_i}{X} + \delta_{ki}\, \frac{X_j}{X} - 3\, P_{ijk}^{L}\,, \tag{2.117}$$

and of fourth order

$$P^L_{ijkl} \;=\; \frac{X_i\,X_j\,X_k\,X_l}{X^4}\,, \tag{2.118}$$

$$P^T_{ijkl} = \delta_{ij}\frac{X_k\,X_l}{X^2} + \delta_{jk}\frac{X_i\,X_l}{X^2} + \delta_{kl}\frac{X_i\,X_j}{X^2} + \delta_{li}\frac{X_k\,X_j}{X^2} + \delta_{jl}\frac{X_k\,X_i}{X^2} + \delta_{ik}\frac{X_j\,X_l}{X^2} - 6P^L_{ijkl}\,, \tag{2.119}$$

$$P^E_{ijkl} \;=\; \delta_{ij}\,\delta_{kl} + \delta_{ik}\,\delta_{jl} + \delta_{il}\,\delta_{jk} - 3\,P^L_{ijkl} - 3\,P^T_{ijkl}\,. \tag{2.120}$$

Analogously to (2.70)–(2.73), we determine the following properties:

$$P^L_{ijk}\frac{X_k}{X} \;=\; P^L_{ij}\,, \qquad P^T_{ijk}\frac{X_k}{X} \;=\; P^T_{ij}\,, \tag{2.121}$$

$$P^L_{ijk}\,P^T_{ilm} \;=\; P^L_{jk}\,P^T_{lm}\,, \qquad P^T_{ijk}\,P^L_{ilm} \;=\; P^T_{jk}\,P^L_{lm}\,, \tag{2.122}$$

$$P^L_{ij}\,P^L_{ikl} = P^L_{jkl}\,, \quad P^T_{ij}\,P^T_{ikl} = P^T_{jl}\frac{X_k}{X} + P^T_{jk}\frac{X_l}{X}\,, \quad P^T_{ij}\,P^L_{ikl} = 0\,, \quad P^L_{ij}\,P^T_{ikl} = P^T_{kl}\frac{X_j}{X}\,, \tag{2.123}$$

$$P^L_{ijk}\,P^L_{ilm} = P^L_{jklm}\,, \quad P^T_{ijk}\,P^T_{ilm} = P^T_{jk}\,P^T_{lm} + P^L_{jl}\,P^T_{km} + P^L_{jm}\,P^T_{kl} + P^L_{kl}\,P^T_{jm} + P^L_{km}\,P^T_{jl}\,, \tag{2.124}$$

$$P^L_{ij}\,P^L_{ijkl} \;=\; P^L_{kl}\,, \qquad P^T_{ij}\,P^T_{ijkl} \;=\; (D-1)\,P^L_{kl}\,, \tag{2.125}$$

$$P^L_{ij}\,P^T_{ijkl} \;=\; P^T_{kl}\,, \qquad P^T_{ij}\,P^L_{ijkl} \;=\; 0\,, \tag{2.126}$$

$$P^L_{ij}\,P^E_{ijkl} \;=\; -2\,P^T_{kl}\,, \qquad P^T_{ij}\,P^E_{ijkl} \;=\; (D+1)\,P^T_{kl} \;-\; 2\,(D-1)\,P^L_{kl}\,. \tag{2.127}$$

With these results, we start calculating the direct diagram (2.112). To this end, we split up the occurring propagators in accordance with (2.97), insert the fourth derivative (2.115) and use the relations (2.71), (2.73), and (2.125)–(2.127), yielding

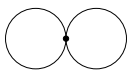

$$\begin{aligned} &= -\frac{1}{\hbar}\int_0^{\hbar\beta} d\tau \left\{ G_L^2(\tau,\tau)\,V^{(4)}(X) + (D^2-1)\,G_T^2(\tau,\tau)\left[\frac{V''(X)}{X^2} - \frac{V'(X)}{X^3}\right] \right. \\ &\qquad \left. + \frac{2\,(D-1)}{\omega_L(X)\,\omega_T(X)}\left[\frac{V'''(X)}{X} - \frac{2\,V''(X)}{X^2} + \frac{2\,V'(X)}{X^3}\right]\right\}. \end{aligned} \tag{2.128}$$

Due to the locality of the propagators, the integration merely yields a factor $\hbar\beta$ when inserting the propagator (2.102). So we finally obtain

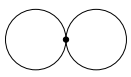

$$\begin{aligned} &= -\frac{\hbar^2\beta}{4\,M^2}\left\{\frac{V^{(4)}(X)}{\omega_L^2\,(X)} + \frac{(D^2-1)}{\omega_T^2\,(X)}\left[\frac{V''(X)}{X^2} - \frac{V'(X)}{X^3}\right]\right. \\ &\qquad \left. + \frac{2\,(D-1)}{\omega_L(X)\,\omega_T(X)}\left[\frac{V'''(X)}{X} - \frac{2\,V''(X)}{X^2} + \frac{2V'(X)}{X^3}\right]\right\}. \end{aligned} \tag{2.129}$$

Next we calculate the sunset diagram (2.113). As before, we split up the occurring propagators in accordance with (2.101), insert the third derivative (2.114) and use the relations (2.71), (2.73), and (2.125)–(2.127), which lead to

$$= \frac{1}{\hbar^2}\int_0^{\hbar\beta} d\tau_1 \int_0^{\hbar\beta} d\tau_2 \Bigg\{ G_L^3(\tau_1,\tau_2)\,[V'''(X)]^2 + 3\,(D-1)\,G_L(\tau_1,\tau_2)\,G_T^2(\tau_1,\tau_2)\left[\frac{V''(X)}{X} - \frac{V'(X)}{X^2}\right]^2 \Bigg\}. \tag{2.130}$$

After inserting the longitudinal and transversal propagators (2.102), both τ-integrations can be executed and we obtain the final result for the sunset diagram

$$= \frac{\hbar^2\,\beta}{12\,M^3\,\omega_L^4}\big[V'''(X)\big]^2 + \frac{3\,\hbar^2\,\beta\,(D-1)}{4\,M^3\,\omega_L\,\omega_T^2\,(2\,\omega_T+\omega_L)}\left[\frac{V''(X)}{X} - \frac{V'(X)}{X^2}\right]^2 . \tag{2.131}$$

The weights of the second-order diagrams have been calculated explicitly in (2.106). As it is worked out in Ref. [25], for instance, they can also be obtained from combinatorial considerations. The weights w of the diagrams with three- and four-vertices are given by

$$w = \frac{1}{2!^{S+D}\,3!^{T}\,4!^{F}\,P}\,. \tag{2.132}$$

Here, S, D, T, F denote the number of self, double, triple, fourfold connections, and P is the number of vertex permutations that leave the topology of the diagram unchanged. Finally, we sum up our results (2.87), (2.107), (2.129), and (2.131) and obtain the effective potential (2.59) up to the second loop order in the low-temperature limit $\beta\to\infty$:

$$\begin{aligned} V_{\text{eff}}(X) &= V(X) + \frac{\hbar\,\omega_L(X)}{2} + (D-1)\,\frac{\hbar\,\omega_T(X)}{2} + \frac{\hbar^2}{32}\Bigg\{ \frac{(D^2-1)}{\omega_T^2}\left[\frac{V''(X)}{X^2} - \frac{V'(X)}{X^3}\right] \\ &\quad + \frac{1}{\omega_L^2(X)}\,V^{(4)}(X) + \frac{2\,(D-1)}{\omega_L(X)\,\omega_T(X)}\left[\frac{V'''(X)}{X} - \frac{2\,V''(X)}{X^2} + \frac{2\,V'(X)}{X^3}\right]\Bigg\} \\ &\quad - \frac{\hbar^2}{48}\Bigg\{ \frac{3\,(D-1)}{2\,\omega_T(X)+\omega_L(X)}\,\frac{1}{\omega_L(X)\,\omega_T^2(X)}\left[\frac{V''(X)}{X} - \frac{V'(X)}{X^2}\right]^2 \\ &\quad + \frac{1}{3\,\omega_L^4(X)}\big[V'''(X)\big]^2 + \Bigg\} + \mathcal{O}(\hbar^3)\,. \end{aligned} \tag{2.133}$$

This result is in accordance with the one in Ref. [26, Ch. 5].

2.8. Effective Potential in Third Loop Order

If we carry on with the third order in the same way as we did in the second order, derivatives of fifth and sixth order have to be calculated. Moreover, diagrams contain up to ten projection operators when dividing the propagators and the derivatives into longitudinal and

transversal contributions. It would be extremely tedious to calculate all these contractions in order to obtain expressions analogously to (2.129) and (2.131). Therefore, we restrict our calculations to $D=1$ dimension, which corresponds to the contraction with all projection operators being longitudinal. This allows us to investigate the convergence of VPT with increasing order at least in $D=1$ dimension. As we will show later on in connection with the second loop order, VPT yields better results the higher dimensions we consider, which justifies restricting to the second order in higher dimensions.

In $D=1$ dimension, there exists only one X-dependent frequency $\omega(X)$ which corresponds to the longitudinal one in (2.81). Likewise, the propagator $G(\tau_i,\tau_j)$ has no longer a decomposition into longitudinal and transversal parts and reads

$$\lim_{T\to 0} G(\tau_1,\tau_2) = \frac{\hbar}{2M\omega(X)}\, e^{-\omega(X)|\tau_1-\tau_2|}. \tag{2.134}$$

The third loop order consists of eight Feynman diagrams which are evaluated along similar lines as discussed in the previous section:

$$\begin{aligned} &= \frac{1}{\hbar^2}\left[V^{(4)}(X)\right]^2 \int_0^{\hbar\beta} d\tau_1 \int_0^{\hbar\beta} d\tau_2\, G^4(\tau_1,\tau_2) \\ &= \hbar^3\beta \left[\frac{1}{2M\omega(X)}\right]^4 \frac{\left[V^{(4)}(X)\right]^2}{2\,\omega(X)}, \end{aligned} \tag{2.135}$$

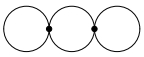

$$\begin{aligned} &= \frac{1}{\hbar^2}\left[V^{(4)}(X)\right]^2 \int_0^{\hbar\beta} d\tau_1 \int_0^{\hbar\beta} d\tau_2\, G(\tau_1,\tau_1)\, G(\tau_2,\tau_2)\, G^2(\tau_1,\tau_2) \\ &= \hbar^3\beta \left[\frac{1}{2M\omega(X)}\right]^4 \frac{\left[V^{(4)}(X)\right]^2}{\omega(X)}, \end{aligned} \tag{2.136}$$

$$\begin{aligned} &= -\frac{1}{\hbar^3}V^{(4)}(X)\left[V^{(3)}(X)\right]^2 \int_0^{\hbar\beta} d\tau_1 \int_0^{\hbar\beta} d\tau_2 \int_0^{\hbar\beta} d\tau_3\, G^2(\tau_1,\tau_2)\, G^2(\tau_1,\tau_3)\, G(\tau_2,\tau_2) \\ &= -\hbar^3\beta \left[\frac{1}{2M\omega(X)}\right]^5 \frac{5\,V^{(4)}(X)\left[V^{(3)}(X)\right]^2}{9\,\omega^2(X)}, \end{aligned} \tag{2.137}$$

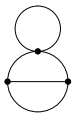

$$\begin{aligned} &= -\frac{1}{\hbar^3}V^{(4)}(X)\left[V^{(3)}(X)\right]^2 \int_0^{\hbar\beta} d\tau_1 \int_0^{\hbar\beta} d\tau_2 \int_0^{\hbar\beta} d\tau_3\, G(\tau_1,\tau_1)\, G(\tau_1,\tau_2)\, G(\tau_1,\tau_3)\, G^2(\tau_2,\tau_2) \\ &= -\hbar^3\beta \left[\frac{1}{2M\omega(X)}\right]^5 \frac{8\,V^{(4)}(X)\left[V^{(3)}(X)\right]^2}{9\,\omega^2(X)}, \end{aligned} \tag{2.138}$$

$$\begin{aligned} &= \frac{1}{\hbar^4}\left[V^{(3)}(X)\right]^4 \int_0^{\hbar\beta} d\tau_1 \int_0^{\hbar\beta} d\tau_2 \int_0^{\hbar\beta} d\tau_3 \int_0^{\hbar\beta} d\tau_4 \\ &\quad \times G(\tau_1,\tau_2)\, G(\tau_1,\tau_3)\, G(\tau_1,\tau_4)\, G(\tau_2,\tau_3)\, G(\tau_2,\tau_4)\, G(\tau_3,\tau_4) \\ &= \hbar^3\beta \left[\frac{1}{2M\omega(X)}\right]^6 \frac{2\left[V^{(3)}(X)\right]^4}{3\,\omega^3(X)}, \end{aligned} \tag{2.139}$$

$$= \frac{1}{\hbar^4}\left[V^{(3)}(X)\right]^4 \int_0^{\hbar\beta} d\tau_1 \int_0^{\hbar\beta} d\tau_2 \int_0^{\hbar\beta} d\tau_3 \int_0^{\hbar\beta} d\tau_4\, G^2(\tau_1,\tau_2)\, G^2(\tau_3,\tau_4)\, G(\tau_1,\tau_4)\, G(\tau_2,\tau_3)$$
$$= \hbar^3\beta \left[\frac{1}{2M\omega(X)}\right]^6 \frac{22\left[V^{(3)}(X)\right]^4}{27\,\omega^3(X)}\,, \tag{2.140}$$

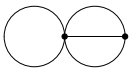

$$= \frac{1}{\hbar^2} V^{(3)}(X) V^{(5)}(X) \int_0^{\hbar\beta} d\tau_1 \int_0^{\hbar\beta} d\tau_2\, G(\tau_1,\tau_1)\, G^3(\tau_1,\tau_2)$$
$$= \hbar^3\beta \left[\frac{1}{2M\omega(X)}\right]^4 \frac{2\,V^{(3)}(X)V^{(5)}(X)}{3\,\omega(X)}\,, \tag{2.141}$$

$$= -\frac{1}{\hbar^3}\, V^{(6)}(X) \int_0^{\hbar\beta} d\tau\, G^2(\tau,\tau)$$
$$= -\hbar^3\beta\, \frac{V^{(6)}(X)}{\left[2M\omega(X)\right]^3}\,. \tag{2.142}$$

The respective weights of these Feynman diagrams follow from (2.132). Adding up all third-order diagrams (2.135)–(2.142) to the second order (2.133) for $D=1$, we obtain the effective potential up to the third order in $\hbar$:

$$\begin{aligned}\lim_{\beta\to\infty} V_{\rm eff}(X) \;=\; & V(X) + \frac{\hbar\omega(X)}{2} + \frac{\hbar^2}{32\,M^2\omega^2(X)}\, V^{(4)}(X) - \frac{\hbar^2}{144\,M^3\omega^4(X)}\left[V^{(3)}(X)\right]^2 \\ & - \frac{17\hbar^3}{13824\,M^6\omega^9(X)}\left[V^{(3)}(X)\right]^4 + \frac{13\hbar^3}{2304\,M^5\omega^7(X)}\, V^{(4)}(X)\left[V^{(3)}(X)\right]^2 \\ & - \frac{7\hbar^3}{1536\,M^4\omega^5(X)}\left[V^{(4)}(X)\right]^2 - \frac{\hbar^3}{288\,M^4\omega^5(X)}\, V^{(3)}(X)\, V^{(5)}(X) \\ & + \frac{\hbar^3}{64\,M^3\omega^3(X)}\, V^{(6)}(X) + \mathcal{O}(\hbar^4)\,. \end{aligned} \tag{2.143}$$

If we specify on a quartic potentials like the double-well, the last two diagrams (2.141) and (2.142) do not contribute to the effective potential due to the vanishing fifth and sixth derivative and our result coincides with Ref. [26, Ch. 2].

3. Variational Perturbation Theory in Quantum Mechanics

In this chapter, we apply variational perturbation theory (VPT) to the effective potential that we derived in the previous chapter. We specialize it both to the double-well, i.e., $D=1$ dimension, and the mexican hat in $D=2$ dimensions. Since we have taken the low-temperature limit in our calculations, we consider the case of quantum mechanics. After a short overview concerning the double-well potential, we give an introduction to VPT. Afterwards, we start with $D=1$ dimension and investigate the convergence of VPT with regard to the loop order. Then, we proceed to $D=2$ dimensions where a second variational parameter is introduced. Finally, we consider the large-D limit.

3.1. Anharmonic Oscillator and Double-Well Potential

In this section, we concentrate on the mexican-hat potential in D dimensions in quantum mechanics, which reads in analogy to (1.1)

$$V(\mathbf{x}) = \frac{M}{2}\,\omega^2\mathbf{x}^2 + \frac{1}{4}\,g\,(\mathbf{x}^2)^2 + \frac{1}{4g}\,, \qquad \omega^2 < 0\,, \tag{3.1}$$

where ω denotes the frequency, M the mass of the particle, and the coupling constant g determines the strength of anharmonicity. We have chosen an additional constant $1/4g$ in order to set the potential' s minimum to zero as it is shown in Figure 3.1a for different values of the coupling constant. In the case of the anharmonic oscillator

$$V(\mathbf{x}) = \frac{M}{2}\,\omega^2\,\mathbf{x}^2 + \frac{1}{4}\,g\,(\mathbf{x}^2)^2\,, \qquad \omega^2 > 0\,, \tag{3.2}$$

it is not necessary to add a constant to the potential. Due to the positive frequency square ω^2, the minimum is equal to zero, see Figure 3.1b.

For large coupling constants g, the mexican-hat potential has the shape of a quartic potential with no significant barrier in the middle. The smaller the coupling constant g, the stronger the shape of the mexican hat distinguishes from the anharmonic oscillator because of the increasing barrier in the middle. For very small coupling constants, the potential can be regarded to consist of two separated potentials. Particles can merely tunnel through the barrier. Raising g, the particles start sliding from one side to the other instead of tunneling.

From our calculations of the effective potential we obtain the ground-state energy in accordance with (2.30) and (2.32). This gives us the possibility to investigate the accuracy of our

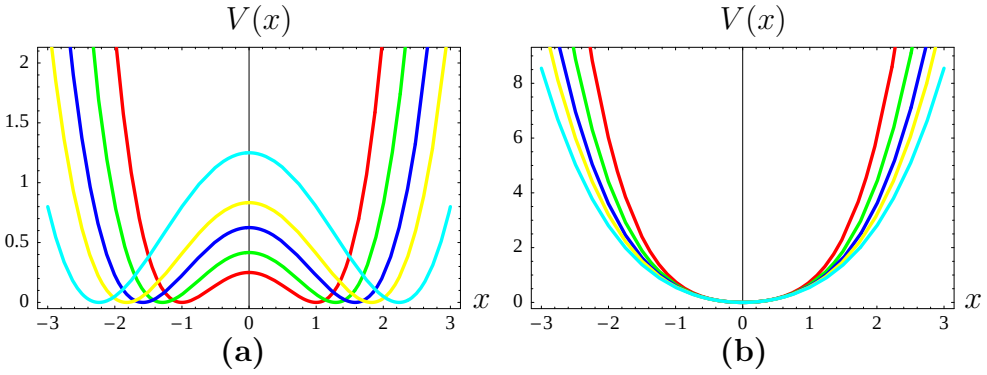

Figure 3.1.: **(a)** Double-well potential (3.1) for $M = 1$, $\omega^2 = -1$, and coupling constants $g = 1.0$ (red), $g = 0.6$ (green), $g = 0.4$ (blue), $g = 0.3$ (yellow), and $g = 0.2$ (light blue). The smaller the coupling constant, the more distinctive the barrier in the middle. **(b)**: Anharmonic oscillator (3.2) for $M=1$, $\omega^2=1$ and the same coupling constants as in (a).

approximations by comparing these results with those calculated numerically with the help of the shooting method [26, App. C]. This method consists of the numerical integration of the Schrödinger equation that reads in one dimension

$$\left[-\frac{\hbar^2}{2M}\frac{d^2}{dx^2} + V(x)\right]\psi(x) = E\,\psi(x)\,. \tag{3.3}$$

The results for the ground-state energy of the double-well potential for different values of g can be found in Table A.1. In arbitrary dimension D, the Schrödinger equation for a rotationally symmetric potential reads

$$\left[-\frac{\hbar^2}{2M}\left(\frac{d^2}{dx^2} + \frac{D-1}{x}\frac{d}{dx}\right) + V(x)\right]\psi(x) = E\,\psi(x) \tag{3.4}$$

with the modulus $x = |\mathbf{x}|$. Again, we apply the shooting method to obtain the ground-state energies and choose $D = 2, 3, 4, 5, 10$ dimensions as it is shown in the Tables A.5–A.8.

3.2. Variational Perturbation Theory

Most physical systems are too complex and too difficult to be calculated analytically. Therefore, approximations are applied, e.g., perturbation series or loop expansions which we will concentrate on. These series can be truncated at a certain order. In the case of a suitable expansion, the first few terms should yield a satisfying approximation. Variational perturbation theory (VPT) is an additional method to increase the accuracy of these expansions in a given order. The basic principle is to introduce an artificial parameter that will be optimized afterwards. This principle resembles *Ritz method* which we therefore recall shortly. For details see Ref. [27, Ch. 18], for instance.

3.2.1. Ritz Method

Let $\hat{H}$ be the Hamiltonian of a system

$$\hat{H}|n\rangle \;=\; E_n|n\rangle\,, \tag{3.5}$$

whose eigenvalues E_n and orthonormal eigenstates $|n\rangle$ cannot be determined analytically. We have

$$\frac{\langle\psi|\hat{H}|\psi\rangle}{\parallel\psi\parallel^2} \geq E_0\,, \tag{3.6}$$

with E_0 being the ground-state energy and ψ being an arbitrary wave function. The evidence of (3.6) is supplied straightforwardly:

$$\begin{aligned}\langle\psi|\hat{H}|\psi\rangle &= \sum_n \langle\psi|n\rangle\langle n|\hat{H}|\psi\rangle = \sum_n E_n\langle\psi|n\rangle\langle n|\psi\rangle \\ &\geq E_0\sum_n\langle\psi|n\rangle\langle n|\psi\rangle = E_0\langle\psi|\psi\rangle.\end{aligned} \tag{3.7}$$

Here, we have applied the completeness $\sum_n |n\rangle\langle n| = 1$ of the eigenstates. With regard to (3.6), we determine the ground-state energy to be the infimum concerning all possible wave functions

$$E_0 = \inf_{\psi}\frac{\langle\psi|\hat{H}|\psi\rangle}{\parallel\psi\parallel^2}\,. \tag{3.8}$$

Note that if ψ is an eigenfunction of $\hat{H}$, the infimum becomes a minimum. We choose trial functions $\psi = \psi(\lambda_1, \lambda_2, ..., \lambda_N)$ containing one or more variational parameters $\lambda_1, \lambda_2, ..., \lambda_N$. Then, we calculate the corresponding energy as a function of these parameters

$$E(\lambda_1, \lambda_2, ..., \lambda_N) = \frac{\big\langle\psi(\lambda_1, \lambda_2, ..., \lambda_N)\big|\hat{H}\big|\psi(\lambda_1, \lambda_2, ..., \lambda_N)\big\rangle}{\parallel\psi(\lambda_1, \lambda_2, ..., \lambda_N)\parallel^2}\,. \tag{3.9}$$

The parameters are varied in such a way that $E(\lambda_1, \lambda_2, ..., \lambda_N)$ becomes minimal. As a result, we obtain an upper bound for the actual ground-state energy E_0

$$E_0 \leq \min_{\{\lambda_1,\lambda_2,...,\lambda_N\}} E(\lambda_1, \lambda_2, ..., \lambda_N)\,. \tag{3.10}$$

In the case of one parameter, we extremize (3.9) by setting its first derivative to zero

$$\left.\frac{dE(\lambda)}{d\lambda}\right|_{\lambda=\lambda^{(\mathrm{ex})}} = 0\,, \tag{3.11}$$

and obtain the approximation

$$E_0 \leq E\left(\lambda^{(\mathrm{ex})}\right). \tag{3.12}$$

Analogously, two parameters yield

$$E_0 \leq E\left(\lambda_1^{(\mathrm{ex})}, \lambda_2^{(\mathrm{ex})}\right) \tag{3.13}$$

with both conditions

$$\left.\frac{\partial E(\lambda_1, \lambda_2)}{\partial\lambda_1}\right|_{\lambda_1=\lambda_1^{(\mathrm{ex})}} = 0\,, \qquad \left.\frac{\partial E(\lambda_1, \lambda_2)}{\partial\lambda_2}\right|_{\lambda_2=\lambda_2^{(\mathrm{ex})}} = 0\,. \tag{3.14}$$

In many cases, satisfying results are obtained with only one parameter. A typical application is the helium atom [27, Ch. 18]: we take advantage of the fact that the wave functions and the energies of the hydrogen atom are well-known and that helium mainly differs from hydrogen in the nuclear charge Z. Qualitatively speaking, both systems resemble very much. For this reason, we take over the hydrogen's wave functions and the nuclear charge Z becomes the variational parameter which is optimized afterwards.

3.2.2. Basic Principles

With the aid of the helium example, we make out the basic idea of Ritz method and VPT: the unknown system that cannot be calculated analytically is regarded as a deviation from a qualitatively similar, analytically solvable one. The deviations are described by a variational parameter which is optimized subsequently in such a way that it describes the deviations as well as one possibly can.

Consider the anharmonic oscillator (3.2) as an example of VPT. Introducing an additional frequency Ω, we may rewrite (3.2) according to

$$V(\mathbf{x}) \;=\; \frac{M}{2}\,\Omega^2\,\mathbf{x}^2 + \frac{1}{4}\,g\,(\mathbf{x}^2)^2 \;+\; \frac{M}{2}\left(\omega^2-\Omega^2\right)\mathbf{x}^2\,. \tag{3.15}$$

This corresponds to the potential of a harmonic oscillator with frequency Ω plus a deviation. Writing (3.15) as

$$V(\mathbf{x}) = \frac{M}{2}\left[\Omega\sqrt{1+\hbar\,\frac{\omega^2-\Omega^2}{\hbar\,\Omega^2}}\;\right]^2\mathbf{x}^2 + \frac{1}{4}\,g\,(\mathbf{x}^2)^2\,, \tag{3.16}$$

we identify the transformation (3.15) with Kleinert's square-root substitution [1, Ch. 5]

$$\omega \to \Omega\sqrt{1+\hbar\,r}\,, \qquad r = \frac{\omega^2-\Omega^2}{\hbar\,\Omega^2}\,. \tag{3.17}$$

By varying the parameter Ω, the deviation from the exactly solvable harmonic oscillator is optimized. The square-root substitution (3.17) is the basic principle of VPT [1, Ch. 5]. It is traced back to the approach of R. Feynman and H. Kleinert in 1986 [28], which has been extended to a systematic and uniformly convergent variational perturbation expansion [29–32]. In particular, it is powerful method to transform divergent weak-coupling series into convergent strong-coupling ones. In this part, VPT is applied to the effective potential of the mexican hat (3.1). The loop expansion of the interaction part (2.107) is truncated at a certain order and we perform the square-root substitution (3.17), yielding

$$V_{\text{eff}}(X) \overset{(3.17)}{\to} V_{\text{eff}}(X,\Omega)\,. \tag{3.18}$$

Whereas in Ritz method, the parameter corresponds to a physical quantity, e.g., the effective nuclear charge of helium, the variational parameter in VPT is artificially introduced. By truncating the loop expansion at a certain order, we obtain an actual dependence of the

effective potential on the variational parameter. Therefore, we minimize its influence, i.e., the dependence of the effective potential on this parameter. This so-called *principle of minimal sensitivity* [33] gives rise to a minimization analogously to (3.11). By doing so, we obtain an approximation for the ground-state energy E_0 in the low-temperature limit $T \to 0$ when we insert the optimized frequency Ω into the effective potential and optimize it with respect to the background X. Thus, we have

$$E_0 \;=\; V_{\text{eff}}\left(X^{(\text{opt})}, \Omega^{(\text{opt})}\right) \tag{3.19}$$

with

$$\left.\frac{\partial\, V_{\text{eff}}(X,\Omega)}{\partial X}\right|_{X=X^{(\text{opt})}} = 0\,, \qquad \left.\frac{\partial\, V_{\text{eff}}(X,\Omega)}{\partial\, \Omega}\right|_{\Omega=\Omega^{(\text{opt})}} = 0\,. \tag{3.20}$$

In some cases, the first derivative with respect to the variational parameter has no zero or only for complex Ω, which is no physical solution. Then, we apply the second derivative and look for turning points instead of minima

$$\left.\frac{\partial^2\, V_{\text{eff}}(X,\Omega)}{\partial \Omega^2}\right|_{\Omega=\Omega^{(\text{opt})}} = 0\,. \tag{3.21}$$

By comparing these results with those obtained from the shooting method, we have a criterion on how fast the loop expansion (2.107) converges with the aid of VPT. To this end, we consider the second and third order of the loop expansion.

3.3. Variational Perturbation Theory in One Dimension

In Ref. [1, Ch. 5], VPT has already been applied to the effective potential of the double-well in quantum mechanics. These calculations have been restricted to the second loop order without the sunset term. It is an interesting question whether this simplification is justified or not, i.e., whether the sunset term increases the accuracy distinctively. Whereas in quantum mechanics or quantum statistics, the sunset term is easy enough to calculate, it will become much more difficult in statistical field theory. Our intention is to investigate the importance of the sunset term in quantum mechanics first. To this end, we apply VPT to both cases with and without sunset term and compare the accuracies with the help of the numerically calculated ground-state energies. These calculations are done at first in $D=1$ dimension. In a second step, we extend our calculations to $D=2$ dimensions where the theory is canonically extended to two variational parameters. This enables us to compare the results with one and two variational parameters, i.e., to examine the significance of a second parameter. Finally, we choose higher dimensions to check the convergence of VPT with increasing dimension.

Consider the double-well potential, i.e., the potential (3.1) in $D=1$ dimension

$$V(x) \;=\; \frac{M}{2}\,\omega^2\, x^2 \;+\; \frac{1}{4}\, g\, x^4 \;+\; \frac{1}{4g}\,. \tag{3.22}$$

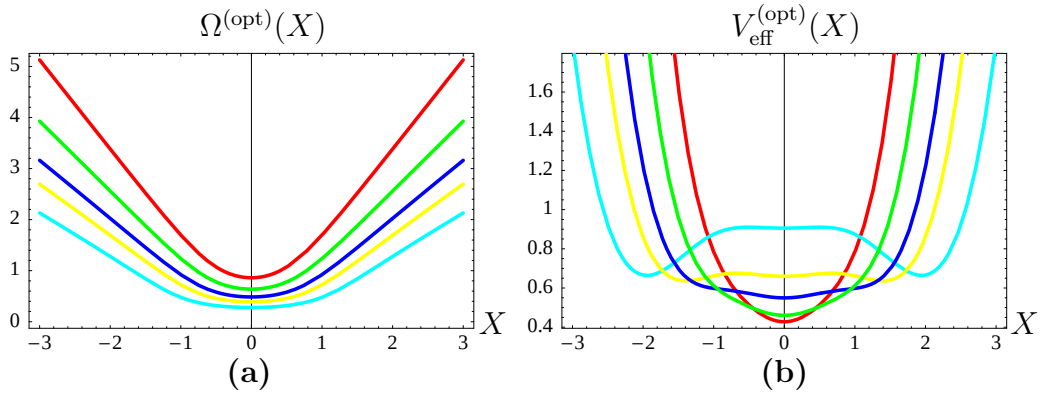

Figure 3.2.: Optimized variational parameter **(a)** and corresponding optimized effective potential **(b)** of the double-well (3.28) in second loop order without sunset ($D=1$). The different values of the coupling constant are denoted by $g=1.0$ (red), $g=0.6$ (green), $g=0.4$ (blue), $g=0.3$ (yellow), and $g=0.2$ (light blue).

Until the end of this chapter, we set the mass $M=1$. The corresponding effective potential in third loop order can be obtained from (2.143) when setting

$$\omega^2(X) \;=\; \omega^2 \,+\, 3\,g\,X^2\,, \tag{3.23}$$

as defined in (2.81) for the longitudinal frequency. The transversal one merely occurs in higher dimensions. It is important to distinguish between the frequency ω of the potential itself and the X-dependent frequency (3.23). For the double-well potential (3.22), the effective potential (2.143) reads

$$\begin{aligned} V_{\mathrm{eff}}(X) \;=\; & \frac{1}{2}\,\omega^2\,X^2 \,+\, \frac{1}{4}\,g\,X^4 \,+\, \frac{1}{4g} \,+\, \frac{\hbar}{2}\,\omega(X) \,+\, \frac{3\,\hbar^2\,g}{16\,\omega^2(X)} \,-\, \frac{\hbar^2\,g^2\,X^2}{4\,\omega^4(X)} \\ & -\,\frac{21\,\hbar^3\,g^2}{128\,\omega^5(X)} \,+\, \frac{39\,\hbar^3\,g^3\,X^2}{32\,\omega^7(X)} \,-\, \frac{51\,\hbar^3\,g^4\,X^4}{32\,\omega^9(X)} \,+\, \mathcal{O}(\hbar^4)\,. \end{aligned} \tag{3.24}$$

In contrast to the usual application of VPT as exemplarily shown for the anharmonic oscillator, we apply the substitution (3.17) not to the frequency ω of the potential (3.22) but to the X-dependent frequency $\omega(X)$ which is obviously of crucial importance for the effective potential instead of the bare frequency. Thus, we have

$$\omega(X) \;\to\; \Omega\sqrt{1+\hbar\,r}\,, \qquad r \;=\; \frac{1}{\hbar}\frac{\omega^2(X)-\Omega^2}{\Omega^2}. \tag{3.25}$$

This substitution makes allowance for the fact that the minimum of the potential is located at $X\neq 0$. Analogously to perturbation expansions which have to be performed around the potential's minimum in order to guarantee stability, the shifted minimum has to be taken into account when applying VPT. We will later on give a more detailed explanation in connection with phase transitions in statistical field theory.

3.3.1. Second Loop Order Without Sunset

First of all, we consider the effective potential in second loop order without the sunset term. In accordance with (3.24), it reads

$$V_{\mathrm{eff}}(X) \;=\; \frac{1}{2}\,\omega^2\,X^2 \,+\, \frac{1}{4}\,g\,X^4 \,+\, \frac{1}{4g} \,+\, \frac{\hbar}{2}\,\omega(X) \,+\, \hbar^2\,\frac{3\,g}{16\,\omega^2(X)}\,. \tag{3.26}$$

Performing the substitution (3.25) and expanding the occurring square root up to the second order with respect to $\hbar$ yields the intermediate result

$$V_{\text{eff}}(X,\Omega) \;=\; \frac{1}{2}\,\omega^2\,X^2 \;+\; \frac{1}{4}\,g\,X^4 \;+\; \frac{1}{4g} \;+\; \frac{\hbar}{2}\,\Omega \;+\; \hbar^2\,\frac{\Omega\,r}{4} \;+\; \hbar^2\,\frac{3\,g}{16\,\Omega^2}\,. \tag{3.27}$$

After replacing r in accordance with (3.23) and (3.25), we obtain

$$V_{\text{eff}}(X,\Omega) \;=\; \frac{1}{2}\,\omega^2\,X^2 \;+\; \frac{1}{4}\,g\,X^4 \;+\; \frac{1}{4g} \;+\; \frac{\hbar}{4}\,\Omega \;+\; \frac{\hbar}{4}\,\frac{\omega^2+3gX^2}{\Omega} \;+\; \hbar^2\,\frac{3\,g}{16\,\Omega^2}\,. \tag{3.28}$$

Due to (3.23), the variational parameter Ω becomes X-dependent itself. In order to calculate the optimized effective potential, we take the first derivative of (3.28) with respect to Ω and set it to zero for a fixed X

$$\frac{\partial\,V_{\text{eff}}(X,\Omega)}{\partial\,\Omega} \;=\; \frac{\hbar}{4} \;-\; \hbar\,\frac{3gX^2+\omega^2}{4\,\Omega^2} \;-\; \frac{3\,g\,\hbar^2}{8\,\Omega^3} \;\stackrel{!}{=}\; 0\,. \tag{3.29}$$

This equation is solved numerically for different values of X and coupling constant g. The X-dependence of the optimized variational parameter $\Omega^{(\text{opt})}(X)$ is interpolated afterwards as it is shown in Figure 3.2a. Inserting $\Omega^{(\text{opt})}(X)$ into (3.28), we obtain the optimized effective potential $V_{\text{eff}}^{(\text{opt})}(X)$ in Figure 3.2b. Merely for coupling constants smaller than $g\approx 0.4$, it has its minimum at non-vanishing background. For large coupling constants, it has the shape of the anharmonic potential in Figure 3.1 b with a minimum at $X=0$. If not denoted otherwise, we always choose $\omega^2=-1$. Finally, we calculate the ground-state energy

$$E_0 \;=\; V_{\text{eff}}^{(\text{opt})}(X_0) \qquad \text{with} \qquad \left.\frac{d\,V_{\text{eff}}^{(\text{opt})}(X)}{dX}\right|_{X=X_0} = 0\,. \tag{3.30}$$

Our results are shown in the Tables A.1 and A.2 compared with those of the shooting method.

3.3.2. Second Loop Order With Sunset

Now we consider the full second order, i.e., including the sunset term. In accordance with (3.24), the corresponding effective potential reads

$$V_{\text{eff}}(X) \;=\; \frac{1}{2}\,\omega^2\,X^2 \;+\; \frac{1}{4}\,g\,X^4 \;+\; \frac{1}{4g} \;+\; \frac{\hbar}{2}\,\omega(X) \;+\; \hbar^2\,\frac{3\,g}{16\,\omega^2(X)} \;-\; \hbar^2\,\frac{g^2\,X^2}{4\,\omega^4(X)}\,. \tag{3.31}$$

Comparing (3.26) and (3.31), we see that the additional term goes with X^2. In other words: as long as the minimum of the effective potential can be found at $X=0$, i.e., for large coupling constants g, the second order with and without sunset term yield the same results concerning the ground-state energy.

After performing the square-root substitution (3.25) in (3.31), we obtain, analogously to the previous section, the effective potential as a function of the variational parameter

$$V_{\text{eff}}(X,\Omega) \;=\; \frac{1}{2}\,\omega^2\,X^2 + \frac{1}{4}\,g\,X^4 + \frac{1}{4g} + \frac{\hbar}{4}\,\Omega + \frac{\hbar}{4}\,\frac{\omega^2+3gX^2}{\Omega} + \hbar^2\,\frac{3\,g}{16\,\Omega^2} - \hbar^2\,\frac{g^2X^2}{4\,\Omega^4}\,. \tag{3.32}$$

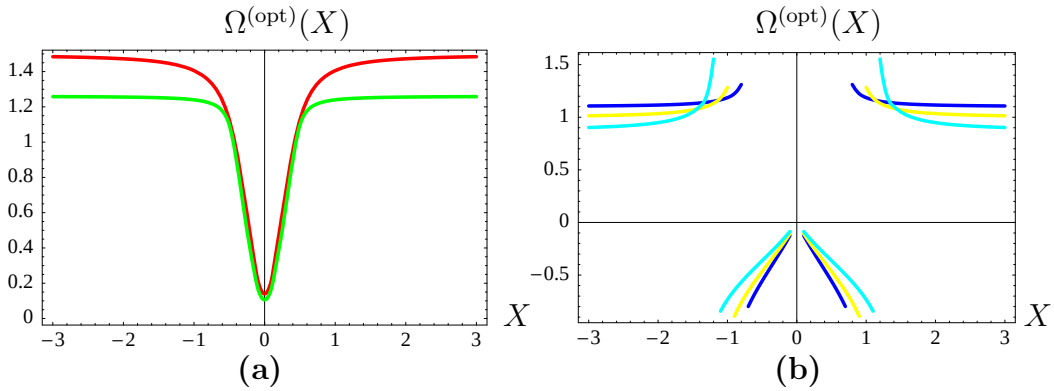

Figure 3.3.: Optimized variational parameter $\Omega^{(\mathrm{opt})}(X)$ of the effective potential (3.32) in second loop order ($D=1$). The run of the curve is continuous for larger coupling constants **(a)** $g=1.0$ (red), $g=0.6$ (green). Smaller values **(b)** $g=0.4$ (blue), $g=0.3$ (yellow), and $g=0.2$ (light blue) yield discontinuous parameters which moreover become negative.

Setting the first derivative to zero

$$\frac{\partial\, V_{\mathrm{eff}}(X,\Omega)}{\partial\,\Omega} = \frac{\hbar}{4} - \hbar\,\frac{3gX^2+\omega^2}{4\,\Omega^2} - \frac{3\,g\,\hbar^2}{8\,\Omega^3} + \frac{g^2\,\hbar^2\,X^2}{\Omega^5} \stackrel{!}{=} 0\,, \tag{3.33}$$

yields the desired optimized variational parameters. The run of the curves distinguishes crucially between larger, Figure 3.3 a, and smaller values, Figure 3.3 b, of the coupling strength g. In contrast to the calculations without sunset term, the frequencies can become negative and their X-dependence is not necessarily continuous. Consequently, the optimized effective potential in Figure 3.5 a is not that smooth any more than it has been without the sunset term in Figure 3.2 b. Analogously to (3.30), we calculate the ground-state energies in Table A.1. The effective potential's minimum is located at $X=0$ for $g \geq 1.3$. As expected, our results for the ground-state energy coincide within this range with those without sunset term.

3.3.3. Third Loop Order

Finally, we consider all terms of the effective potential (3.24) up to the third order with respect to $\hbar$. The square-root substitution (3.25) yields together with (3.23)

$$\begin{aligned} V_{\mathrm{eff}}(X,\Omega) \;=\; & \frac{1}{2}\,\omega^2\,X^2 + \frac{1}{4}\,g\,X^4 + \frac{1}{4g} + \frac{3\,\hbar\,\Omega}{16} + \frac{3\,\hbar\,\left(\omega^2+3gX^2\right)}{8\,\Omega} - \frac{\hbar\,(\omega^2+3gX^2)^2}{16\,\Omega^3} \\ & + \frac{3\,\hbar^2\,g}{8\,\Omega^2} - \frac{3\,\hbar^2\,\left(7g^2X^2+g\omega^2\right)}{16\,\Omega^4} - \frac{21\,\hbar^3\,g^2}{128\,\Omega^5} + \frac{\hbar^2\,g^2\,X^2\,(3gX^2+\omega^2)}{2\,\Omega^6} \\ & + \frac{39\,\hbar^3\,g^3\,X^2}{32\,\Omega^7} - \frac{51\,\hbar^3\,g^4\,X^4}{32\,\Omega^9}\,. \end{aligned} \tag{3.34}$$

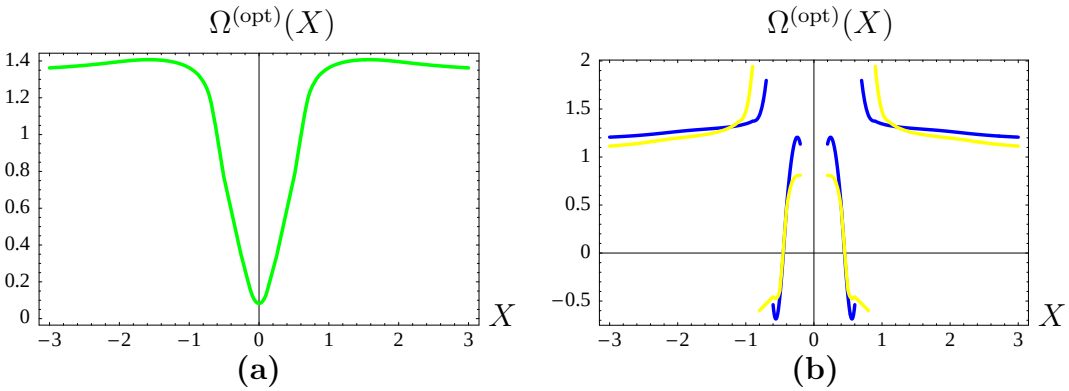

Figure 3.4.: Optimized variational parameter $\Omega^{(\mathrm{opt})}(X)$ of the effective potential (3.34) in third loop order ($D=1$). Similarly to Figure 3.3, the run of the curve is continuous **(a)** for larger coupling constants $g=0.6$ (green) and discontinuous **(b)** for smaller values $g=0.4$ (blue) and $g=0.3$ (yellow).

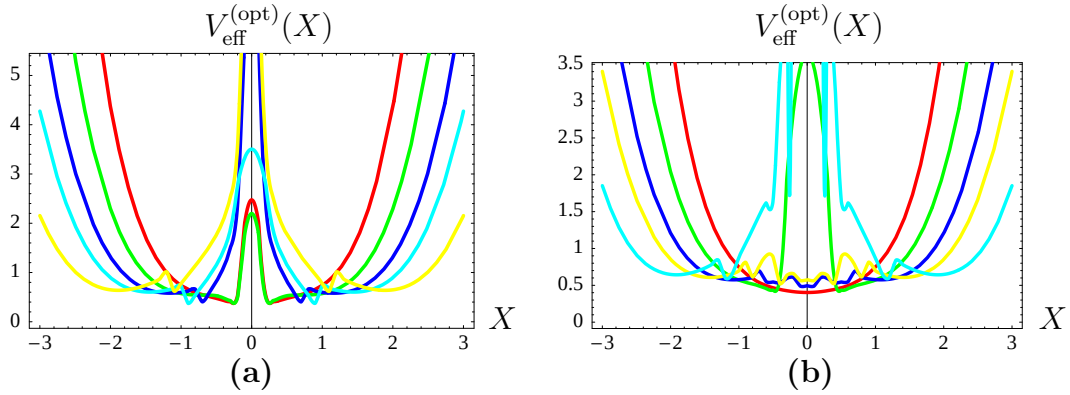

Figure 3.5.: Optimized effective potential (3.32) and (3.34) in second **(a)** and third loop order **(b)**, respectively ($D=1$). The different values of the coupling constants are indicated by $g=1.0$ (red), $g=0.6$ (green), $g=0.4$ (blue), $g=0.3$ (yellow), and $g=0.2$ (light blue).

Since the first derivative yields no real values for Ω, we choose the second derivative when optimizing $V_{\mathrm{eff}}(X,\Omega)$ with respect to Ω

$$\begin{aligned}\frac{\partial^2 V_{\mathrm{eff}}(X,\Omega)}{\partial\,\Omega^2} \;=\; & \frac{3\,\hbar\,(3gX^2+\omega^2)}{4\,\Omega^3}+\frac{9\,g\,\hbar^2}{4\,\Omega^4}-\frac{3\,\hbar\,(3gX^2+\omega^2)^2}{4\,\Omega^5}\\ & -\frac{15\,g\,\hbar^2\,(7gX^2+\omega^2)}{4\,\Omega^6}-\frac{315g^2\hbar^3}{64\,\Omega^7}+\frac{21\,g^2\hbar^2X^2(3gX^2+\omega^2)}{\Omega^8}\\ & +\frac{273\,g^3\hbar^3X^2}{4\,\Omega^9}-\frac{2295\,g^4\hbar^3X^4}{16\,\Omega^{11}}\stackrel{!}{=}0\,. \end{aligned} \tag{3.35}$$

Similar to the previous section, the shape of the X-dependent optimized parameter $\Omega^{(\mathrm{opt})}(X)$ varies with the coupling constant in so far that it becomes discontinuous for small g. Three examples are given in Figure 3.4. The optimized effective potential resembles the full second order just as much as the frequencies do, see Figure 3.5 b. The approximations for the ground-state energies are listed in Table A.3 .

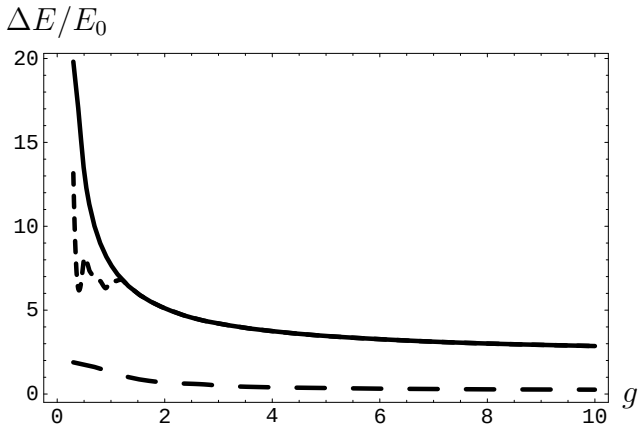

Figure 3.6.: Deviations in per cent of the VPT ground-state energies from the numerically calculated ones as a function of the coupling constant g ($D=1$). The solid line denotes the second order without sunset, the long-dashed line corresponds to the third order. As far as the results with sunset differ from those without, they are indicated by the short-dashed curve.

3.3.4. Convergence with Increasing Loop Order

Now we consider the convergence of VPT, i.e., the accuracy with increasing order of $\hbar$. To this end, we compare the deviations of our approximations in second order with and without sunset term and in third order from the numerical results that are listed in the Tables A.1–A.3. Figure 3.6 shows the deviations as a function of the coupling constant g. The approximation becomes the better the larger the coupling constant is. This is not surprising since in the strong-coupling limit $g\to\infty$, the double-well passes into the anharmonic potential which is conspicuously more incomplex due to the missing barrier in the middle. The sunset term increases the accuracy merely slightly and additionally just for small coupling constants $g\leq 1.3$ where the effective potential's minimum passes over to $X\neq 0$. For larger values of the coupling constant, the minimum is located at $X=0$, which annihilates the influence of the sunset term $\sim X^2$, see Eq. (3.31). This result shows that the sunset term is of particular importance for potentials with minima at $X\neq 0$, i.e., potentials which are not convex: the more this characteristic is formed (small g), the more the influence of the sunset increases. By contrast, we have the anharmonic potential, for instance, which has its minimum at $X=0$. In this case, we can neglect the sunset without losing accuracy.

Taking the third loop order into account, however, increases the accuracy crucially. This is in accordance with the fact that VPT converges exponentially, as it is shown in Ref. [6, Ch. 19]. Furthermore, it is remarkable that even in the third order, the approximations become abruptly seriously worse at about $g=0.4$. This phenomenon has already been observed in Ref. [1, Ch. 5] and can be explained as follows: for very small coupling constants, the potential can be regarded to consist of two separated potentials, see Figure 3.1. Particles can merely tunnel through the barrier in the middle. For large coupling constants, the double-well potential has the shape of a quartic potential with no significant barrier in the middle. At about $g\approx 0.4$, particles start sliding from one side to the other. This modification is

directly reflected in the VPT results. If we wish to obtain satisfying results in such regions, it is obviously necessary to go to higher orders.

3.4. Variational Perturbation Theory in Two Dimensions

In the previous section, we have investigated the accuracy of VPT with respect to the loop order. As expected, the approximations improve when taking more terms of the loop expansion (2.107) into account. But there exist still another way to increase the accuracy that has already been mentioned in conjunction with Ritz method: instead of one variational parameter we choose two parameters, which is canonically possible for dimensions $D \geq 2$ because of the arising longitudinal and transversal X-dependent frequencies (2.81). Now we perform the square-root substitution (3.25) twice

$$V_{\text{eff}}(X) \overset{(3.25)}{\rightarrow} V_{\text{eff}}(X, \Omega_L, \Omega_T)\,, \tag{3.36}$$

and optimize with respect to both variational parameters and X

$$\left.\frac{\partial\, V_{\text{eff}}(X, \Omega_L, \Omega_T)}{\partial\, \Omega_L}\right|_{\Omega_L = \Omega_L^{(\text{opt})}} = 0\,, \tag{3.37}$$

$$\left.\frac{\partial\, V_{\text{eff}}(X, \Omega_L, \Omega_T)}{\partial\, \Omega_T}\right|_{\Omega_T = \Omega_T^{(\text{opt})}} = 0\,, \tag{3.38}$$

$$\left.\frac{\partial\, V_{\text{eff}}(X, \Omega_L, \Omega_T)}{\partial\, X}\right|_{X = X_0} = 0\,. \tag{3.39}$$

Thus, we can compare the accuracy of the approximations with one and two parameters in second order.

Consider the mexican-hat potential (3.1) in $D = 2$ dimensions. Then, the X-dependent frequencies (2.81) read

$$\omega_L^2(X) = \omega^2 + 3\,g\,X^2\,, \qquad \omega_T^2(X) \,=\, \omega^2 + g\,X^2\,. \tag{3.40}$$

The corresponding effective potential in full second loop order follows from (2.133), yielding

$$\begin{aligned} V_{\text{eff}}(X) \;=\; & \frac{1}{2}\,\omega^2\,X^2 + \frac{1}{4}\,g\,X^4 + \frac{1}{4g} + \frac{\hbar}{2}\Big[\omega_L(X) + \omega_T(X)\Big] + \hbar^2\Bigg\{\frac{3\,g}{16\,\omega_L^2(X)} + \frac{3\,g}{16\,\omega_T^2(X)} \\ & + \frac{g}{8\,\omega_L(X)\,\omega_T(X)} - \frac{g^2X^2}{4\,\omega_L^4(X)} - \frac{g^2X^2}{4\,\omega_L(X)\,\omega_T^2(X)\big[2\omega_L(X) + \omega_T(X)\big]}\Bigg\}\,. \end{aligned} \tag{3.41}$$

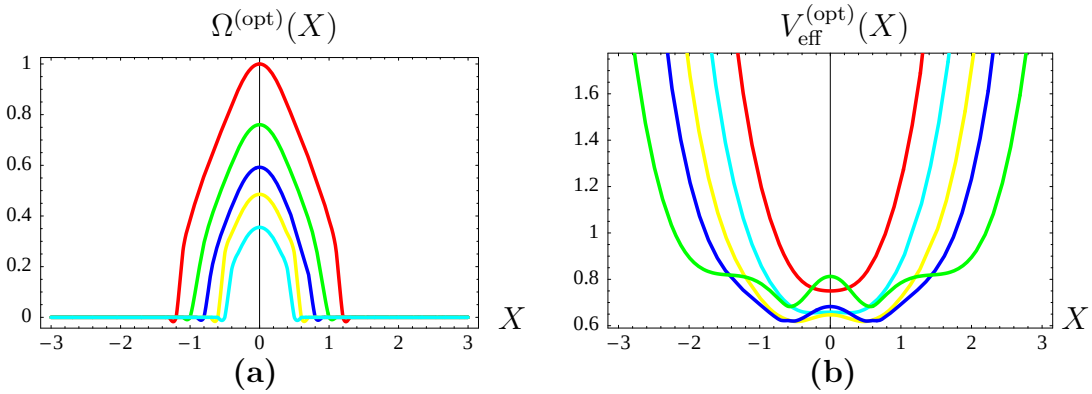

Figure 3.7.: Optimized variational parameter **(a)** of the effective potential (3.41) and the thereby optimized effective potential **(b)** ($D=2$). The different curves correspond to the coupling constants $g=1.0$ (red), $g=0.6$ (green), $g=0.4$ (blue), $g=0.3$ (yellow), and $g=0.2$ (light blue).

3.4.1. One Variational Parameter

Before calculating with two variational parameters, we insert a section with only one parameter in $D=2$ dimensions in order to investigate the significance of an additional parameter afterwards. To this end, we apply the square-root substitution (3.17) to the potential's frequency ω and not, as announced before, to the X-dependent longitudinal and transversal frequencies (3.40), which would canonically lead to two variational parameters. In this section, we consider the second loop order with the sunset term. The X-dependence of the resulting optimized parameter is shown in Figure 3.7 a. It is interesting to see that the frequency is non-vanishing just in a surrounding of $X=0$. The smaller the coupling strength g, the smaller this area is. This matter of fact shows that it is, indeed, reasonable to apply the square-root substitution to the X-dependent frequencies as done in the previous section, if we consider a potential with minima at $X\neq 0$. Otherwise, the variational parameter has no influence on the effective potential, which makes VPT useless and redundant. As a consequence, the optimized effective potential in Figure 3.7 b shows a very smooth course for vanishing values of $\Omega^{(\mathrm{opt})}(X)$. The barrier of the potential itself in the middle is again only reflected for small coupling constants. After determining the effective potential's minimum, we obtain the ground-state energies in Table A.4 for some values of g. For about $g\geq 0.8$, it turns out that there is no difference in the ground-state energies for one or two variational parameters, since the minimum lies at $X=0$ where both frequencies are equal.

3.4.2. Two Variational Parameters

Now we proceed with two variational parameters, applying (3.17) to both longitudinal and transversal frequencies (3.40):

$$\omega_L(X)\to\Omega_L\sqrt{1+\hbar r_L}\,,\qquad r_L=\frac{\omega_L^2(X)-\Omega_L^2}{\hbar\,\Omega_L^2}\,, \tag{3.42}$$

$$\omega_T(X)\to\Omega_T\sqrt{1+\hbar r_T}\,,\qquad r_T=\frac{\omega_T^2(X)-\Omega_T^2}{\hbar\,\Omega_T^2}\,.$$

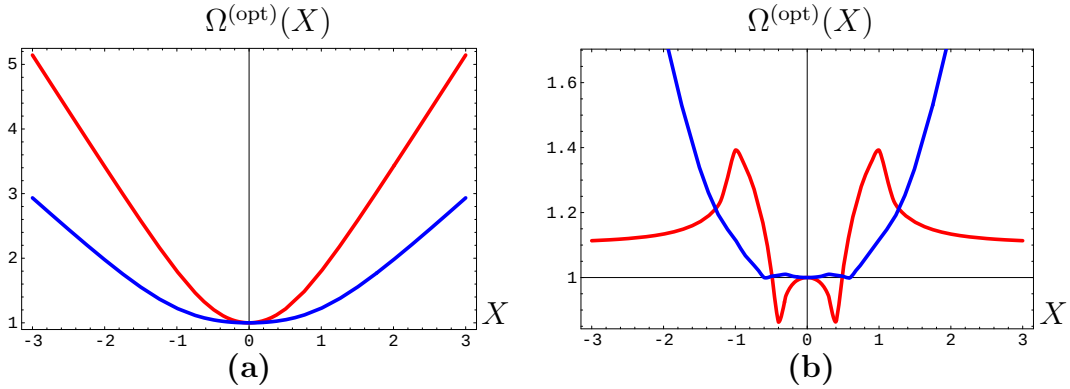

Figure 3.8.: The blue (red) curves show the optimized transversal (longitudinal) variational parameter of the effective potential (3.41) for $g = 1$ without **(a)** and with **(b)** the sunset ($D=2$).

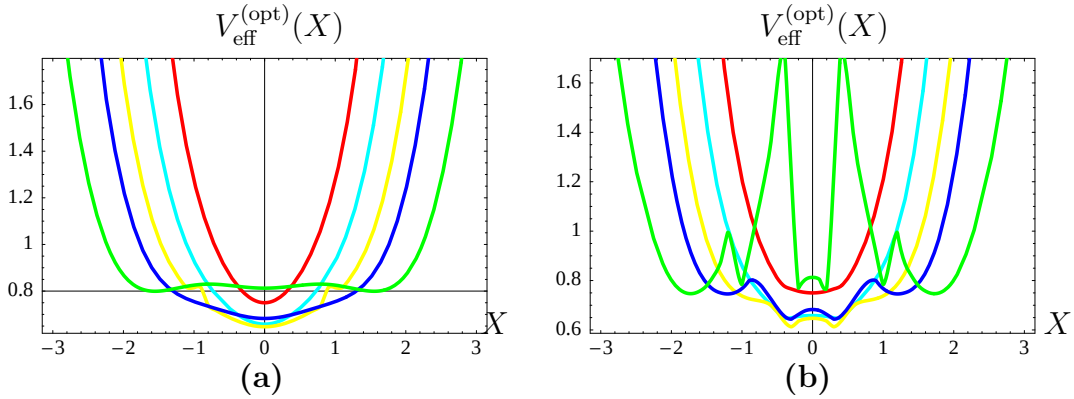

Figure 3.9.: Optimized effective potential (3.41) without **(a)** and with sunset **(b)** and with two variational parameters ($D = 2$) for coupling constants $g = 1.0$ (red), $g = 0.6$ (green), $g=0.4$ (blue), $g=0.3$ (yellow), and $g=0.2$ (light blue).

We obtain the optimized effective potential after calculating the conditions (3.37) and (3.38), which leads to the equations

$$\begin{aligned}\frac{\partial V_{\mathrm{eff}}(X,\Omega_L,\Omega_T)}{\partial \Omega_L} &= \frac{\hbar^2 g^2 X^2}{2\Omega_L^3\Omega_T^2} - \frac{\hbar^2(12g^2X^2+g\Omega_L^2)}{8\,\Omega_L^4\Omega_T} + \frac{\hbar^2 g^2 X^2}{\Omega_L^3(\Omega_L+2\Omega_T)^2} + \frac{3\hbar^2 g^2 X^2}{\Omega_L^4(\Omega_L+2\Omega_T)} \\ &\quad - \frac{\hbar\left(-8g^2X^2+3g\Omega_L^2+6gX^2\Omega_L^3+2\omega^2\Omega_L^3-2\Omega_L^5\right)}{8\,\Omega_L^5} \stackrel{!}{=} 0\,, \end{aligned} \tag{3.43}$$

$$\begin{aligned}\frac{\partial V_{\mathrm{eff}}(X,\Omega_L,\Omega_T)}{\partial \Omega_T} &= \frac{\hbar}{4} + \frac{\hbar^2(4g^2X^2-3g\Omega_L^2)}{8\,\Omega_L^2\,\Omega_T^3} - \frac{4\hbar^2g^2X^2+\hbar^2g\Omega_L^2+2\hbar gX^2\Omega_L^3+2\hbar\omega^2\Omega_L^3}{8\,\Omega_L^3\,\Omega_T^2} \\ &\quad + \frac{2\hbar^2g^2X^2}{\Omega_L^3\left(\Omega_L+2\Omega_T\right)^2} \stackrel{!}{=} 0. \end{aligned} \tag{3.44}$$

The optimized longitudinal and transversal frequencies coincide for $X = 0$, which is not surprising because of their definition (3.40). Whereas the transversal frequency shows a quadratic behavior both in second loop order with and without sunset term, the run of the longitudinal frequency distinguish crucially in both cases: taking the sunset term into account, this frequency is restricted and converges to a finite value as it is shown in Figure

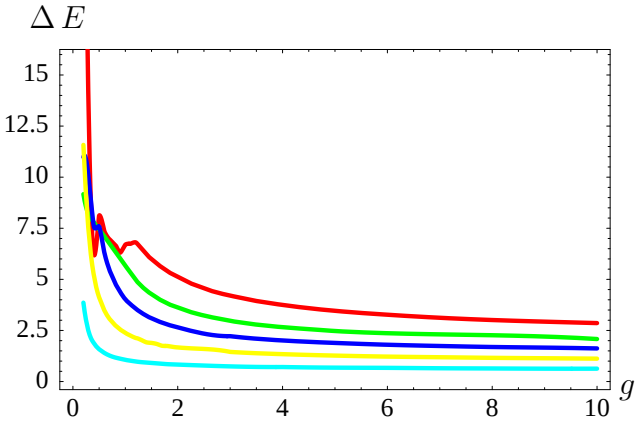

Figure 3.10.: Deviation in per cent of the numerical values from the ground-state energies calculated via VPT for the effective potential (2.133) in second loop order. The different colors denote the dimensions $D=1$ (red), $D=2$ (green), $D=3$ (blue), $D=5$ (yellow), and $D=10$ (light blue).

3.8 a and Figure 3.8 b respectively. The corresponding optimized effective potentials are illustrated in Figure 3.9, the ground-state energies in second loop order can be found in Table A.5. Comparing the Tables A.4 and A.5, we state that a second variational parameter does not increase the accuracy distinctively. For large coupling constants g where the effective potential has its minimum at $X=0$, there is no difference at all because both frequencies $\omega_L(X)$ and $\omega_T(X)$ coincide at $X=0$. Consequently, this holds also for the corresponding variational parameters. Thus, when calculating the free energy, the second parameter turns out to be redundant. Our investigations with regard to the sunset term or a second variational parameter show that it is important to introduce methods to increase the accuracy for potentials that have their minima at $X\neq 0$, i.e., potentials that have broken symmetry and are thus not convex. Potentials like the anharmonic one, however, can be treated without any additional methods.

3.5. Variational Perturbation Theory in Higher Dimensions

We are also interested in the convergence of VPT with respect to the dimension D. Starting from the effective potential (2.133) in second loop order for arbitrary dimension D, we calculate the ground-state energies for different values of D as a function of the coupling constant g by applying VPT with two variational parameters analogously to the procedure in $D=2$ dimensions. The results are given in the Tables A.5–A.8 and are graphically shown in Figure 3.10. In Ref. [34], it is demonstrated for the anharmonic oscillator, that the accuracy of VPT increases for higher dimensions. Figure 3.10 indicates that the same behavior also holds for the mexican hat. This phenomenon is in accordance with the large-N limit in statistical field theory where the $O(N)$-symmetric ϕ^4-theory becomes exactly solvable [35, Ch. 18]. We will come back to this point in Chapter 8.

Part II.

Statistical Field Theory

4. Effective Potential of One Real Field

As mentioned in the introduction, we are primarily interested in statistical field theory rather than in quantum statistics. The previous chapters were intended to prepare our calculations in statistical field theory which we now turn our attention to. In the following, we derive the effective potential analogously to our procedure in quantum statistics. Instead of D-dimensional space coordinates $\mathbf{x}$, we consider N real fields $\phi(\mathbf{x})$ as functions of space-time coordinates $\mathbf{x}$ in D dimensions. In this chapter, we focus on a potential $V\big(\phi(\mathbf{x})\big)$ for $N=1$ field in D spatial dimensions. As the field-theoretic results have to pass for $D=1$ into those derived in quantum statistics for the low-temperature limit, we can check our calculations by comparing them to the results of Chapter 2. Note, that we return now to the original notation m for the mass.

4.1. Background Method

We start deriving the effective potential in the same way as before in quantum statistics. The field theoretic analogue to the partition function (2.15) in quantum statistics reads

$$\mathcal{Z} \;=\; \int \mathcal{D}\phi \, e^{-\mathcal{A}[\phi]} \tag{4.1}$$

with the action

$$\mathcal{A}[\phi] \;=\; \int d^D x \, \left\{ \frac{1}{2} \left[\nabla \, \phi(\mathbf{x}) \right]^2 \;+\; V\big(\phi(\mathbf{x})\big) \right\} . \tag{4.2}$$

The background method now amounts to dividing the field $\phi(\mathbf{x})$ into a constant background Φ and fluctuations $\delta\phi(\mathbf{x})$ according to

$$\phi(\mathbf{x}) \;=\; \Phi \;+\; \delta\phi(\mathbf{x}) \, . \tag{4.3}$$

We insert the ansatz (4.3) into the potential $V\big(\phi(\mathbf{x})\big)$ and perform a functional Taylor expansion around the background Φ. For reasons of simplicity, we define the partial derivatives

$$\left. \frac{\partial^n V\big(\phi(\mathbf{x})\big)}{\partial \, \phi^n(\mathbf{x})} \right|_{\phi(\mathbf{x})=\Phi} \;=:\; V^{(n)}(\Phi) \, . \tag{4.4}$$

Thus, the Taylor expansion reads

$$\begin{aligned} V\big(\Phi + \delta\phi(\mathbf{x})\big) \;\;=\;\; & V(\Phi) + V'(\Phi) \, \delta\phi(\mathbf{x}) \;+\; \frac{1}{2} \, V''(\Phi) \, \delta\phi^2(\mathbf{x}) \;+\; \frac{1}{6} \, V'''(\Phi) \, \delta\phi^3(\mathbf{x}) \\ & + \frac{1}{24} \, V^{(4)}(\Phi) \, \delta\phi^4(\mathbf{x}) \;+\; \cdots \, . \end{aligned} \tag{4.5}$$

Now we insert the Taylor expansion (4.5) into the action (4.2), yielding

$$\begin{aligned}\mathcal{A}[\Phi+\delta\phi] &= \mathrm{v}\,V(\Phi) + \int d^Dx\Big\{\frac{1}{2}\,\delta\phi(\mathbf{x})\Big[-\Delta+V''(\Phi)\Big]\delta\phi(\mathbf{x}) \\ &\quad + \frac{1}{6}\,V'''(\Phi)\,\delta\phi^3(\mathbf{x}) + \frac{1}{24}\,V^{(4)}(\Phi)\,\delta\phi^4(\mathbf{x}) + \cdots\Big\} \\ &\equiv \mathcal{A}^{(\mathrm{cl})}(\Phi) + \mathcal{A}^{(\mathrm{fluc})}\big[\Phi+\delta\phi\big] \end{aligned} \tag{4.6}$$

with volume v. Analogously to quantum statistics, the term linear in $\delta\phi(\mathbf{x})$ vanishes within the background method. With regard to the classical and the fluctuation part of the action (4.6), we likewise decompose the partition function (4.1) into

$$\begin{aligned}\mathcal{Z}(\Phi) &= e^{-\mathcal{A}^{(\mathrm{cl})}(\Phi)}\int\mathcal{D}\delta\phi\; e^{-\mathcal{A}^{(\mathrm{fluc})}[\Phi+\delta\phi]} \\ &\equiv \mathcal{Z}^{(\mathrm{cl})}(\Phi)\,\mathcal{Z}^{(\mathrm{fluc})}(\Phi)\,. \end{aligned} \tag{4.7}$$

For the following calculations, it is useful to define

$$\tilde{\mathcal{A}}\big[\Phi+\delta\phi\big] := \int d^Dx\,\frac{1}{2}\,\delta\phi(\mathbf{x})\Big[-\Delta+V''(\Phi)\Big]\delta\phi(\mathbf{x})\,. \tag{4.8}$$

The fluctuation part of the partition function (4.7) is calculated by expanding the exponential function with terms of third and higher powers regarding the fluctuations. In accordance with (4.6), we obtain

$$\begin{aligned}\mathcal{Z}^{(\mathrm{fluc})}(\Phi) &= \int\mathcal{D}\delta\phi\; e^{-\tilde{\mathcal{A}}[\Phi+\delta\phi]}\Bigg[1 - \frac{V'''(\Phi)}{6}\int d^Dx\;\delta\phi^3(\mathbf{x}) \\ &\quad - \frac{V^{(4)}(\Phi)}{24}\int d^Dx\;\delta\phi^4(\mathbf{x}) + \frac{\big[V'''(\Phi)\big]^2}{72}\int d^Dx\int d^Dy\;\delta\phi^3(\mathbf{x})\,\delta\phi^3(\mathbf{y}) + \cdots\Bigg]. \end{aligned} \tag{4.9}$$

Now we introduce the expectation value

$$\langle\bullet\rangle_\Phi := \frac{1}{\mathcal{Z}^{(1)}(\Phi)}\int\mathcal{D}\delta\phi\;\bullet\;e^{-\tilde{\mathcal{A}}[\Phi+\delta\phi]} \tag{4.10}$$

with the first-order partition function

$$\mathcal{Z}^{(1)}(\Phi) := \int\mathcal{D}\delta\phi\;e^{-\tilde{\mathcal{A}}[\Phi+\delta\phi]}\,. \tag{4.11}$$

For symmetry reasons, expectation values with odd powers of the fluctuations vanish. Therefore, (4.9) reduces to

$$\begin{aligned}\mathcal{Z}^{(\mathrm{fluc})}(\Phi) &= \mathcal{Z}^{(1)}(\Phi)\Bigg[1 - \frac{V'''(\Phi)}{6}\int d^Dx\,\big\langle\delta\phi^3(\mathbf{x})\big\rangle_\Phi - \frac{V^{(4)}(\Phi)}{24}\int d^Dx\,\big\langle\delta\phi^4(\mathbf{x})\big\rangle_\Phi \\ &\quad + \frac{\big[V'''(\Phi)\big]^2}{72}\int d^Dx\int d^Dy\,\big\langle\delta\phi^3(\mathbf{x})\,\delta\phi^3(\mathbf{y})\big\rangle_\Phi + \cdots\Bigg]. \end{aligned} \tag{4.12}$$

The expectation value consisting of two fluctuations $\delta\phi(\mathbf{x})\,\delta\phi(\mathbf{y})$, for instance, is defined to be the propagator

$$G_\Phi(\mathbf{x},\mathbf{y}) \;=\; \big\langle \delta\phi(\mathbf{x})\,\delta\phi(\mathbf{y})\big\rangle_\Phi\,. \tag{4.13}$$

The effective potential follows immediately by expanding the logarithm $V_{\text{eff}}(\Phi)=-\ln\mathcal{Z}(\Phi)$. With regard to (4.6), (4.7), and (4.12), we obtain

$$\begin{aligned} V_{\text{eff}}(\Phi) \;&=\; \mathrm{v}\,V(\Phi) \,-\, \ln\mathcal{Z}^{(1)}(\Phi) \,+\, \frac{V^{(4)}(\Phi)}{24}\int d^Dx\,\big\langle\delta\phi^4(\mathbf{x})\big\rangle_\Phi \\ &\quad -\frac{\big[V'''(\Phi)\big]^2}{72}\int d^Dx\int d^Dy\,\big\langle\delta\phi^3(\mathbf{x})\,\delta\phi^3(\mathbf{y})\big\rangle_\Phi \,+\,\cdots \\ &\equiv\; \mathrm{v}\,V(\Phi) \,+\, V_{\text{eff}}^{(1)}(\Phi) \,+\, V_{\text{eff}}^{(\text{int})}(\Phi)\,. \end{aligned} \tag{4.14}$$

4.2. Effective Potential in First Loop Order

In the first place, we calculate the first-order term $\mathcal{Z}^{(1)}(\Phi)$ and $V_{\text{eff}}^{(1)}(\Phi)$, respectively. Defining the integral kernel

$$G_\Phi^{-1}(\mathbf{x},\mathbf{x}') \;:=\; \Big[-\Delta+V''(\Phi)\Big]\,\delta(\mathbf{x}-\mathbf{x}') \tag{4.15}$$

associated with the propagator (4.13), we write the first-order partition function (4.11) in accordance with (4.8) as

$$\mathcal{Z}^{(1)}(\Phi) \;=\; \int\mathcal{D}\delta\phi\,\exp\left\{-\int d^Dx\int d^Dx'\,\frac{1}{2}\,\delta\phi(\mathbf{x})\,G_\Phi^{-1}(\mathbf{x},\mathbf{x}')\,\delta\phi(\mathbf{x}')\right\}. \tag{4.16}$$

Similar to (2.65), the functional integral (4.16) can be regarded as a functional generalization of a Gaussian integral, resulting in

$$\mathcal{Z}^{(1)}(\Phi) \;=\; \frac{1}{\sqrt{\det G_\Phi^{-1}}} \;=\; \exp\left[-\frac{1}{2}\,\mathrm{Tr}\ln G_\Phi^{-1}\right] \tag{4.17}$$

and the first-order effective potential

$$V_{\text{eff}}^{(1)}(\Phi) \;=\; \frac{1}{2}\,\mathrm{Tr}\ln\Big[-\Delta+V''(\Phi)\Big]\,. \tag{4.18}$$

In terms of the momentum basis, (4.18) reads

$$V_{\text{eff}}^{(1)}\,(\Phi) \;=\; \frac{\mathrm{v}}{2}\int\frac{d^Dk}{(2\pi)^D}\,\ln\Big[\mathbf{k}^2+V''(\Phi)\Big]\,, \tag{4.19}$$

where the spacial integration merely leads to a volume factor v. Reminding Schwinger's proper time representation of the logarithm in (C.33), we continue

$$V_{\text{eff}}^{(1)}(\Phi) \;=\; \frac{\mathrm{v}}{2}\left(-\frac{\partial}{\partial x}\right)\left\{\frac{1}{\Gamma(x)}\int_0^\infty d\tau\;\tau^{x-1}\,e^{-\tau\,V''(\Phi)}\int\frac{d^Dk}{(2\pi)^D}\,e^{-\tau\,\mathbf{k}^2}\right\}\Bigg|_{x=0}. \tag{4.20}$$

The momentum integral corresponds to a Gaussian integral and the τ-integral can be evaluated with the aid of the Gamma function (C.1), so we obtain

$$V_{\text{eff}}^{(1)}(\Phi) \;=\; \frac{\mathrm{v}}{2\,(4\pi)^{D/2}} \left(-\frac{\partial}{\partial x}\right) \left\{ \frac{\Gamma\,(x-D/2)}{\Gamma(x)\,\big[V''(\Phi)\big]^{x-D/2}} \right\} \Bigg|_{x=0} . \tag{4.21}$$

Because of the poles of the Gamma function at negative integers, we have to treat even dimensions carefully when further calculating (4.21). Therefore, we start with assuming that D is odd. In this case, the only pole is caused by $\Gamma(x)$ in the denominator, so our first task is to evaluate $1/\Gamma(x)$ at $x=0$. To this end, we perform a Taylor expansion of $\Gamma(x)$ around $x=0$ with regard to (C.2),

$$\Gamma(x) \;=\; \frac{\Gamma\,(x+1)}{x} \;=\; \frac{1}{x} \,+\, \Gamma'(1) \,+\, \cdots\,, \tag{4.22}$$

and expand the reciprocal value, yielding

$$\frac{1}{\Gamma(x)} \;=\; \frac{x}{1 \,+\, x\,\Gamma'(1) \,+\cdots} \;=\; x \,-\, x^2\,\Gamma'(1) \,+\, \cdots\,. \tag{4.23}$$

Performing the derivative in (4.21) at $x=0$, all terms cancel apart from one:

$$\begin{aligned} V_{\text{eff}}^{(1)}(\Phi) \;&=\; -\,\frac{\mathrm{v}}{2\,(4\pi)^{D/2}}\, \frac{\Gamma\,(x-D/2\,)}{\big[V''(\Phi)\big]^{x-D/2}} \Bigg|_{x=0} \\ &=\; -\,\frac{\mathrm{v}}{2\,(4\pi)^{D/2}}\, \Gamma\!\left(\frac{D}{2}\right) \big[V''(\Phi)\big]^{D/2} . \end{aligned} \tag{4.24}$$

In $D=1$ dimension and for the potential (1.1) in $N=1$ field dimension, (4.24) reduces to

$$V_{\text{eff}}^{(1)}(\Phi) \;\overset{D=1}{=}\; \frac{\mathrm{v}}{2}\, M\,, \tag{4.25}$$

where the Φ-dependent mass M is just the second derivative $V''(\Phi)$ of (1.1)

$$M^2 \;:=\; m^2 + \frac{g}{2}\,\Phi^2\,. \tag{4.26}$$

Replacing $m^2 \to \omega^2$, $\Phi \to X$ and dividing by the volume v, (4.24) reproduces the former result (2.87) for $D=1$ dimension in quantum mechanics. For $D=3$, we obtain from (4.24)

$$V_{\text{eff}}^{(1)}(\Phi) \;\overset{D=3}{=}\; -\,\frac{\mathrm{v}}{12\pi}\, M^3\,. \tag{4.27}$$

Now let D be even, i.e., $D=2n$ and we start again from (4.21). The ratio of both Gamma functions can be written as

$$\frac{\Gamma\big(x-D/2\big)}{\Gamma(x)} \;=\; \frac{\Gamma\,(x-n)}{\Gamma(x)} \;=\; \frac{1}{(x-n)(x-n+1)\cdots(x-1)}\,. \tag{4.28}$$

Thus, (4.21) amounts to calculating

$$-\frac{\partial}{\partial x}\left\{\frac{1}{(x-n)(x-n+1)\cdots(x-1)}\left[V''(\Phi)\right]^{n-x}\right\}\Bigg|_{x=0} \tag{4.29}$$
$$=\frac{1}{(x-n)\cdots(x-1)}\Bigg|_{x=0}\left[V''(\Phi)\right]^{n}\ln V''(\Phi)\;-\;\left[V''(\Phi)\right]^{n}\;\frac{\partial}{\partial x}\left\{\frac{1}{(x-n)\cdots(x-1)}\right\}\Bigg|_{x=0}.$$

Consider the product

$$(x-n)\,(x-n+1)\,\cdots\,(x-1)\;=\;\sum_{k=0}^{n}b_k\,x^k\;:=\;f_n(x) \tag{4.30}$$

with

$$f_n(0)\;=\;(-1)^n\,n!\,. \tag{4.31}$$

Regarding (4.31), the first term in (4.29) yields straightforwardly

$$\frac{1}{(x-n)\cdots(x-1)}\Bigg|_{x=0}\left[V''(\Phi)\right]^{n}\ln V''(\Phi)\;=\;(-1)^n\,\frac{\left[V''(\Phi)\right]^{n}\ln V''(\Phi)}{n!}\,. \tag{4.32}$$

The derivative in the second term of (4.29) reads:

$$-\frac{\partial}{\partial x}\,\frac{1}{(x-n)\cdots(x-1)}\Bigg|_{x=0}\;=\;-\frac{\partial}{\partial x}\,\frac{1}{f_n(x)}\Bigg|_{x=0}\;=\;\frac{f_n'(x)}{f_n^2(x)}\Bigg|_{x=0}. \tag{4.33}$$

All coefficients b_k in (4.30) are functions of n: $b_k\equiv b_k(n)$. Taking the derivative $f_n'(x)$ at $x=0$, all terms cancel except for $b_1(n)=f_n'(0)$ on which we will therefore focus our attention. Defining $a_n:=b_1(n)$, one can show by induction the recursion formula

$$a_n\;=\;(-1)^{n+1}\Big[n\,|a_{n-1}|\;+\;(n-1)!\Big]\,,\qquad n\geq 2\,,\qquad\text{with}\quad a_1=1\,. \tag{4.34}$$

The first three coefficients are

$$a_2\;=\;-3\,,\qquad a_3\;=\;11\,,\qquad a_4\;=\;-50\,. \tag{4.35}$$

Eq. (4.34) enables us to perform the derivative (4.33). According to (4.31), we obtain

$$\frac{f_n'(x)}{f_n^2(x)}\Bigg|_{x=0}\;=\;\frac{a_n}{\left(n!\right)^2}\,. \tag{4.36}$$

Finally, we insert (4.32) and (4.36) into (4.21) and (4.29), which delivers the first loop order of the effective potential for even dimensions $D=2n$:

$$V_{\rm eff}^{(1)}(\Phi)\;=\;\frac{\left(-1\right)^n\,\mathrm{v}}{2\,n!\,(4\pi)^n}\left[V''(\Phi)\right]^{n}\left[\frac{a_n}{n!}\;-\;\ln V''(\Phi)\right]. \tag{4.37}$$

For $D=2$ dimensions, i.e., $n=1$, (4.37) becomes

$$V_{\rm eff}^{(1)}(\Phi)\;\stackrel{n=1}{=}\;-\frac{\mathrm{v}}{8\pi}\,V''(\Phi)\Big[1\;-\;\ln V''(\Phi)\Big]\,. \tag{4.38}$$

Both results (4.24) and (4.37) are connected by means of renormalization. In fact, they turn out to be equivalent. We will come back to this point in Section 5.4.

4.3. Effective Potential in Second Loop Order

Now we turn our attention to the interaction part of the effective potential (4.14). The expectation values are reduced to products of the propagator (4.13) by applying Wick contractions and we obtain

$$V_{\text{eff}}^{(\text{int})}(\Phi) \;=\; \frac{V^{(4)}(\Phi)}{8}\int d^D x\; G_\Phi^2(\mathbf{x},\mathbf{x}) \;-\; \frac{\big[V'''(\Phi)\big]^2}{12}\int d^D x \int d^D y\; G_\Phi^3(\mathbf{x},\mathbf{y}) \;+\cdots . \tag{4.39}$$

These first two terms can immediately be identified with those in (2.106) in quantum statistics. In fact, we find a direct analogy when we consider the corresponding Feynman rules:

(1) All vertices and their outgoing lines are denoted arbitrarily.

(2) A propagator $G_\Phi(\mathbf{x},\mathbf{y})$ corresponds to a line connecting vertices $\mathbf{x}$ and $\mathbf{y}$

$$\equiv\; G_\Phi(\mathbf{x},\mathbf{y})\,, \tag{4.40}$$

where the propagator is related to the integral kernel $G_\Phi^{-1}(\mathbf{x},\mathbf{y})$ according to

$$\int d^D x'\, G_\Phi^{-1}(\mathbf{x},\mathbf{x}')\, G_\Phi(\mathbf{x}',\mathbf{x}'') \;=\; \delta(\mathbf{x}-\mathbf{x}'')\,. \tag{4.41}$$

(3) n outgoing lines from a vertex $\mathbf{x}$ represent the integration

$$\equiv\; -V^{(n)}(\Phi)\int d^D x \tag{4.42}$$

over the propagators connected with vertex $\mathbf{x}$.

Now we specialize in the potential (1.1) for $N=1$ field dimension. Thus, we have $V''(\Phi)=M^2$ in accordance with (4.26). Comparing the interaction part (4.39) with the Feynman rules (4.40) and (4.42), we obtain the explicit expressions of the second-order diagrams:

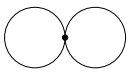

$$\equiv\; -\,g\int d^D x\; G_\Phi^2(\mathbf{x},\mathbf{x})\,, \tag{4.43}$$

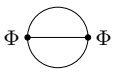

$$\equiv\; g^2\,\Phi^2\int d^D x\int d^D y\; G_\Phi^3(\mathbf{x},\mathbf{y})\,. \tag{4.44}$$

The diagrammatic representation of the second loop order $V_{\text{eff}}^{(2)}(\Phi)$ that includes the weights in (4.39) is the same as (2.111) in quantum statistics. It is much easier to evaluate Feynman diagrams in the momentum space. Due to translational invariance, the propagator $G_\Phi(\mathbf{x},\mathbf{y})$ has a Fourier representation

$$G_\Phi(\mathbf{x},\mathbf{y}) \;=\; \int \frac{d^D k}{(2\pi)^D}\; e^{\imath\,\mathbf{k}\,(\mathbf{x}-\mathbf{y})}\; G_\Phi(\mathbf{k})\,. \tag{4.45}$$

In the same way, the integral kernel (4.15) can be written as

$$G_\Phi^{-1}(\mathbf{x},\mathbf{y}) \;=\; \int \frac{d^D k}{(2\pi)^D}\, e^{\imath\,\mathbf{k}\,(\mathbf{x}-\mathbf{y})}\; G_\Phi^{-1}(\mathbf{k})\,, \qquad G_\Phi^{-1}(\mathbf{k}) \;=\; \mathbf{k}^2 \;+\; M^2\,. \tag{4.46}$$

Moreover, we apply the Fourier transform of the δ-function

$$\delta(\mathbf{x}-\mathbf{y}) \;=\; \int \frac{d^D k}{(2\pi)^D}\, e^{\imath\,\mathbf{k}\,(\mathbf{x}-\mathbf{y})}\,. \tag{4.47}$$

In order to calculate the propagator in momentum space, we insert (4.45)–(4.47) into (4.41), yielding

$$G_\Phi(\mathbf{k}) \;=\; \frac{1}{G_\Phi^{-1}(\mathbf{k})} \;=\; \frac{1}{\mathbf{k}^2+M^2}\,. \tag{4.48}$$

The direct diagram (4.43) follows from (C.30) without any problems since all propagators are local and the spatial integration only gives a volume factor v:

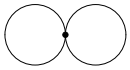

$$\begin{aligned} &\equiv && -\,g\int d^D x\left[\int \frac{d^D k}{(2\pi)^D}\, G_\Phi(\mathbf{k})\right]^2 \\ &= && -g\,\mathrm{v}\left[\int \frac{d^D k}{(2\pi)^D}\,\frac{1}{\mathbf{k}^2+M^2}\right]^2 \\ &= && \frac{-\,g\,\mathrm{v}\,\Gamma^2\,(\,1-D/2\,)}{(4\pi)^D\,\left(M^2\right)^{2-D}}\,. \end{aligned} \tag{4.49}$$

For even dimensions, (4.49) is infinite due to the Gamma function's poles at negative integers. However, we are primarily interested in $D=3$ dimensions, so we do not have to pay attention to this problem at the moment.

The sunset diagram (4.44) turns out to be much more complicated since the propagators are actual bilocal quantities. In a first step, we insert the Fourier representation (4.45) of the propagators. Due to the translational invariance, one of the spatial integrations gives a volume factor v and we obtain

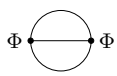

$$\begin{aligned} &= && g^2\Phi^2\int d^D x\; d^D y\int \frac{d^D p\; d^D q\; d^D k}{(2\pi)^{3\,D}}\; e^{\imath[\mathbf{k}+\mathbf{p}+\mathbf{q}](\mathbf{x}-\mathbf{y})}\; G_\Phi(\mathbf{k})\, G_\Phi(\mathbf{p})\, G_\Phi(\mathbf{q}) \\ &= && g^2\Phi^2\int d^D y\int \frac{d^D p\; d^D q\; d^D k}{(2\pi)^{2\,D}}\int \frac{d^D z}{(2\pi)^D}\; e^{\imath[\mathbf{k}+\mathbf{p}+\mathbf{q}]\mathbf{z}}\; G_\Phi(\mathbf{k})\, G_\Phi(\mathbf{p})\, G_\Phi(\mathbf{q})\,. \end{aligned} \tag{4.50}$$

Using the Fourier transformed propagator (4.48), this reduces to

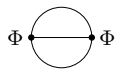

$$\begin{aligned} &= && g^2\Phi^2\,\mathrm{v}\int \frac{d^D p\; d^D q}{(2\pi)^{2\,D}}\;\frac{1}{\mathbf{p}^2+M^2}\;\frac{1}{\mathbf{q}^2+M^2}\;\frac{1}{(\mathbf{p}+\mathbf{q})^2+M^2} \\ &:= && g^2\Phi^2\,\mathrm{v}\,I(D)\,. \end{aligned} \tag{4.51}$$

The remaining integral $I(D)$ has been solved in Appendix D. With regard to (D.8), the sunset diagram yields

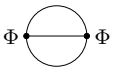

$$= g^2\Phi^2\,\mathrm{v}\,\frac{(M^2)^{D-3}\,\Gamma\big(1-D/2\big)}{(4\pi)^D}\left\{\Gamma\left(2-D/2\right)\,F\left(1,2-\frac{D}{2};\frac{3}{2};\frac{1}{4}\right)\right.$$
$$\left.-\,\frac{2^{D-3}\,\sqrt{\pi}\,\Gamma(3-D)}{\Gamma\big((5-D)/2\big)}\,F\left(1,3-D;\frac{5-D}{2};\frac{1}{4}\right)\right\}. \tag{4.52}$$

By now, we realize that we do have to deal with infinities occurring in Feynman integrals: due to the Gamma and the hypergeometric functions in (4.52), the sunset integral has divergencies in $D=3$ dimensions as well as for even dimensions. Therefore, we leave (4.52) at that for the moment and insert a whole chapter on regularization and renormalization of Feynman integrals before dealing with this very diagram.

5. Regularization and Renormalization

In statistical field theory, many Feynman integrals do not converge due to two different types of divergencies: ultraviolet (UV)-divergencies arise from an integrand falling off too slowly at large momenta, infrared (IR)-divergencies occur for small momenta in the zero-mass limit. Since all fields we consider are massive, the latter divergencies do not occur during our present calculations.

Usually, a Feynman integral is primarily defined for a certain region of convergence, i.e., merely for certain dimensions. Due to analytic continuation, it is possible to extend this region to all real numbers except for some discrete poles. To this end, one uses the Gamma function $\Gamma(x)$, defined for all $x \in \mathbb{R} \setminus \{-1, -2, -3, ...\}$, and applies its identity

$$\Gamma(x+1) \;=\; x\,\Gamma(x)\,. \tag{5.1}$$

Since these discrete poles are usually located at integer dimensions which are just of physical interest, the regularization procedure has to go further. Via ε-expansion, we approach the pole from one side where the integral is now defined, so we can localize and characterize the divergency. Finally, we perform renormalization by absorbing all divergencies in so-called renormalized quantities.

5.1. Dimensional Regularization

In order to demonstrate the idea of dimensional regularization, we consider the elementary Feynman integral

$$= I_1(D) \;=\; \int \frac{d^D k}{(2\pi)^D}\,\frac{1}{\mathbf{k}^2 + M^2}\,, \tag{5.2}$$

which is originally convergent for $0 < D < 2$. We assume the dimension D to be an arbitrary complex number and write (5.2) – benefiting from the rotationally invariant integrand – in terms of polar coordinates

$$I_1(D) \;=\; \frac{S_D}{(2\pi)^D}\int_0^\infty dk\; k^{D-1}\,\frac{1}{k^2 + M^2}\,, \tag{5.3}$$

with S_D being the surface of the $D-$dimensional unit sphere

$$S_D = \frac{2\pi^{D/2}}{\Gamma(D/2)}\,. \tag{5.4}$$

The integral (5.2) can be reduced to the one of the Beta function (C.9). Thus, the result reads

$$I_1(D) \;=\; \frac{\Gamma\left(1-D/2\right)}{(4\pi)^{D/2}}\,(M^2)^{D/2-1}\,. \tag{5.5}$$

By means of (5.1), the Gamma function continues the integral from $0<D<2$ to all D except for even dimensions $D=2,4,6,...$ where the occurring Gamma function has poles.

5.2. ε-Expansion of Feynman Integrals

Despite of analytic continuation, divergencies can remain at dimensions which shall be considered, e.g., $D=4$ in (5.5). Since all remaining poles are discrete, we are able to approach them through a region in which the integral is well-defined choosing a dimension close to the desired one, e.g., $D=4-\varepsilon$. Inserting this into (5.5), an expansion for small ε leads to

$$I(4+\varepsilon) \;=\; \frac{M^2}{8\,\pi^2}\left[-\frac{1}{\varepsilon}\;-\;\ln 2\;+\;\frac{1}{2}\left(\gamma-1+\ln M^2-\ln\pi\right)\right]\;+\;\mathcal{O}(\varepsilon)\,, \tag{5.6}$$

with Euler's constant γ defined in (C.7). All terms of order ε and higher can be neglected since we consider the limit $\varepsilon\to 0$. From the leading term $\sim 1/\varepsilon$, we read off that we deal with a pole of first order.

The ε-expansion of the sunset integral for $D=3+\varepsilon$ has been calculated in Appendix D (D.15), yielding

$$\overset{D=3+\varepsilon}{=}\quad -\frac{1}{32\,\pi^2\,\varepsilon}\;+\;\frac{1}{32\,\pi^2}\left\{-\ln M^2\;+\;\ln\frac{4\pi}{9}\;+\;1\;-\;\gamma\right\}+\mathcal{O}(\varepsilon)\,. \tag{5.7}$$

Again, the divergency turns out to be a first-order pole, whereas for $D=4-\varepsilon$, we find a pole of second order as it is shown in detail in (D.19). An approach from above, i.e., $D=4+\varepsilon$, would lead to the same result. However, it is common to remain within the most important physical interval $2\leq D\leq 4$.

5.3. Renormalization

After localizing and characterizing all divergencies, we continue with renormalization. The basic idea is to introduce renormalized parameters in which all divergencies are absorbed. These parameters transform initial quantities such as mass, coupling constant, and field into renormalized physical quantities. Of course, not all theories can be renormalized. In this context, the so-called *power counting* is a very illuminating method to investigate UV-divergencies. In accordance with the Feynman rules, each internal line of a Feynman diagram I_{F} corresponds to a propagator $\sim p^{-2}$, so I internal lines yield $2I$ powers of momentum p in the denominator. Furthermore, v vertices give rise to

$$L \;=\; I\;-\;v\;+\;1 \tag{5.8}$$

D-dimensional loop integrations [6, Ch. 9]. Thus, we have $DL = D\,(I - v + 1)$ powers of momentum in the numerator. Altogether, a Feynman integral yields

$$\omega(I_{\mathrm{F}}) \;=\; (D-2)\,I \;+\; D\,(1-v) \tag{5.9}$$

powers of momentum, which characterizes the integral's power behavior at large momenta. Therefore, we have

$$I_{\mathrm{F}} \;\sim\; \lambda^{\omega(I_{\mathrm{F}})} \qquad \text{if} \qquad \lambda \to \infty\,, \tag{5.10}$$

after rescaling the momentum $\mathbf{p} \to \lambda\mathbf{p}$. The quantity $\omega(I_{\mathrm{F}})$ in (5.9) is called *superficial degree of divergence*. The Feynman diagram I_F is called *superficially divergent* if $\omega(I_{\mathrm{F}}) \geq 0$. The sunset integral (D.1), for instance, has $\omega(I_{\mathrm{F}}) = 0$ for $D = 3$ dimensions, which is called *logarithmically divergent*. In $D = 4$ dimensions, however, it has $\omega(I_{\mathrm{F}}) = 2$, referred to as *quadratically divergent*. In ϕ^4-theory without background, the numbers I and n of internal and external lines are connected by [6, Ch. 9]

$$I \;=\; 2v \,-\, \frac{n}{2}\,. \tag{5.11}$$

Inserting (5.11) into (5.9) yields

$$\omega(I_{\mathrm{F}}) \;=\; D \;+\; n\,\left(1 - \frac{D}{2}\right) \;+\; v\,(D-4)\,. \tag{5.12}$$

In four dimensions, the corresponding superficial degree of divergence

$$\omega(I_F) \;=\; 4 \,-\, n \tag{5.13}$$

shows that at any given perturbative order, merely vacuum diagrams, two- and four-point one-particle irreducible diagrams lead to $\omega(I_{\mathrm{F}}) \geq 0$, thus they are the only superficially divergent diagrams. All other n-point functions are finite, hence the theory is *renormalizable*. However, since (5.13) is independent of the number v of vertices, divergencies can occur at any given perturbation order. In three dimensions, (5.12) simplifies to

$$\omega(I_{\mathrm{F}}) \;=\; 3 \,-\, \frac{n}{2} \,-\, v\,. \tag{5.14}$$

In this case, only a few low-order diagrams can be superficially divergent, all others are finite. Consider, for instance, vacuum diagrams where $n = 0$. Due to (5.14), divergencies merely arise up to the third perturbation order $v = 3$. Such a theory is called *superrenormalizable*. In more than four dimensions, (5.12) can be positive at any given order and not only for two- or four-point diagrams. Hence, new divergencies arise again and again, which makes the theory *nonrenormalizable*. For a ϕ^4-theory, $D_c = 4$ is called the *upper critical dimension* above which the theory becomes nonrenormalizable. More generally, the upper critical dimension of a ϕ^r-theory reads [6, Ch. 9]

$$D_c \;=\; \frac{r}{r/2 \,-\, 1}\,. \tag{5.15}$$

In a renormalizable theory, all quantities like mass, field, and coupling constant have to be renormalized. In the case of a superrenormalizable theory, however, the renormalization procedures of these quantities are independent of each other and not implicitly necessary to absorb all divergencies. Thus, we concentrate on the mass renormalization which turns out to be the only infinite renormalization. The renormalization of the field and coupling constant merely leads to additional constants which may be disregarded due to renormalization invariance. We will dwell upon this fact in Section 8.4 in connection with VPT.

5.4. Subtraction Method

When we calculated the first order of the effective potential in Section 4.2, we implicitly derived a further method of regularization that is referred to as *subtraction method*. In this section, we introduce the basic principles and explain that our results are correct although they seem to be inconsistent so far.

First of all, note that the integral example (5.2) points out another possibility to calculate the first-order diagram (4.19). The integral (5.2) represents the derivative of the trace-log term with regard to M^2 as defined in (4.26). In fact, the integral (5.5) results from (4.24) after differentiation or the other way round: the first-order diagram is obtained by integrating (5.5) with respect to M^2. The result (5.5), however, is valid for arbitrary dimensions, in particularly for even dimensions. Therefore, it must be possible to extend (4.24) to even dimensions, although it was originally intended to be valid only for odd dimensions. The result has to be equivalent to (4.37) which was explicitly derived for even dimension. In other words, both results have to be equal when taking renormalization invariance into account.

The subtraction method was introduced in 1984 by Collins [36]. It was originally intended to deal with IR-divergencies. More precisely, it consists of subtracting IR-divergencies of an integral, which arise if we extend the dimension to $D<0$. The resulting integral can be solved analytically and yields an expression in terms of Gamma or Beta functions. These functions, however, provide analytic continuation to dimensions $D>0$ in such a way that this method can also be applied to UV-divergencies. A detailed discussion is presented in Ref. [6, Ch. 8], for instance. Here, we restrict ourselves to summarizing the basic principle.

Consider an integral with a finite region of convergence $0 < D < D'$ and a rotationally invariant integrand $f(\mathbf{k}^2)$. This integral is continued to dimensions $-2<D<0$ by

$$\int \frac{d^D k}{(2\pi)^D} f(\mathbf{k}^2) = \frac{S_D}{(2\pi)^D} \left\{ \int_0^C dk\, k^{D-1} \left[f(k^2) - f(0) \right] + f(0)\, \frac{C^D}{D} + \int_C^\infty dk\, k^{D-1} f(k^2) \right\}. \tag{5.16}$$

Due to the negative dimension D, the limit $C \to \infty$ leads to

$$\int \frac{d^D k}{(2\pi)^D} f(\mathbf{k}^2) = \frac{S_D}{(2\pi)^D} \int_0^\infty dk\, k^{D-1} \left[f(k^2) - f(0) \right] . \tag{5.17}$$

This procedure is applied again and again until all divergencies are subtracted and the right-hand side of (5.17) yields a finite result.

Now consider the integral (4.19) of the effective potential in first order. The term to subtract with regard to (5.17) is just $\ln M^2$. In fact, this is what our calculations in Section 4.2 amount to, compare with Eq. (4.37). For this reason, we conclude that both results (4.24) and (4.37) are equivalent with regard to renormalization invariance. For even dimensions, however, the subtraction method has to be favored. In doing so, all divergencies are removed without any further measures.

5.5. Renormalization of Effective Potential

In this section, we turn back to the original problem, i.e., the renormalization of the sunset diagram (4.52) in $D = 3$ dimensions. The regularization procedure and the ε-expansion as introduced in Section 5.2 are worked out in detail in Appendix D, yielding the result (D.15). Thus, we obtain

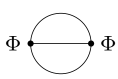

$$\overset{D=3+\varepsilon}{=} \frac{g^2 \Phi^2\, \mathrm{v}}{32\, \pi^2} \left\{ -\frac{1}{\varepsilon} - \ln \frac{M^2}{\mu^2} + \ln \frac{4\pi}{9} + 1 - \gamma \right\} + \mathcal{O}(\varepsilon)$$

$\equiv$ 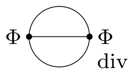 $+$ 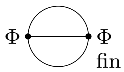 , (5.18)

with M^2 defined in (4.26). The divergent part consists of the term $\sim 1/\varepsilon$, the finite part contains all other terms. The full effective potential (4.14) in terms of Feynman diagrams can hence be written as

$V_{\text{eff}}(\Phi) = \frac{\mathrm{v}}{2} m^2 \Phi^2 + \frac{\mathrm{v}\, g}{24} \Phi^4 + \frac{\hbar}{2}$ 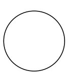 $- \frac{\hbar^2}{8}$ 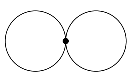 $- \frac{\hbar^2}{12}$ 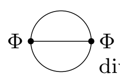 $- \frac{\hbar^2}{12}$ 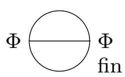 . (5.19)

Here, we have introduced the artificial smallness parameter $\hbar$ whose powers denote the respective loop orders. In order to renormalize (5.19), we consider the harmonic contribution of the potential itself and the divergent contribution of the sunset diagram. With regard to (5.18), both are proportional to Φ^2, thus they can be merged as follows:

$\frac{\mathrm{v}}{2} m^2 \Phi^2 - \frac{\hbar^2}{12}$ 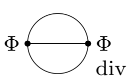 $= \frac{\mathrm{v}}{2} m^2 \Phi^2 + \frac{\hbar^2 g^2 \Phi^2\, \mathrm{v}}{32\, \pi^2} \frac{1}{\varepsilon} \equiv \frac{\mathrm{v}}{2} m_r^2 \Phi^2 ,$ (5.20)

where m_r denotes the physical renormalized mass that absorbs all divergencies. In accordance with (4.27), (4.49), and (5.18)–(5.20), the renormalized effective potential $V_{\text{eff}}^{(r)}(\Phi)$ in second loop order for $D = 3$ dimensions and volume $\mathrm{v} = 1$ results in

$$\begin{aligned} V_{\text{eff}}^{(r)}(\Phi) \;=\; & \frac{1}{2} m_r^2 \Phi^2 + \frac{g}{24} \Phi^4 - \frac{\hbar}{12\, \pi} \left(m_r^2 + \frac{g}{2} \Phi^2 \right)^{3/2} + \frac{\hbar^2 g}{128 \pi^2} \left(m_r^2 + \frac{g}{2} \Phi^2 \right) \\ & + \frac{\hbar^2 g^2 \Phi^2}{384\, \pi^2} \ln \left[\frac{1}{\mu^2} \left(m_r^2 + \frac{g}{2} \Phi^2 \right) \right] - \frac{\hbar^2 g^2 \Phi^2}{384\, \pi^2} \left(\ln \frac{4\pi}{9} + 1 - \gamma \right) . \end{aligned} \tag{5.21}$$

In all terms of first and higher loop order, the bare mass can be replaced by the renormalized one as the additional terms are of higher order and do not contribute to the second loop order. To simplify matters, we omit the index r of the renormalized mass and the renormalized effective potential in the following unless otherwise noted.

6. Self-Energy

The calculation of the self-energy allows another access to renormalization. We present it in this chapter in order to verify the result of the previous renormalization procedure in another way.

When we approach a many-particle system, we usually begin by assuming that the particles are point-like. This simplification can cause essential non-physical infinities: via the interaction, a point-like particle acquires an infinite mass, but the actual physical mass is, of course, finite. Thus, all infinities caused by the theory have to be removed by a renormalization scheme. In order to illustrate this procedure, we consider a particle propagating from $\mathbf{x}_1$ to $\mathbf{x}_2$. In Feynman's formalism, we describe this process with the propagator

$$\mathbf{x}_1 \text{ —— } \mathbf{x}_2 \;=\; G_0\left(\mathbf{x}_1, \mathbf{x}_2\right). \tag{6.1}$$

However, the particle will also interact with the vacuum. In the ϕ^4-theory, such interactions are, for instance,

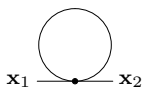

or

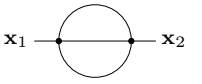

. (6.2)

Since physics includes all possible processes, (6.1) is only a zeroth approximation. Let us denote the full propagator by

$$\mathbf{x}_1 \text{ ═══ } \mathbf{x}_2 \;=\; G(\mathbf{x}_1, \mathbf{x}_2)\,. \tag{6.3}$$

Whereas $G_0(\mathbf{x}_1, \mathbf{x}_2)$ describes the propagation of a point-like particle, $G(\mathbf{x}_1, \mathbf{x}_2)$ characterizes a real physical particle interacting with the vacuum. The self-energy Σ collects all these interactions with the vacuum. More precisely, Σ denotes the interaction energy and can therefore be absorbed in the full integral kernel G^{-1} in addition to the other contributions of the free integral kernel G_0^{-1}:

$$G^{-1}(\mathbf{x}_1, \mathbf{x}_2) \;=\; G_0^{-1}(\mathbf{x}_1, \mathbf{x}_2) \;-\; \Sigma(\mathbf{x}_1, \mathbf{x}_2)\,. \tag{6.4}$$

The contributions of the self-energy Σ can be regarded as modifications of quantities like the mass m. Therefore, it is obvious to associate the self-energy with renormalization, which we demonstrate in this chapter.

6.1. Definition of Self-Energy

Consider the free action

$$\mathcal{A}^{(0)}[\phi] \;=\; \frac{1}{2}\int d^D x\; d^D x'\; \phi(\mathbf{x})\, G_0^{-1}(\mathbf{x},\mathbf{x}')\, \phi(\mathbf{x}') \tag{6.5}$$

of the potential (1.1). Its name denotes that in contrast to the full action (4.2), we have no interaction. In analogy to (4.15), the free integral kernel reads

$$G_0^{-1}(\mathbf{x},\mathbf{x}') \;=\; \Big(-\Delta + m^2\Big)\,\delta(\mathbf{x}-\mathbf{x}')\,. \tag{6.6}$$

Since it merely depends on the difference of the coordinates, it has the Fourier representation

$$G_0^{-1}(\mathbf{x},\mathbf{x}') \;=\; \int \frac{d^D k}{(2\pi)^D}\; e^{\imath\,\mathbf{k}(\mathbf{x}-\mathbf{x}')}\; G_0^{-1}(\mathbf{k})\,. \tag{6.7}$$

The integral kernel in Fourier space can directly be calculated from (6.6) by means of inverse Fourier transform, yielding

$$G_0^{-1}(\mathbf{k}) \;=\; \mathbf{k}^2 \;+\; m^2\,. \tag{6.8}$$

Note that for $\mathbf{k}=0$, the integral kernel just yields the mass m^2:

$$G_0^{-1}(\mathbf{k}=0) \;=\; m^2\,. \tag{6.9}$$

The free propagator $G_0(\mathbf{x},\mathbf{x}')$ is related to (6.6) by an integral identity that reads in analogy to (4.41)

$$\int d^D x'\; G_0^{-1}(\mathbf{x},\mathbf{x}')\, G_0(\mathbf{x}',\mathbf{x}'') \;=\; \delta(\mathbf{x}-\mathbf{x}'')\,. \tag{6.10}$$

Its Feynman diagram has already been introduced in (6.1). Now we take the interaction part of the potential (1.1) into account

$$\mathcal{A}^{(\mathrm{int})}[\phi] \;=\; \frac{g}{24}\int d^D x\; \phi^4(\mathbf{x})\,. \tag{6.11}$$

The full action $\mathcal{A}[\phi] = \mathcal{A}^{(0)}[\phi] + \mathcal{A}^{(\mathrm{int})}[\phi]$ leads to the full integral kernel $G^{-1}(\mathbf{x},\mathbf{x}')$ and the corresponding full propagator (6.3). In accordance with (6.4), the difference of both integral kernels is referred to as self-energy. Whereas we found the free integral kernel at zero momentum to be the bare mass, we define the renormalized physical mass as

$$m_r^2 \;:=\; G^{-1}(\mathbf{k}=0) \;=\; m^2 - \Sigma(\mathbf{k}=0)\,. \tag{6.12}$$

In terms of the self-energy, mass renormalization therefore amounts to calculating the self-energy at zero momentum.

The self-energy is determined by the so-called *Dyson equation* which can be derived from (6.4). We multiply with $G(\mathbf{x}, \mathbf{x}_1)$ and $G_0(\mathbf{x}_2, \mathbf{x}')$ and integrate over $\mathbf{x}_1$ and $\mathbf{x}_2$, yielding

$$\begin{aligned}
&\int d^D x_2\, G_0(\mathbf{x}_2, \mathbf{x}') \int d^D x_1\, G^{-1}(\mathbf{x}_1, \mathbf{x}_2)\, G(\mathbf{x}, \mathbf{x}_1) \\
&= \int d^D x_1\, G(\mathbf{x}, \mathbf{x}_1) \int d^D x_2\, G_0^{-1}(\mathbf{x}_1, \mathbf{x}_2)\, G_0(\mathbf{x}_2, \mathbf{x}') \\
&- \int d^D x_1 \int d^D x_2\, G(\mathbf{x}, \mathbf{x}_1)\, \Sigma(\mathbf{x}_1, \mathbf{x}_2)\, G_0(\mathbf{x}_2, \mathbf{x}')\,. \qquad (6.13)
\end{aligned}$$

Taking into account the orthonormality condition for G_0 in (6.10) and a corresponding one for G, (6.13) simplifies to

$$G(\mathbf{x}, \mathbf{x}') \;=\; G_0(\mathbf{x}, \mathbf{x}') \;+\; \int d^D x_1 \int d^D x_2\, G(\mathbf{x}, \mathbf{x}_1)\, \Sigma(\mathbf{x}_1, \mathbf{x}_2)\, G_0(\mathbf{x}_2, \mathbf{x}')\,. \qquad (6.14)$$

The Dyson equation (6.14) can also be expressed in terms of Feynman diagrams. To this end, we introduce a new symbol for the self-energy

$\Sigma(\mathbf{x}, \mathbf{x}') \;=$  . (6.15)

It has two *stumps* which, however, have to be distinguished from actual lines that are described by propagators like (6.1) and (6.3). Such full lines can be attached to the self-energy at each of its stumps $\mathbf{x}$ and $\mathbf{x}'$, which corresponds analytically to integrate over $\mathbf{x}$ and $\mathbf{x}'$, respectively. With this prescription, we identify (6.14) with

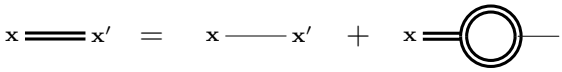 . (6.16)

The Dyson equation (6.14) is a self-consistent equation [37, Ch. 7] for the propagator $G(\mathbf{x}, \mathbf{x}')$ because it appears both on the left- and the right-hand side of the equation. Solving (6.16) iteratively up to any desired order by inserting the left-hand side into the right-hand side again and again, we obtain the Dyson series

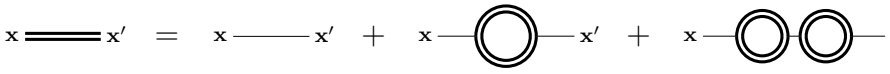 (6.17)

6.2. Self-Energy via Effective Action

Each vacuum diagram of the effective potential has a corresponding self-energy diagram. In this section, we derive the self-energy for $N = 1$ field from the point of view of loop expansion. We proceed similarly to Chapter 4, starting from (4.1) and (4.2), but in contrast to the calculation of the effective potential where we assumed a constant background, we now choose a $\mathbf{x}$-dependent background function $\Phi(\mathbf{x})$. This yields the effective action $\Gamma[\Phi(\mathbf{x})]$, which differs from the effective potential merely in the non-constant background function.

Thus, instead of the effective potential and the partition function being a function of the background, they are functionals now:

$$\mathcal{Z}[\Phi] \;=\; e^{-\Gamma[\Phi]}\,. \tag{6.18}$$

Evaluating the effective action $\Gamma[\Phi(\mathbf{x})]$ for a constant background Φ, we recover the effective potential

$$\Gamma[\Phi]\Big|_{\Phi(\mathbf{x})=\Phi} \;=\; V_{\text{eff}}(\Phi)\,. \tag{6.19}$$

Moreover, we specialize in the potential (1.1) from the very beginning instead of assuming an arbitrary potential as we did before. The corresponding ansatz in the background method (4.3) reads

$$\phi(\mathbf{x}) \;=\; \Phi(\mathbf{x}) \;+\; \delta\phi(\mathbf{x})\,. \tag{6.20}$$

Analogously to (4.5), we perform a Taylor expansion of the potential (1.1) around the background $\Phi(\mathbf{x})$ and insert it into the action (4.2). With vanishing terms linear in $\delta\phi(\mathbf{x})$, the action yields

$$\begin{aligned}\mathcal{A}[\Phi+\delta\phi] \;=\; & \int d^Dx \left\{ \frac{1}{2}\,\Phi(\mathbf{x})\left[-\Delta+m^2\right]\Phi(\mathbf{x}) \;+\; \frac{g}{24}\,\Phi^4(\mathbf{x}) \;+\; \frac{g}{4}\,\Phi^2(\mathbf{x})\,\delta\phi^2(\mathbf{x}) \right. \\ & \left. +\,\frac{g}{6}\,\Phi(\mathbf{x})\,\delta\phi^3(\mathbf{x}) \;+\; \frac{g}{24}\,\delta\phi^4(\mathbf{x}) \;+\; \frac{1}{2}\,\delta\phi(\mathbf{x})\left[-\Delta+m^2\right]\delta\phi(\mathbf{x}) \right\}. \end{aligned} \tag{6.21}$$

Inserting the action (6.21) of the background formalism into (4.1), we divide again the partition function into a classical and a fluctuation part by means of

$$\mathcal{Z}[\Phi] \;=\; \mathcal{Z}^{(\text{cl})}[\Phi]\;\mathcal{Z}^{(\text{fluc})}[\Phi]\,. \tag{6.22}$$

Here, the classical partition function is defined by

$$\mathcal{Z}^{(\text{cl})}[\Phi] \;:=\; \exp\left\{ -\int d^Dx \left[\frac{1}{2}\,\Phi(\mathbf{x})\left[-\Delta \;+\; m^2\right]\Phi(\mathbf{x}) \;+\; \frac{g}{24}\,\Phi^4(\mathbf{x}) \right] \right\}. \tag{6.23}$$

The fluctuation part in (6.22) reads

$$\mathcal{Z}^{(\text{fluc})}[\Phi] = \int \mathcal{D}\delta\phi\; e^{-\tilde{\mathcal{A}}[\Phi+\delta\phi]} \exp\left\{ -\int d^Dx \left[\frac{g}{6}\,\Phi(\mathbf{x})\,[\,\delta\phi(\mathbf{x})\,]^3 + \frac{g}{24}\,[\,\delta\phi(\mathbf{x})\,]^4 \right] \right\}, \tag{6.24}$$

where we defined

$$\tilde{\mathcal{A}}[\Phi+\delta\phi] \;=\; \int d^Dx\,\frac{1}{2}\,\delta\phi(\mathbf{x})\Big[-\Delta+m^2+\frac{g}{2}\,\Phi^2(\mathbf{x})\Big]\delta\phi(\mathbf{x})\,. \tag{6.25}$$

With regard to (6.18) and (6.22), we write the effective action in a loop expansion analogously to (4.14)

$$\Gamma[\Phi] \;=\; \mathcal{A}[\Phi] \;+\; \Gamma^{(1)}[\Phi] \;+\; \Gamma^{(\text{int})}[\Phi]\,. \tag{6.26}$$

The zero-loop order of the effective action follows straightforwardly from (6.23), as the integral can no longer be calculated explicitly due to the non-constant background

$$\mathcal{A}[\Phi] \;=\; -\ln \mathcal{Z}^{(\mathrm{cl})}[\Phi] \;=\; \int d^D x \left[\frac{1}{2}\, \Phi(\mathbf{x}) \left[-\,\Delta \,+\, m^2 \right] \Phi(\mathbf{x}) \,+\, \frac{g}{24}\, \Phi^4(\mathbf{x}) \right]. \tag{6.27}$$

We are merely interested in the second functional derivative of $\mathcal{A}[\Phi]$ with respect to the background $\Phi(\mathbf{x})$, which cancels the spatial integration anyway

$$\frac{\delta^2 \mathcal{A}[\Phi]}{\delta\, \Phi(\mathbf{x})\, \delta\, \Phi(\mathbf{x}')} \;=\; \Big[-\Delta + m^2 + \frac{g}{2}\, \Phi^2(\mathbf{x}) \Big]\, \delta(\mathbf{x} - \mathbf{x}')\,. \tag{6.28}$$

Note that for a constant background Φ, the second functional derivative (6.28) reproduces the Φ-dependent integral kernel (4.15):

$$\left. \frac{\delta^2 \mathcal{A}[\Phi]}{\delta\, \Phi(\mathbf{x})\, \delta\, \Phi(\mathbf{x}')} \right|_{\Phi(\mathbf{x})=\Phi} \;=\; \Big[-\Delta + m^2 + \frac{g}{2}\, \Phi^2 \Big]\, \delta(\mathbf{x} - \mathbf{x}') \;=\; G_\Phi^{-1}(\mathbf{x}, \mathbf{x}')\,. \tag{6.29}$$

Thus, in the background method, the Φ-dependent integral kernel (6.28) plays the role of the free integral kernel (6.6). It is obvious to identify the full integral kernel analogously with the second derivative of the full effective action [6, Ch. 5]

$$\left. \frac{\delta^2 \Gamma[\Phi]}{\delta\, \Phi(\mathbf{x})\, \delta\, \Phi(\mathbf{x}')} \right|_{\Phi(\mathbf{x})=\Phi} \;=\; G^{-1}(\mathbf{x}, \mathbf{x}')\,. \tag{6.30}$$

Comparing (6.4), (6.26), (6.29), and (6.30), we see that the self-energy diagrams follow from the second functional derivative of $\Gamma^{(1)}[\Phi]$ and $\Gamma^{(\mathrm{int})}[\Phi]$ evaluated at a constant background. In order to calculate the effective action in first and higher loop orders, we expand the fluctuation part (6.24) as follows

$$\begin{aligned} \mathcal{Z}^{(\mathrm{fluc})}[\Phi] \;&=\; \int \mathcal{D}\delta\phi\; e^{-\,\tilde{\mathcal{A}}[\Phi+\delta\phi]} \,-\, \frac{g}{6} \int d^D x\; \Phi(\mathbf{x}) \oint \mathcal{D}\delta\phi\, \big[\, \delta\phi(\mathbf{x}) \,\big]^3\; e^{-\,\tilde{\mathcal{A}}[\Phi+\delta\phi]} \\ &\quad - \frac{g}{24} \int d^D x \oint \mathcal{D}\delta\phi\; \big[\, \delta\phi(\mathbf{x}) \,\big]^4\; e^{-\,\tilde{\mathcal{A}}[\Phi+\delta\phi]} \\ &\quad + \frac{g^2}{72} \int d^D x \int d^D x' \oint \mathcal{D}\delta\phi\; \big[\, \delta\phi(\mathbf{x}) \,\big]^3 \big[\, \delta\phi(\mathbf{x}') \,\big]^3\; e^{-\,\tilde{\mathcal{A}}[\Phi+\delta\phi]} + \cdots \\ &\equiv\; \mathcal{Z}^{(1)}[\Phi] \,+\, \mathcal{Z}^{(2)}[\Phi] \,+\, \cdots\,. \end{aligned} \tag{6.31}$$

The logarithm of $\mathcal{Z}^{(1)}[\Phi]$ yields the first loop order of the effective action

$$\Gamma^{(1)}[\Phi] \;=\; -\ln \mathcal{Z}^{(1)}[\Phi] \;=\; -\ln \left\{ \int \mathcal{D}\delta\phi\; e^{-\,\tilde{\mathcal{A}}[\Phi+\delta\phi]} \right\}. \tag{6.32}$$

Our next task is to calculate the second functional derivative of (6.32) as we did in (6.28) for the zero-loop order

$$\begin{aligned}\frac{\delta^2\,\Gamma^{(1)}[\Phi]}{\delta\,\Phi(\mathbf{x})\;\delta\,\Phi(\mathbf{x}')} \;=\; & \frac{g^2}{4}\,\frac{\Phi(\mathbf{x})\,\Phi(\mathbf{x}')}{\big(\mathcal{Z}^{(1)}[\Phi]\big)^2}\left[\int\mathcal{D}\delta\phi\;[\,\delta\phi(\mathbf{x})\,]^2\,e^{-\tilde{\mathcal{A}}[\Phi+\delta\phi]}\right]\left[\int\mathcal{D}\delta\phi\;[\,\delta\phi(\mathbf{x}')\,]^2\,e^{-\tilde{\mathcal{A}}[\Phi+\delta\phi]}\right]\\ & +\frac{1}{\mathcal{Z}^{(1)}[\Phi]}\int\mathcal{D}\delta\phi\;\frac{g}{2}\,\delta(\mathbf{x}-\mathbf{x}')\;[\,\delta\phi(\mathbf{x})\,]^2\;e^{-\tilde{\mathcal{A}}[\Phi+\delta\phi]}\\ & -\frac{1}{\mathcal{Z}^{(1)}[\Phi]}\int\mathcal{D}\delta\phi\;\frac{g^2}{4}\,\Phi(\mathbf{x})\,\Phi(\mathbf{x}')\;[\,\delta\phi(\mathbf{x})\,]^2\;[\,\delta\phi(\mathbf{x}')\,]^2\,e^{-\tilde{\mathcal{A}}[\Phi+\delta\phi]}\,. \qquad (6.33)\end{aligned}$$

Specializing in a constant background $\Phi(\mathbf{x})\equiv\Phi$, (6.33) reduces to

$$\begin{aligned}\left.\frac{\delta^2\,\Gamma^{(1)}[\Phi]}{\delta\,\Phi(\mathbf{x})\;\delta\,\Phi(\mathbf{x}')}\right|_{\Phi(\mathbf{x})\,=\,\Phi} \;=\; & \frac{g^2}{4}\,\Phi^2\big\langle\delta\phi^2(\mathbf{x})\big\rangle_\Phi\big\langle\delta\phi^2(\mathbf{x}')\big\rangle_\Phi\;+\;\frac{g}{2}\,\delta(\mathbf{x}-\mathbf{x}')\,\big\langle\delta\phi^2(\mathbf{x}')\big\rangle_\Phi\\ & -\frac{g^2}{4}\,\Phi^2\big\langle\delta\phi^2(\mathbf{x})\,\delta\phi^2(\mathbf{x}')\big\rangle_\Phi\,, \qquad (6.34)\end{aligned}$$

with the expectation value $\langle\bullet\rangle_\Phi$ already defined in (4.10). Furthermore, the propagator $G_\Phi(\mathbf{x},\mathbf{x}')$ is defined by means of (4.13). Applying Wick contractions, we write in accordance with (4.13)

$$\big\langle\delta\phi^2(\mathbf{x})\,\delta\phi^2(\mathbf{x}')\big\rangle_\Phi \;=\; G_\Phi(\mathbf{x},\mathbf{x})\;G_\Phi(\mathbf{x}',\mathbf{x}')\;+\;2\,G_\Phi^2(\mathbf{x},\mathbf{x}')\,, \qquad (6.35)$$

which simplifies (6.34) to

$$\left.\frac{\delta^2\,\Gamma^{(1)}[\Phi]}{\delta\,\Phi(\mathbf{x})\;\delta\,\Phi(\mathbf{x}')}\right|_{\Phi(\mathbf{x})=\Phi} \;=\; -\,\frac{g^2}{2}\,\Phi^2\,G_\Phi^2(\mathbf{x},\mathbf{x}')\;+\;\frac{g}{2}\,\delta(\mathbf{x}-\mathbf{x}')\,G_\Phi(\mathbf{x}',\mathbf{x}')\,. \qquad (6.36)$$

Analogously to the vacuum diagrams of the effective potential, Feynman rules can be derived for the self-energy diagrams. A detailed derivation is given, for instance, in Ref. [38]. In doing so, the terms in (6.36) are attributed to the first-order diagrams of the self-energy

$$\frac{g^2}{2}\,\Phi^2\,G_\Phi^2(\mathbf{x},\mathbf{x}') \;=\; \frac{1}{2}$$

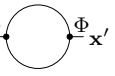

$$\,, \qquad (6.37)$$

$$\frac{g}{2}\,\delta(\mathbf{x}-\mathbf{x}')\,G_\Phi(\mathbf{x},\mathbf{x}') \;=\; \frac{1}{2}$$

$$\,. \qquad (6.38)$$

Thus, the second functional derivative of the first-order effective action evaluated at a constant background is just the self-energy in first loop order:

$$-\left.\frac{\delta^2\,\Gamma^{(1)}[\Phi]}{\delta\,\Phi(\mathbf{x})\;\delta\,\Phi(\mathbf{x}')}\right|_{\Phi(\mathbf{x})\,=\,\Phi} \;=\; \frac{1}{2}$$

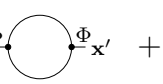

$$\;+\;\frac{1}{2}$$

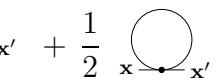

$$\,. \qquad (6.39)$$

Consequently, we obtain the second-order diagrams of the self-energy from the second order of the effective action. There exists still a further connection between vacuum diagrams

and self-energy diagrams by means of Feynman's formalism. Comparing (6.39) with the second-order diagrams of the effective potential as they are given, for instance, in (2.111), we find the following correlation: the self-energy diagrams and their corresponding weights follow graphically from the vacuum diagrams by amputating one line. Amputating one line, however, means decreasing the loop order. Thus, we obtain the first-order self-energy diagrams (6.39) graphically from the second-order vacuum diagrams (2.111). The second-order diagrams of the self-energy might hence be derived from (2.135)–(2.142) and translated to analytic expressions by means of Feynman rules. Alternatively, we might extend the present calculations to the next higher order of the effective action. Since it turns out that we need just one single second-order diagram to renormalize the mass, we take the second-loop order Feynman diagrams for the self-energy from Ref. [38] instead of calculating them explicitly.

6.3. Renormalization with Self-Energy

Now we turn back to our original intention, i.e., the renormalization of the effective potential in Chapter 4 in $D=3$ dimensions with the self-energy. In (6.12), we have defined the renormalized mass to be the difference of the bare mass and the self-energy with zero momentum. Strictly speaking, we have to calculate all self-energy diagrams in second loop order when we wish to calculate the renormalized mass in second loop order. However, we benefit from the fact that ϕ^4-theory in three dimensions is superrenormalizable, see Chapter 5. Most self-energy diagrams are finite, among others the first-order diagrams (6.37) and (6.38). These diagrams merely lead to finite contributions to the effective potential, which can be omitted because of renormalization invariance as further discussed in Section 8.4. Hence, it is sufficient to concentrate on the only infinite second-order diagram which gives us the required mass renormalization. In accordance with Ref. [38], it reads

$$\Sigma_{\ominus}\left(\mathbf{x},\mathbf{x}'\right) \;=\; \frac{1}{6}\;\mathbf{x}\;\;\mathbf{x}' \;=\; \frac{1}{6}\,g^2\,G_\Phi^3(\mathbf{x},\mathbf{x}')\,. \tag{6.40}$$

For the purpose of mass renormalization (6.12), it is sufficient to calculate (6.40) in momentum space for $\mathbf{k}=0$. Here, we benefit from the fact that the propagator is a function only of the coordinate difference $\mathbf{y}:=\mathbf{x}-\mathbf{x}'$. We perform a Fourier transform of (6.40) and calculate the spatial integral, yielding

$$\begin{aligned}\Sigma_{\ominus}\left(\mathbf{k}\right) &= \frac{1}{6}\,g^2\int d^Dy\;e^{-\imath\mathbf{k}\mathbf{y}}\;G_\Phi^3\left(\mathbf{y}\right)\\ &= \frac{1}{6}\,g^2\int\frac{d^Dk'd^Dk''}{(2\pi)^{2D}}\;\frac{1}{\mathbf{k}'^2+M^2}\;\frac{1}{\mathbf{k}''^2+M^2}\;\frac{1}{(\mathbf{k}-\mathbf{k}'-\mathbf{k}'')^2+M^2}\end{aligned} \tag{6.41}$$

with the mass M defined in (4.26). Evaluating the integral (6.41) at $\mathbf{k}=0$ leads to

$$\Sigma_{\ominus}\left(\mathbf{k}=0\right) \;=\; \frac{1}{6}\,g^2\int\frac{d^Dk'\,d^Dk''}{(2\pi)^{2D}}\;\frac{1}{\mathbf{k}'^2+M^2}\;\frac{1}{\mathbf{k}''^2+M^2}\;\frac{1}{(\mathbf{k}'+\mathbf{k}'')^2+M^2}\,, \tag{6.42}$$

which coincides with the sunset diagram (4.51) except for the prefactor Φ^2. In accordance with (5.18) and (6.12), the renormalized mass m_r^2 results in

$$m_r^2 \;=\; m^2 \;+\; \frac{g^2}{192\pi^2}\,\frac{1}{\varepsilon} \;-\; \Sigma_{\ominus}^{(\mathrm{fin})}(\mathbf{k}=0)\,. \tag{6.43}$$

All finite terms of (5.18) have been absorbed in $\Sigma_{\ominus}^{(\mathrm{fin})}(\mathbf{k}=0)$ defined by

$$\frac{1}{6}$$ 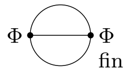 $$= \Phi^2\,\Sigma_{\ominus}^{(\mathrm{fin})}(\mathbf{k}=0)\,. \tag{6.44}$$

In contrast to the previous renormalization procedure in Chapter 5 where we started with the bare mass and came to defining the renormalized one, we now proceed contrarily: we consider the quadratic term of the potential with the renormalized mass and the sunset diagram from the second loop order, insert (5.18) and (6.43) and notice that all divergencies cancel:

$$\frac{1}{2}\,m_r^2\,\Phi^2 \;-\; \frac{\hbar^2}{12}$$ 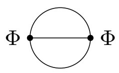

$$\begin{aligned}
&= \frac{1}{2}\left[m^2 + \frac{\hbar^2\,g^2}{192\,\pi^2}\,\frac{1}{\varepsilon} - \hbar^2\,\Sigma_{\ominus}^{(\mathrm{fin})}(\mathbf{k}=0)\right]\Phi^2 - \frac{\hbar^2\,g^2\,\Phi^2}{384\,\pi^2}\,\frac{1}{\varepsilon} + \frac{\hbar^2}{2}\,\Sigma_{\ominus}^{(\mathrm{fin})}(\mathbf{k}=0)\\
&= \frac{1}{2}\,m^2\,\Phi^2\,.
\end{aligned} \tag{6.45}$$

Here, we have again introduced the formal smallness parameter $\hbar$. By means of this renormalization procedure, the renormalized effective potential in second loop order reads in accordance with (4.26)

$$\begin{aligned}
V_{\mathrm{eff}}^{(\mathrm{r})}(\Phi) \;=\;& \frac{1}{2}\,m^2\,\Phi^2 + \frac{g}{24}\,\Phi^4 - \frac{\hbar}{12\,\pi}\left(m^2 + \frac{g}{2}\,\Phi^2\right)^{3/2} + \frac{\hbar^2\,g}{128\,\pi^2}\left(m^2 + \frac{g}{2}\,\Phi^2\right)\\
&+ \frac{\hbar^2\,g^2\,\Phi^2}{384\,\pi^2}\ln\left[\frac{1}{\mu^2}\left(m^2 + \frac{g}{2}\,\Phi^2\right)\right]\,.
\end{aligned} \tag{6.46}$$

Note, that we might also omit the finite part of the self-energy in (6.45): the divergencies cancel anyway, we merely add a finite term from the second-order diagram to the renormalized effective potential. This modification does not change physics due to the superrenormalizability of the ϕ^4-theory in $D=3$ dimensions. We will dwell upon this point in Chapter 8. If we omitted the finite part of the self-energy, we would obtain our former result (5.21) instead of (6.46).

7. Effective Potential of N Real Fields

In order to apply VPT with two variational parameters in statistical field theory, we have to extend our calculations to N real fields and derive the corresponding effective potential. Furthermore, we require a general result for an arbitrary number of fields to connect VPT with the Hubbard-Stratonovich transformation which represents the large-N limit. To this end, we take advantage of our calculations in quantum statistics in Chapter 2, which are completely analogous to our present procedure. Moreover, we have already calculated the effective potential in statistical field theory for $N=1$ real field in Chapter 4. Therefore, we go succinctly through this chapter and refer to our former results.

7.1. Background Method

Consider the partition function

$$\mathcal{Z} \;=\; \int \mathcal{D}\phi \; e^{-\mathcal{A}[\boldsymbol{\phi}]} \,, \tag{7.1}$$

with the field $\boldsymbol{\phi}$ consisting of N components, i.e. $\boldsymbol{\phi} \equiv (\phi_1, \phi_2, \cdots, \phi_N)$. Assuming an arbitrary potential $V\big(\boldsymbol{\phi}(\mathbf{x})\big)$, the action reads

$$\mathcal{A}[\boldsymbol{\phi}] \;=\; \int d^D x \, \left[-\frac{1}{2}\, \boldsymbol{\phi}(\mathbf{x})\, \Delta\, \boldsymbol{\phi}(\mathbf{x}) \;+\; V(\boldsymbol{\phi}(\mathbf{x})) \right] . \tag{7.2}$$

The background method for a constant background yields the ansatz

$$\boldsymbol{\phi}(\mathbf{x}) \;=\; \boldsymbol{\Phi} \;+\; \boldsymbol{\delta\phi}(\mathbf{x}) \,. \tag{7.3}$$

We perform a Taylor expansion of the potential $V\big(\boldsymbol{\phi}(\mathbf{x})\big)$ around the background $\boldsymbol{\Phi}$ and insert the result into the action (7.2) analogously to (2.50) and (2.51), which leads to

$$\begin{aligned} \mathcal{A}\big[\boldsymbol{\Phi} + \boldsymbol{\delta\phi}\big] \;&=\; \mathrm{v}\, V(\boldsymbol{\Phi}) + \int d^D x \Big\{ \frac{1}{2}\, \delta\phi_i(\mathbf{x}) \big[-\Delta + V_{ij}(\boldsymbol{\Phi}) \big] \delta\phi_j(\mathbf{x}) \\ &\quad + \frac{V_{ijk}(\boldsymbol{\Phi})}{6}\, \delta\phi_i(\mathbf{x}) \delta\phi_j(\mathbf{x}) \delta\phi_k(\mathbf{x}) + \frac{V_{ijkl}(\boldsymbol{\Phi})}{24}\, \delta\phi_i(\mathbf{x}) \delta\phi_j(\mathbf{x}) \delta\phi_k(\mathbf{x}) \delta\phi_l(\mathbf{x}) + \cdots \Big\} \\ &\equiv\; \mathcal{A}^{(\mathrm{cl})}(\boldsymbol{\Phi}) + \mathcal{A}^{(\mathrm{fluc})}\big[\boldsymbol{\Phi} + \boldsymbol{\delta\phi}\big] \,. \end{aligned} \tag{7.4}$$

Here, we have denoted the partial derivatives of the potential analogously to (2.49) by

$$\left. \frac{\partial^n V\big(\boldsymbol{\phi}(\mathbf{x})\big)}{\partial\phi_i(\mathbf{x})\, \partial\phi_j(\mathbf{x}) \cdots \partial\phi_m(\mathbf{x})} \right|_{\boldsymbol{\phi}(\mathbf{x}) = \boldsymbol{\Phi}} \;=:\; V_{ij\cdots m}(\boldsymbol{\Phi}) \,. \tag{7.5}$$

Terms linear in the fluctuations vanish in (7.4). The partition function (7.1) is divided into the classical partition function $\mathcal{Z}^{(\mathrm{cl})}(\mathbf{\Phi})$ and the fluctuating partition function $\mathcal{Z}^{(\mathrm{fluc})}(\mathbf{\Phi})$ as it has likewise been done in (4.7). We expand the fluctuation part and write it in terms of the expectation values that are defined similar to (4.10) and (4.11) for $N=1$ field. Finally, we obtain the loop expansion of the effective potential $V_{\mathrm{eff}}(\mathbf{\Phi})=-\ln\mathcal{Z}(\mathbf{\Phi})$ in accordance with (2.59) and (4.14)

$$\begin{aligned} V_{\mathrm{eff}}(\mathbf{\Phi}) \;&=\; \mathrm{v}\,V(\mathbf{\Phi}) \;-\; \ln\mathcal{Z}^{(1)}(\mathbf{\Phi}) \;+\; \frac{V_{ijkl}(\mathbf{\Phi})}{24}\int d^Dx\big\langle\delta\phi_i(\mathbf{x})\,\delta\phi_j(\mathbf{x})\,\delta\phi_k(\mathbf{x})\,\delta\phi_l(\mathbf{x})\big\rangle \\ &-\frac{V_{ijk}(\mathbf{\Phi})V_{lmn}(\mathbf{\Phi})}{72}\int d^Dx\int d^Dy\big\langle\delta\phi_i(\mathbf{x})\,\delta\phi_j(\mathbf{x})\,\delta\phi_k(\mathbf{x})\,\delta\phi_l(\mathbf{y})\,\delta\phi_m(\mathbf{y})\,\delta\phi_n(\mathbf{y})\big\rangle+\cdots \\ &\equiv\; \mathrm{v}\,V(\mathbf{\Phi}) \;+\; V^{(1)}_{\mathrm{eff}}(\mathbf{\Phi}) \;+V^{(\mathrm{int})}_{\mathrm{eff}}(\mathbf{\Phi})\,. \end{aligned} \tag{7.6}$$

7.2. Effective Potential in First Loop Order

The first-order term can be adopted from (4.18), yielding

$$V^{(1)}_{\mathrm{eff}}(\mathbf{\Phi}) \;=\; -\frac{1}{2}\,\mathrm{Tr}\ln G^{-1}\,. \tag{7.7}$$

Analogously to (2.61), we define the operator

$$\hat{O}_{ij}(\mathbf{x}) \;:=\; \Big[-\Delta \;+\; V_{ij}(\mathbf{\Phi})\Big]\,, \tag{7.8}$$

which enables us to write the integral kernel in (7.7) in the form

$$G^{-1}_{ij}(\mathbf{x},\mathbf{x}') \;=\; \hat{O}_{ij}(\mathbf{x})\,\delta(\mathbf{x}-\mathbf{x}')\,. \tag{7.9}$$

Strictly speaking, we would have to denote the integral kernel (7.9) by a subscript Φ referring to the background as we did in Chapter 4. In order to avoid too many indices, we omit the subscript during this chapter. Now we specialize the potential in a rotationally symmetric one $V(\mathbf{\Phi})=V(\Phi)$. In accordance with (2.69), we define the longitudinal and transversal projection operators

$$P^L_{mn} \;:=\; \frac{\Phi_m\Phi_n}{\Phi^2}\,, \qquad P^T_{mn} \;:=\; \delta_{mn} \;-\; P^L_{mn}\,. \tag{7.10}$$

All properties follow from the quantum statistical results (2.70)–(2.73) when replacing $X_i\rightarrow\Phi_i$. The second partial derivative of the potential in terms of the projection operators (7.10) reads

$$V_{ij}(\Phi) \;=\; V''(\Phi)\,P^L_{ij} \;+\; \frac{V'(\Phi)}{\Phi}\,P^T_{ij} \tag{7.11}$$

where $V'(\Phi)$ and $V''(\Phi)$ denote the first and the second derivative with respect to the modulus $\Phi=|\mathbf{\Phi}|$, respectively. We obtain a decomposition of the operator (7.8) into longitudinal and transversal part by inserting (7.11):

$$\hat{O}_{ij}(\mathbf{x}) \;=\; P^L_{ij}\Big[-\Delta \;+\; V''(\Phi)\Big] \;+\; P^T_{ij}\,\left[-\Delta \;+\; \frac{V'(\Phi)}{\Phi}\right]\,. \tag{7.12}$$

Thus, the calculation of (7.7) amounts to finding the longitudinal and transversal eigenvalues of the operator (7.12). The corresponding eigenvalue equation reads

$$\hat{O}_{ij}(\mathbf{x})\, v_j^{(\mathbf{k},n)}(\mathbf{x}) \;=\; \lambda^{(\mathbf{k})}\, v_i^{(\mathbf{k},n)}(\mathbf{x})\,, \qquad n \;=\; 1,2,...,N\,, \tag{7.13}$$

with a decomposition of the eigenfunctions analogously to Section 2.5. For the longitudinal eigenfunction $n=1$, we choose the ansatz

$$v_j^{(\mathbf{k},1)}(\mathbf{x}) \;=\Phi_j\, e^{-\imath\,\mathbf{k}\,\mathbf{x}}\,, \tag{7.14}$$

which yields in accordance with (7.11) the eigenvalue

$$\lambda_L^{(\mathbf{k})} \;=\; \mathbf{k}^2 \;+\; V''(\Phi)\,. \tag{7.15}$$

For the transversal eigenfunctions

$$v_j^{(\mathbf{k},n)}(\mathbf{x}) \;=\Psi_j^{(n)}\, e^{-\imath\,\mathbf{k}\,\mathbf{x}}\,, \qquad n \;=\; 2,3,...,N\,, \tag{7.16}$$

we choose fields $\Psi_j^{(n)}$ being perpendicular among each other and with respect to the background field $\Psi_j^{(n)}\Psi_j^{(m)}=0$ for $n\neq m$ and $\Psi_j^{(n)}\Phi_j=0$. Due to the symmetry, the corresponding eigenvalues do not depend on n and are therefore $(N-1)$-fold degenerated

$$\lambda_T^{(\mathbf{k})} \;=\; \mathbf{k}^2 \;+\; \frac{V'(\Phi)}{\Phi}\,. \tag{7.17}$$

Therewith, all eigenvalues are determined and the first-order term (7.7) reads in analogy to (2.84)

$$V_{\text{eff}}^{(1)}(\Phi) \;=\; -\,\frac{\mathrm{v}}{2}\int\frac{d^Dk}{(2\pi)^D}\Big[\ln\lambda_L^{(\mathbf{k})} \;+\; (N-1)\ln\lambda_T^{(\mathbf{k})}\Big]\,. \tag{7.18}$$

The remaining momentum integrals have already been solved in (4.24). Thus, we obtain

$$V_{\text{eff}}^{(1)}(\Phi) \;=\; \frac{\mathrm{v}\,\Gamma\big(-D/2\big)}{2\,(4\pi)^{D/2}}\left\{\,\big[V''(\Phi)\big]^{D/2} + (N-1)\,\left[\frac{V'(\Phi)}{\Phi}\right]^{D/2}\right\}. \tag{7.19}$$

The integral over the momentum space in (7.18) can be regarded as the field-theoretic analogy of the Matsubara sum (2.84) in quantum statistics. Therefore, it is obvious to define longitudinal and transversal Φ-dependent masses analogously to (2.81):

$$m_L^2(\Phi) \;=:\; V''(\Phi)\,, \qquad m_T^2(\Phi) \;=:\; \frac{V'(\Phi)}{\Phi}\,. \tag{7.20}$$

Since we assume a rotationally symmetric potential, the masses (7.20) only depend on the modulus of the background. Specializing to the potential (1.1), the masses (7.20) reduce to

$$m_L^2(\Phi) \;\;=:\;\; m^2 \;+\; \frac{g}{2}\,\Phi^2\,, \tag{7.21}$$

$$m_T^2(\Phi) \;\;=:\;\; m^2 \;+\; \frac{g}{6}\,\Phi^2\,. \tag{7.22}$$

7.3. Calculation of Propagator

For all calculations in higher orders, we need the propagator $G_{ij}(\mathbf{x},\mathbf{x}')$ which we derive next. It is defined as a generalization of (4.41) by the functional inverse of the integral kernel (7.9)

$$\int d^D x'\; G^{-1}_{ij}(\mathbf{x},\mathbf{x}')\, G_{jk}(\mathbf{x}',\mathbf{x}'') \;=\; \delta_{ik}\,\delta(\mathbf{x}-\mathbf{x}'')\,. \tag{7.23}$$

Inserting (7.12) and (7.20) into (7.9), the decomposition of the integral kernel into longitudinal and transversal parts reads

$$G^{-1}_{ij}(\mathbf{x},\mathbf{x}') \;=\; \left\{ P^L_{ij}\Big[-\Delta_x + m_L^2(\Phi)\Big] \;+\; P^T_{ij}\Big[-\Delta_x + m_T^2(\Phi)\Big] \right\} \delta(\mathbf{x}-\mathbf{x}')\,. \tag{7.24}$$

The coefficients of the Fourier transform

$$G^{-1}_{ij}(\mathbf{x},\mathbf{x}') \;=\; \int \frac{d^D k}{(2\pi)^D}\, G^{-1}_{ij}(\mathbf{k})\, e^{-\imath\mathbf{k}(\mathbf{x}-\mathbf{x}')}\,. \tag{7.25}$$

can therefore similarly be written as a sum of longitudinal and transversal contributions

$$G^{-1}_{ij}(\mathbf{k}) \;=\; P^L_{ij}\left[\mathbf{k}^2 + m_L^2(\Phi)\right] \;+\; P^T_{ij}\left[\mathbf{k}^2 + m_T^2(\Phi)\right]. \tag{7.26}$$

Inserting the Fourier representations

$$G_{jk}(\mathbf{x}',\mathbf{x}'') \;=\; \int \frac{d^D k'}{(2\pi)^D}\, G_{jk}(\mathbf{k})\, e^{-\imath\mathbf{k}'(\mathbf{x}'-\mathbf{x}'')}\,, \tag{7.27}$$

$$\delta(\mathbf{x}-\mathbf{x}'') \;=\; \int \frac{d^D k}{(2\pi)^D}\, e^{-\imath\mathbf{k}(\mathbf{x}-\mathbf{x}'')}\,, \tag{7.28}$$

as well as (7.25) into (7.23) and performing the $\mathbf{x}'$- and $\mathbf{k}'$-integrations, we obtain

$$\int \frac{d^D k}{(2\pi)^D}\, G^{-1}_{ij}(\mathbf{k})\, G_{jk}(\mathbf{k})\, e^{-\imath\mathbf{k}(\mathbf{x}-\mathbf{x}'')} \;=\; \int \frac{d^D k}{(2\pi)^D}\, \delta_{ik}\, e^{-\imath\mathbf{k}(\mathbf{x}-\mathbf{x}'')}\,. \tag{7.29}$$

Both integrands imply the relation

$$G^{-1}_{ij}(\mathbf{k})\, G_{jk}(\mathbf{k}) \;=\; \delta_{ik}\,. \tag{7.30}$$

Because of orthonormality, the Fourier transform of the propagator has a decomposition into longitudinal and transversal part analogously to the integral kernel (7.26)

$$G_{ij}(\mathbf{k}) \;=\; P^L_{ij}\, G_L(\mathbf{k}) \;+\; P^T_{ij}\, G_T(\mathbf{k})\,, \tag{7.31}$$

which enables us to determine longitudinal and transversal propagators in Fourier space:

$$G_L(\mathbf{k}) \;=\; \frac{1}{\mathbf{k}^2 + m_L^2(\Phi)}\,, \qquad G_T(\mathbf{k}) \;=\; \frac{1}{\mathbf{k}^2 + m_T^2(\Phi)}\,. \tag{7.32}$$

With respect to (7.26) and (7.31), the full propagator results in

$$G_{ij}(\mathbf{x},\mathbf{x}') \;=\; P^L_{ij}\, G_L(\mathbf{x},\mathbf{x}') \;+\; P^T_{ij}\, G_T(\mathbf{x},\mathbf{x}')\,, \tag{7.33}$$

with the longitudinal and transversal parts

$$G_L(\mathbf{x},\mathbf{x}') \;=\; \int \frac{d^Dk}{(2\pi)^D}\,\frac{1}{\mathbf{k}^2+m_L^2(\Phi)}\,e^{-i\mathbf{k}(\mathbf{x}-\mathbf{x}')}\,, \tag{7.34}$$

$$G_T(\mathbf{x},\mathbf{x}') \;=\; \int \frac{d^Dk}{(2\pi)^D}\,\frac{1}{\mathbf{k}^2+m_T^2(\Phi)}\,e^{-i\mathbf{k}(\mathbf{x}-\mathbf{x}')}\,. \tag{7.35}$$

7.4. Effective Potential in Second Loop Order

Now we come back to the interaction part of the effective potential (7.6). The expectation values are reduced to products of the propagator (7.33) by applying Wick contractions and we obtain two second-order terms analogously to (4.39). In order to attribute them to Feynman diagrams, we briefly transfer the Feynman rules (4.40) and (4.42) to the present case of a rotationally symmetric potential $V(\Phi)$ consisting of N constant background fields $\mathbf{\Phi}\equiv(\Phi_1,\Phi_2,\cdots,\Phi_N)$:

(1) All vertices and their outgoing lines are denoted arbitrarily.

(2) A propagator $G_{ij}(\mathbf{x},\mathbf{y})$ corresponds to a line connecting lines i and j between the vertices $\mathbf{x}$ and $\mathbf{y}$

$$\mathbf{x} \overset{\;i\quad j\;}{\text{———}} \mathbf{x}' \quad\equiv\quad G_{ij}(\mathbf{x},\mathbf{x}')\,, \tag{7.36}$$

with the propagator defined by (7.33)–(7.35).

(3) n outgoing lines from a vertex $\mathbf{x}$ represent the integration

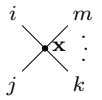

$$\equiv\; -V_{ijk\cdots m}(\Phi)\int d^Dx \tag{7.37}$$

over all propagators connected with the vertex $\mathbf{x}$ and the partial derivatives defined in (7.5).

With regard to (7.36) and (7.37), we identify the second-order diagrams which have to be one-particle irreducible with

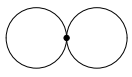

$$= \quad -V_{ijkl}(\Phi)\int d^Dx\; G_{ij}(\mathbf{x},\mathbf{x})\; G_{kl}(\mathbf{x},\mathbf{x})\,, \tag{7.38}$$

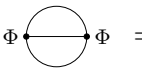

$$= V_{ijk}(\Phi)\; V_{lmn}(\Phi)\int d^Dx\int d^Dx'\; G_{il}(\mathbf{x},\mathbf{x}')\; G_{jm}(\mathbf{x},\mathbf{x}')\; G_{kn}(\mathbf{x},\mathbf{x}')\,. \tag{7.39}$$

Our proceeding is the same as the one in quantum mechanics: we express the higher derivatives in terms of projection operators, decompose the propagators into longitudinal and transversal parts and perform all contractions of the resulting projection operators. To this end, we calculate the third and fourth derivatives of the rotationally symmetric potential $V(\Phi)$ in accordance with (7.5), yielding

$$V_{ijk}(\Phi) \;=\; P^L_{ijk}\,V'''(\Phi) \,+\, P^T_{ijk}\left[\frac{V''(\Phi)}{\Phi} \,-\, \frac{V'(\Phi)}{\Phi^2}\right], \tag{7.40}$$

$$V_{ijkl}(\Phi) \;=\; P^L_{ijkl}\,V^{(4)}(\Phi) \,+\, P^T_{ijkl}\,\frac{V'''(\Phi)}{\Phi} \,+\, P^E_{ijkl}\left[\frac{V''(\Phi)}{\Phi^2} \,-\, \frac{V'(\Phi)}{\Phi^3}\right]. \tag{7.41}$$

Here, we have introduced the projection operators of third order

$$P^L_{ijk} \,:=\, \frac{\Phi_i\,\Phi_j\,\Phi_k}{\Phi^3}\,, \qquad P^T_{ijk} \,:=\, \delta_{ij}\frac{\Phi_k}{\Phi} \,+\, \delta_{ik}\frac{\Phi_j}{\Phi} \,+\, \delta_{jk}\frac{\Phi_i}{\Phi} \,-\, 3\,P^L_{ijk}\,, \tag{7.42}$$

and of fourth order

$$P^L_{ijkl} \;=\; \frac{\Phi_i\,\Phi_j\,\Phi_k\,\Phi_l}{\Phi^4}\,, \tag{7.43}$$

$$P^T_{ijkl} \;=\; \delta_{ij}\frac{\Phi_k\Phi_l}{\Phi^2} + \delta_{ik}\frac{\Phi_j\Phi_l}{\Phi^2} + \delta_{il}\frac{\Phi_j\Phi_k}{\Phi^2} + \delta_{jk}\frac{\Phi_i\Phi_l}{\Phi^2} + \delta_{jl}\frac{\Phi_i\Phi_k}{\Phi^2} + \delta_{kl}\frac{\Phi_i\Phi_j}{\Phi^2} - 6\,P^L_{ijkl}\,, \tag{7.44}$$

$$P^E_{ijkl} \;=\; \delta_{ij}\,\delta_{kl} \,+\, \delta_{ik}\,\delta_{jl} \,+\, \delta_{il}\,\delta_{jk} \,-\, 3\,P^L_{ijkl} \,-\, 3\,P^T_{ijkl}\,. \tag{7.45}$$

Their properties correspond to those of the operators (2.121)–(2.127) in quantum statistics after replacing $X_i \to \Phi_i$. Inserting (7.33) and (7.41) into (7.38), the contractions of the projection operators yield

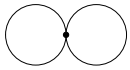

$$\begin{aligned} &= -\int d^Dx \left\{ G_L^2(\mathbf{x},\mathbf{x})\,V^{(4)}(\Phi) \,+ (N^2-1)\,G_T^2(\mathbf{x},\mathbf{x})\left[\frac{V''(\Phi)}{\Phi^2} \,-\, \frac{V'(\Phi)}{\Phi^3}\right] \right. \\ &\qquad \left. + 2\,(N-1)\,G_L(\mathbf{x},\mathbf{x})\,G_T(\mathbf{x},\mathbf{x})\left[\frac{V'''(\Phi)}{\Phi} \,-\, \frac{2\,V''(\Phi)}{\Phi^2} \,+\, \frac{2\,V'(\Phi)}{\Phi^3}\right]\right\}. \end{aligned} \tag{7.46}$$

The $\mathbf{x}$-integration merely leads to a volume factor v since all propagators are local. The remaining momentum integrals (7.34) and (7.35) amount to simple Feynman integrals (5.5), thus (7.46) results in

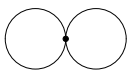

$$\begin{aligned} &= -\,\mathrm{v}\,\frac{\Gamma^2\big(1-D/2\big)}{(4\pi)^D}\left\{ V^{(4)}(\Phi)\left[m_L^2(\Phi)\right]^{D-2} \right. \\ &\qquad + 2\,(N-1)\left[\frac{V'''(\Phi)}{\Phi} - \frac{2\,V''(\Phi)}{\Phi^2} + \frac{2\,V'(\Phi)}{\Phi^3}\right]\left[m_L^2(\Phi)\right]^{D/2-1}\left[m_T^2(\Phi)\right]^{D/2-1} \\ &\qquad \left. + (N^2-1)\left[\frac{V''(\Phi)}{\Phi^2} - \frac{V'(\Phi)}{\Phi^3}\right]\left[m_T^2(\Phi)\right]^{D-2}\right\}. \end{aligned} \tag{7.47}$$

Specializing (7.47) to the potential (1.1), we obtain

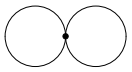

$$= -\mathrm{v}\,\frac{\Gamma^2\big(1-D/2\big)}{(4\pi)^D}\,g\,\Big\{\big[m_L^2(\Phi)\big]^{D-2}+\frac{N^2-1}{3}\,\big[m_T^2(\Phi)\big]^{D-2} + \frac{2\,(N-1)}{3}\,\big[m_L(\Phi)\big]^{D/2-1}\,\big[m_T(\Phi)\big]^{D/2-1}\Big\}, \tag{7.48}$$

with the longitudinal and transversal mass (7.21) and (7.22), respectively. For $N=1$ field, (7.48) coincides with our previous result (4.49).

In order to calculate the sunset diagram (7.39), we insert (7.33) and (7.40) and perform all contractions of the projection operators, yielding

$$\begin{aligned} &= \int d^Dx\,d^Dx'\Big\{G_L^3(\mathbf{x},\mathbf{x}')\,\big[V'''(\Phi)\big]^2 \\ &\qquad + 3\,(N-1)\,G_L(\mathbf{x},\mathbf{x}')\,G_T^2(\mathbf{x},\mathbf{x}')\left[\frac{V''(\Phi)}{\Phi}-\frac{V'(\Phi)}{\Phi^2}\right]^2\Big\} \\ &\equiv \big[V'''(\Phi)\big]^2\,J_1(D)+3\,(N-1)\left[\frac{V''(\Phi)}{\Phi}-\frac{V'(\Phi)}{\Phi^2}\right]^2 J_2(D)\,. \end{aligned} \tag{7.49}$$

The integral $J_1(D)$ coincides with the normal sunset integral (D.1), where the mass M^2 has to be replaced by $m_L^2(\Phi)$

$$\begin{aligned} J_1(D) &= \int d^Dx\,d^Dx'\int\frac{d^Dk\,d^Dk'\,d^Dk''}{(2\pi)^{3D}}\,\frac{e^{-\imath(\mathbf{k}+\mathbf{k}'+\mathbf{k}'')(\mathbf{x}-\mathbf{x}')}}{\big[\mathbf{k}^2+m_L^2(\Phi)\big]\,\big[\mathbf{k}'^2+m_L^2(\Phi)\big]\,\big[\mathbf{k}''^2+m_L^2(\Phi)\big]} \\ &= \mathrm{v}\int\frac{d^Dk\,d^Dk'}{(2\pi)^{2D}}\,\frac{1}{\mathbf{k}^2+m_L^2(\Phi)}\,\frac{1}{\mathbf{k}'^2+m_L^2(\Phi)}\,\frac{1}{(\mathbf{k}+\mathbf{k}')^2+m_L^2(\Phi)} \qquad (7.50) \\ &\equiv \mathrm{v}\,I(D)\,. \qquad (7.51) \end{aligned}$$

The second integral $J_2(D)$ differs from $J_1(D)$ in so far as both longitudinal and transversal masses occur, which complicates the calculation crucially

$$\begin{aligned} J_2(D) &= \int d^Dx\,d^Dx'\int\frac{d^Dk\,d^Dk'\,d^Dk''}{(2\pi)^{3D}}\,\frac{e^{-\imath(\mathbf{k}+\mathbf{k}'+\mathbf{k}'')(\mathbf{x}-\mathbf{x}')}}{\big[\mathbf{k}^2+m_L^2(\Phi)\big]\,\big[\mathbf{k}'^2+m_T^2(\Phi)\big]\,\big[\mathbf{k}''^2+m_T^2(\Phi)\big]} \\ &= \mathrm{v}\int\frac{d^Dk\,d^Dk'}{(2\pi)^{2D}}\,\frac{1}{\mathbf{k}^2+m_L^2(\Phi)}\,\frac{1}{\mathbf{k}'^2+m_T^2(\Phi)}\,\frac{1}{(\mathbf{k}+\mathbf{k}')^2+m_T^2(\Phi)} \\ &\equiv \mathrm{v}\;\mathcal{I}\big(m_L^2(\Phi),m_T^2(\Phi),m_T^2(\Phi)\big)\,. \qquad (7.52) \end{aligned}$$

Therefore, the evaluation of (7.52) is relegated to Appendix E. Both the normal sunset $J_1(D)$ and the integral $J_2(D)$ have a pole for $D=3$. We adopt the result from (E.59) in ε-expansion

for $D=3+\varepsilon$

$$J_2(D=3+\varepsilon) = -\frac{\mathrm{v}}{32\pi^2}\frac{1}{\varepsilon}+\frac{\mathrm{v}}{32\pi^2}\Bigg\{-\gamma+1+\ln 4\pi+\ln\frac{m_L(\Phi)}{\mu} - \ln\left(\frac{2\,m_T(\Phi)-m_L(\Phi)}{\mu}\right)-2\ln\left(\frac{m_L(\Phi)+2\,m_T(\Phi)}{\mu}\right)\Bigg\}+\mathcal{O}(\varepsilon)\,. \quad (7.53)$$

Finally, we insert (D.15), (7.51), and (7.53) into (7.49) and specialize in the potential (1.1):

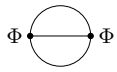

$$= \frac{g^2\,\Phi^2\,\mathrm{v}}{32\,\pi^2}\Bigg\{-\frac{1}{\varepsilon}-\gamma+1+\ln\frac{4\pi}{9}-2\ln\frac{m_L(\Phi)}{\mu}+\frac{N-1}{3}\Bigg[-\frac{1}{\varepsilon}-\gamma+1 +\ln 4\pi+\ln\frac{m_L(\Phi)}{\mu}-\ln\left(\frac{2\,m_T(\Phi)-m_L(\Phi)}{\mu}\right) -2\ln\left(\frac{m_L(\Phi)+2\,m_T(\Phi)}{\mu}\right)\Bigg]\Bigg\}+\mathcal{O}(\varepsilon)\,. \quad (7.54)$$

Note that for $N=1$ field, (7.54) reduces to our previous result (5.18).

7.5. Renormalization of Effective Potential

The divergent part of (7.54) does not depend on the number N of field components and is, thus, analogous to the one in the case of $N=1$ field (5.18). Hence, we may use our previous renormalization calculation (5.20). Inserting (7.19), (7.48), and (7.54) into (5.19), the renormalized effective potential in second loop order for $D=3$ dimensions and volume $\mathrm{v}=1$ results in

$$\begin{aligned} V_{\text{eff}}^{(r)}(\Phi) &= \frac{1}{2}\,m_r^2\,\Phi^2+\frac{g}{24}\,\Phi^4-\frac{\hbar}{12\,\pi}\Big\{m_L^3(\Phi)+(N-1)\,m_T^3(\Phi)\Big\} \\ &+ \frac{\hbar^2\,g}{128\,\pi^2}\Big\{m_L^2(\Phi)+\frac{N^2-1}{3}\,m_T^2(\Phi)+\frac{2\,(N-1)}{3}\,m_L(\Phi)\,m_T(\Phi)\Big\} \\ &+ \frac{\hbar^2\,g^2\Phi^2}{384\,\pi^2}\Bigg\{2\ln\frac{m_L(\Phi)}{\mu}-\ln\frac{4\pi}{9}-1+\gamma-\frac{N-1}{3}\Bigg[-\gamma+1+\ln 4\pi+\ln\frac{m_L(\Phi)}{\mu} \\ &- \ln\left(\frac{2\,m_T(\Phi)-m_L(\Phi)}{\mu}\right)-2\ln\left(\frac{m_L(\Phi)+2\,m_T(\Phi)}{\mu}\right)\Bigg]\Bigg\}\,. \end{aligned} \quad (7.55)$$

Here, we have used again the artificial smallness parameter $\hbar$. In the case of $N=1$ field, this result coincides with (5.21) as required.

8. Variational Perturbation Theory in Statistical Field Theory

Now we proceed to VPT in statistical field theory. At the beginning of this chapter, we argue that an optimization of the effective potential requires its resummation. Afterwards, we apply VPT to the renormalized effective potential in $D=3$ dimensions. As explained in Chapter 5, we have renormalization invariance as we are dealing with a superrenormalizable theory. Thus, we cannot obtain a unique effective potential which would yield a unique ground-state energy. The only actual numerical quantity we might extract from the effective potential is the condensation energy E_c which is invariant with respect to renormalization. This quantity can immediately be read off from a potential by means of the difference between zero and the minimum. Ground-state energies obtained from the optimization of the effective potential are not significant and can therefore not be compared with numerically calculated ones as done in quantum mechanics. However, we apply VPT nevertheless to investigate whether this is, in principle, possible. Analogously to quantum mechanics, we choose one and two variational parameters, which corresponds to the effective potential for one and for several fields. Subsequently, we check whether the phase transition is still continuous after renormalizing and resumming the effective potential. At the end of this chapter, we consider the large-N limit and show that the result from variational resummation passes into the one obtained from the Hubbard-Stratonovich transformation.

8.1. Necessity of Resummation

Without any variational parameters, the effective potential could merely be optimized with respect to the background field Φ. This, however, is impossible since the effective potential turns out to diverge when it is evaluated at the optimal background field. For this reason, it is indispensable to resum it, which we demonstrate in this section.

We try then to optimize the unresummed effective potential by means of the usual procedure [26]. To this end, we take the first derivative of the effective potential (7.55) with respect to Φ^2. This is more reasonable than differentiating it regarding Φ, which would include the solution $\Phi = 0$ belonging to the normal phase. Afterwards, we expand the square of the background in powers of $\hbar$ up to the second order

$$\Phi^2 \;=\; \Phi_0^2 \,+\, \hbar\,\Phi_1^2 \,+\, \hbar^2\,\Phi_2^2 \,+\cdots\,, \tag{8.1}$$

and insert this ansatz into the derivative of the effective potential. The resulting expression is expanded up to the second order in $\hbar$ and set to zero, yielding an equation of the form

$$\frac{\partial\, V_{\text{eff}}(\Phi)}{\partial\,\Phi^2} \;=\; C_0(\Phi_0^2) \,+\, \hbar\, C_1(\Phi_0^2,\Phi_1^2) \,+\, \hbar^2\, C_2(\Phi_0^2,\Phi_1^2,\Phi_2^2) \,+\, \mathcal{O}(\hbar^3) \;\stackrel{!}{=}\, 0\,. \tag{8.2}$$

The explicit expressions of the coefficients in (8.2) read

$$C_0(\Phi_0^2) = m^2 + \frac{g}{6}\,\Phi_0^2\,, \qquad C_1(\Phi_0^2,\Phi_1^2) = \frac{g}{6}\,\Phi_1^2 - \frac{g}{12\,\pi}\left[\frac{N-1}{2}\,m_T(\Phi_0) - \frac{3}{2}\,m_L(\Phi_0)\right], \quad (8.3)$$

$$\begin{aligned} C_2(\Phi_0^2,\Phi_1^2,\Phi_2^2) = {} & \frac{g^2}{192\,\pi^2}\Bigg\{\gamma - 1 - \ln\frac{4\pi}{9} + \ln m_L^2(\Phi_0) + \frac{N-1}{3}\Bigg[\gamma - 1 - \ln 4\pi \\ & + \ln\big[2m^2 + m_T^2(\Phi_0)\big] + \ln\big[2m_T(\Phi_0) + m_L(\Phi_0)\big] - \ln m_L(\Phi_0)\Bigg]\Bigg\} \\ & \frac{g^2}{128\,\pi^2}\left\{1 + \frac{N^2-1}{9} + \frac{N-1}{3}\frac{m_T(\Phi_0)}{m_L(\Phi_0)} + \frac{N-1}{9}\frac{m_L(\Phi_0)}{m_T(\Phi_0)}\right\} + \frac{g^2\Phi_0^2}{384\,\pi^2}\Bigg\{\frac{1}{m_L^2(\Phi_0)} \\ & + \frac{N-1}{3}\left[\frac{1}{6\,m^2 + 3\,m_T^2(\Phi_0)} - \frac{1}{2\,m_L^2(\Phi_0)} + \frac{2\,m_L(\Phi_0) + 3\,m_T(\Phi_0)}{6\,m_L(\Phi_0)\,m_T(\Phi_0)\big[2\,m_T(\Phi_0) + m_L(\Phi_0)\big]}\right]\Bigg\} \\ & + \frac{g}{6}\,\Phi_2^2 - \frac{g^2\Phi_1^2}{12\,\pi}\left[\frac{N-1}{24\,m_T(\Phi_0)} - \frac{3}{8\,m_L(\Phi_0)}\right], \end{aligned} \quad (8.4)$$

with the longitudinal and transversal masses defined in (7.21) and (7.22), respectively. Hence, (8.2) leads to a system of three equations $C_i = 0$, $i = 0, 1, 2$, each corresponding to the respective order of $\hbar$. This system for the extremizing background Φ can be solved consecutively. The first two equations ($i = 0, 1$) are solved without further problems. With regard to (8.3), they lead to the solutions

$$\Phi_0^2 \;=\; -\frac{6\,m^2}{g}\,, \qquad \Phi_1^2 \;=\; \frac{3\sqrt{-2m^2}}{4\,\pi}\,. \quad (8.5)$$

However, if we insert these solutions into the second-order coefficient (8.4), it becomes infinite. This matter of fact becomes obviously when we take (7.22) into account and identify the solution of zeroth order in (8.5) with the transversal mass $m_T^2(\Phi_0)$ being zero. Since this is the very same mass that is also written in the denominator in (8.4), the coefficient C_2 has a pole. Thus, the second-order contribution to the background becomes infinite and we have to resum the effective potential if we wish to proceed to higher loop orders.

8.2. Variational Resummation with One Parameter

In order to apply VPT with one variational parameter, we consider the effective potential for $N = 1$ real field. This case corresponds to $D = 1$ dimension in quantum mechanics. A higher number of fields would require two variational parameters. During the following calculations, we return to the renormalized effective potential (5.21) and omit the superscript r which distinguishes the renormalized potential from the unrenormalized one. Hence, we start with

$$\begin{aligned} V_{\text{eff}}(\Phi) \;=\; & \frac{1}{2}\,m^2\,\Phi^2 \;+\; \frac{g}{24}\,\Phi^4 \;-\; \frac{\hbar}{12\,\pi}\,\big(M^2\big)^{3/2} \;+\; \frac{\hbar^2\,g}{128\,\pi^2}\,M^2 \\ & + \frac{\hbar^2\,g^2\,\Phi^2}{384\,\pi^2}\ln\frac{M^2}{\mu^2} \;-\; \frac{\hbar^2\,g^2\,\Phi^2}{384\,\pi^2}\left(\ln\frac{4\pi}{9} + 1 - \gamma\right) + \mathcal{O}(\hbar^3)\,, \end{aligned} \quad (8.6)$$

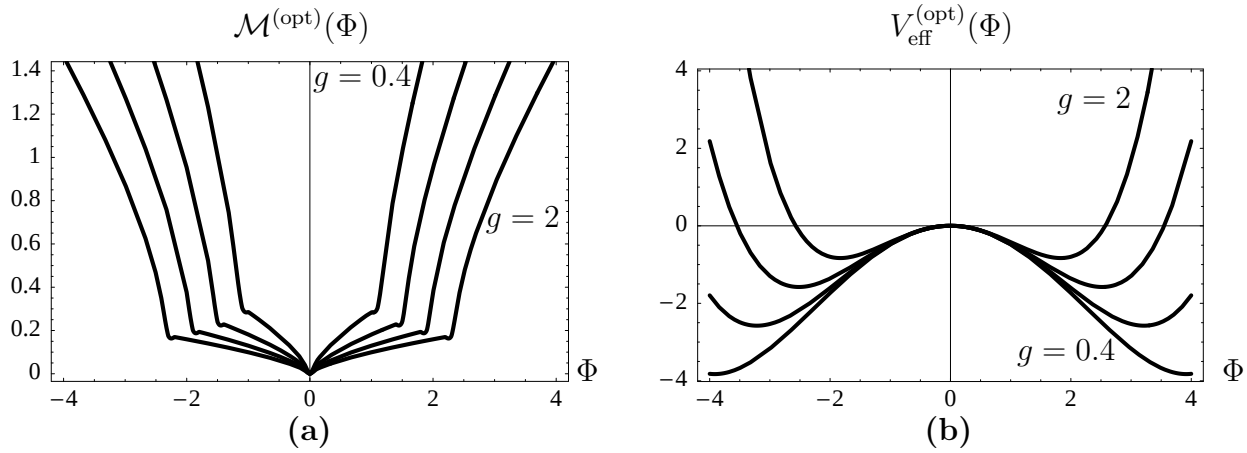

Figure 8.1.: Optimized variational parameter **(a)** and optimized effective potential **(b)** for the effective potential (8.9) in second loop order ($N = 1$) with coupling constants $g = 0.4$, $g = 0.6$, $g = 1$, and $g = 2$.

where M^2 is the Φ-dependent mass (4.26). In the following, we set the mass parameter $\mu = 1$. In statistical field theory, the mass m plays the role of the frequency ω in quantum mechanics, see Section 4.2. Consequently, the square-root substitution (3.17) now refers to the mass. Analogously to (3.25), we choose the Φ-dependent mass (4.26)

$$M \longrightarrow \mathcal{M}\sqrt{1+\hbar\, r}\,, \tag{8.7}$$

$$r = \frac{1}{\hbar}\,\frac{M^2-\mathcal{M}^2}{\mathcal{M}^2}\,. \tag{8.8}$$

Our proceeding is as follows: we insert (8.7) into (8.6) and expand the resulting expression up to the second order with respect to $\hbar$. Afterwards, we resubstitute (8.8), yielding

$$\begin{aligned} V_{\mathrm{eff}}(\Phi,\mathcal{M}) &= \frac{1}{2}\,m^2\,\Phi^2 + \frac{g}{24}\,\Phi^4 + \frac{\hbar}{24\,\pi}\,\mathcal{M}^3 - \frac{\hbar\,M^2}{8\,\pi}\,\mathcal{M} - \frac{\hbar\,g\,\Phi^2}{16\,\pi}\mathcal{M} + \frac{\hbar^2\,g}{128\,\pi^2}\,\mathcal{M}^2 \\ &\quad - \frac{\hbar^2\,g^2\,\Phi^2}{384\,\pi^2}\Big(\ln\frac{4\pi}{9} + 1 - \gamma\Big) + \frac{\hbar^2\,g^2\,\Phi^2}{384\,\pi^2}\ln\mathcal{M}^2 + \mathcal{O}(\hbar^3)\,. \end{aligned} \tag{8.9}$$

Calculating the first derivative of (8.9) with respect to $\mathcal{M}$ and setting it to zero, we obtain the equation

$$\frac{\partial\, V_{\mathrm{eff}}(\Phi,\mathcal{M})}{\partial\mathcal{M}} = \frac{\hbar}{8\,\pi}\,\mathcal{M}^2 - \frac{\hbar\,M^2}{8\,\pi} - \frac{\hbar\,g\,\Phi^2}{16\,\pi} + \frac{\hbar^2\,g}{64\,\pi^2}\,\mathcal{M} + \frac{\hbar^2\,g^2\,\Phi^2}{192\,\pi^2\mathcal{M}} \stackrel{!}{=} 0\,. \tag{8.10}$$

The result of the numerical evaluation is shown in Figure 8.1 a for different values of the coupling constant g. In contrast to the corresponding quantum mechanical results in Figure 3.3, the optimized parameter turns out to be continuous for all coupling strengths. The effective potential yields real values for all Φ and is plotted in Figure 8.1 b. It reflects the typical shape of the double-well, the smaller the coupling constant, the more distinctive the barrier in the middle.

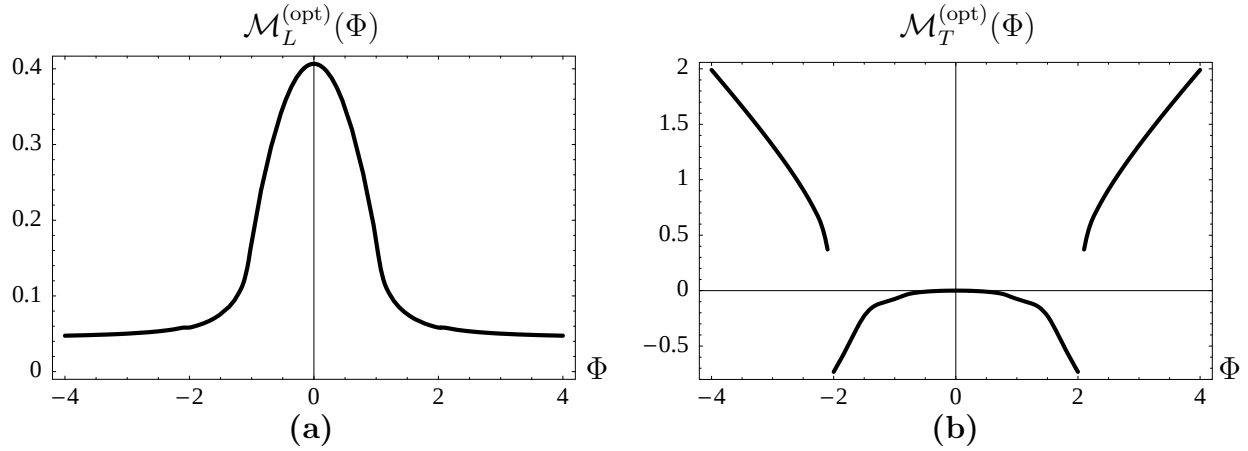

Figure 8.2.: Optimized longitudinal **(a)** and transversal **(b)** variational parameters for the effective potential (8.14) in second loop order ($N=2$) with coupling constant $g=2$.

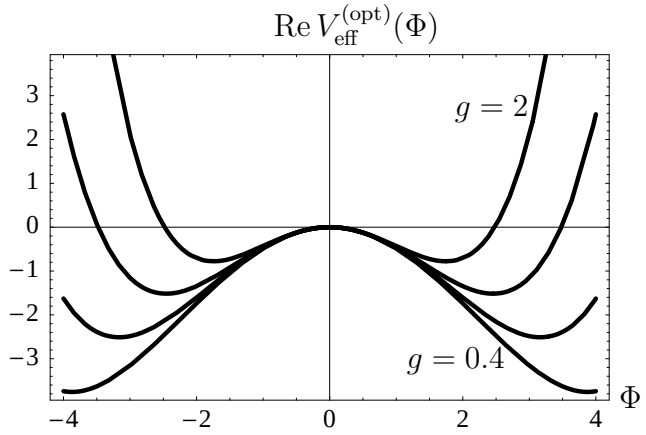

Figure 8.3.: Optimized effective potential (8.14) in second loop order ($N=2$) for coupling constants $g=0.4$, $g=0.6$, $g=1$, and $g=2$.

8.3. Variational Resummation with Two Parameters

In this section, we apply VPT with two variational parameters. To this end, we consider the effective potential for $N=2$ real fields, which reads in accordance with (7.55)

$$\begin{aligned} V_{\mathrm{eff}}(\Phi) &= \frac{1}{2}m^2\Phi^2 + \frac{g}{24}\Phi^4 - \frac{\hbar}{12\,\pi}\Big\{m_L^3(\Phi) + m_T^3(\Phi)\Big\} + \frac{\hbar^2\,g}{128\,\pi^2}\Big\{m_L^2(\Phi) + m_T^2(\Phi) \\ &\quad + \frac{2}{3}\,m_L(\Phi)\,m_T(\Phi)\Big\} + \frac{\hbar^2\,g^2\,\Phi^2}{384\,\pi^2}\Big\{\frac{5}{3}\ln m_L(\Phi) - \ln\frac{4\pi}{9} + \frac{4}{3}\,(\gamma-1) \\ &\quad - \frac{1}{3}\Big[\ln 4\pi - \ln\Big(2m_T(\Phi) - m_L(\Phi)\Big) - 2\ln\Big(m_L(\Phi) + 2m_T(\Phi)\Big)\Big]\Big\}. \end{aligned} \tag{8.11}$$

Here, we have again set the mass parameter $\mu = 1$. The effective potential (8.11) contains longitudinal and transversal Φ-dependent masses $m_L^2(\Phi)$ and $m_T^2(\Phi)$ as defined in (7.21) and (7.22), respectively. For this reason, it is straightforward to generalize (8.7) and (8.8) to two variational parameters $\mathcal{M}_M$, $\mathcal{M}_T$ by means of

$$m_L(\Phi) \longrightarrow \mathcal{M}_L \sqrt{1 + \hbar\, r_L}\,, \qquad m_T(\Phi) \longrightarrow \mathcal{M}_T \sqrt{1 + \hbar\, r_T}\,, \tag{8.12}$$

$$r_L = \frac{1}{\hbar}\,\frac{m_L^2(\Phi) - \mathcal{M}_L^2}{\mathcal{M}_L^2}\,, \qquad r_T = \frac{1}{\hbar}\,\frac{m_T^2(\Phi) - \mathcal{M}_T^2}{\mathcal{M}_T^2}\,. \tag{8.13}$$

Then, we insert (8.12) into (8.11), expand the resulting expression up the to second order in $\hbar$ and apply (8.13), which gives us the effective potential as a function of the variational parameters

$$\begin{aligned} V_{\text{eff}}(\Phi, \mathcal{M}_L, \mathcal{M}_T) \;=\; & \frac{1}{2}\, m^2\, \Phi^2 \,+\, \frac{g}{24}\, \Phi^4 \,-\, \frac{\hbar}{8\,\pi} \Big[m_L^2(\Phi)\, \mathcal{M}_L \,+\, m_T^2(\Phi)\, \mathcal{M}_T \Big] \\ & + \frac{\hbar}{24\,\pi} \Big[\mathcal{M}_L^3 \,+\, \mathcal{M}_T^3 \Big] \,+\, \frac{\hbar^2\, g}{128\,\pi^2} \left[\mathcal{M}_L^2 + \mathcal{M}_T^2 + \frac{2}{3}\, \mathcal{M}_L\, \mathcal{M}_T \right] \\ & + \frac{\hbar^2\, g^2\, \Phi^2}{384\,\pi^2} \left\{ \frac{5}{3} \ln \mathcal{M}_L - \ln \frac{4\pi}{9} \,+\, \frac{4}{3}\,(\gamma - 1) \right. \\ & \left. - \frac{1}{3} \left[\ln 4\pi - \ln\Big(2\, \mathcal{M}_T - \mathcal{M}_L \Big) - 2 \ln\Big(\mathcal{M}_L + 2\, \mathcal{M}_T \Big) \right] \right\}. \end{aligned} \tag{8.14}$$

We obtain the optimization equations for (8.14) by taking the first derivative with respect to both variational parameters $\mathcal{M}_L$ and $\mathcal{M}_T$ and setting them to zero

$$\begin{aligned} \frac{\partial\, V_{\text{eff}}(\Phi, \mathcal{M}_L, \mathcal{M}_T)}{\partial \mathcal{M}_L} \;=\; & \frac{\hbar}{8\,\pi} \Big[\mathcal{M}_L^2 - m_L^2(\Phi) \Big] + \frac{\hbar^2\, g}{64\,\pi^2} \Big[\mathcal{M}_L + \frac{1}{3} \mathcal{M}_T \Big] \\ & + \frac{\hbar^2\, g^2\, \Phi^2}{1152\,\pi^2} \left[\frac{5}{\mathcal{M}_L} - \frac{2\mathcal{M}_L}{4\,\mathcal{M}_T^2 - \mathcal{M}_L^2} + \frac{1}{\mathcal{M}_L + 2\,\mathcal{M}_T} \right] \stackrel{!}{=} 0\,, \end{aligned} \tag{8.15}$$

$$\begin{aligned} \frac{\partial\, V_{\text{eff}}(\Phi, \mathcal{M}_L, \mathcal{M}_T)}{\partial \mathcal{M}_T} \;=\; & \frac{\hbar}{8\,\pi} \Big[\mathcal{M}_T^2 - m_T^2(\Phi) \Big] + \frac{\hbar^2\, g}{64\,\pi^2} \Big[\mathcal{M}_T + \frac{1}{3}\, \mathcal{M}_L \Big] \\ & + \frac{\hbar^2\, g^2\, \Phi^2}{576\,\pi^2} \left[\frac{4\,\mathcal{M}_T}{4\,\mathcal{M}_T^2 - \mathcal{M}_L^2} + \frac{1}{\mathcal{M}_L + 2\,\mathcal{M}_T} \right] \stackrel{!}{=} 0\,. \end{aligned} \tag{8.16}$$

The actual simultaneous evaluation of (8.15) and (8.16) is done numerically. As it is shown in Figure 8.2, the plots of the optimized longitudinal and transversal variational parameters are quite different. The longitudinal parameter 8.2 a is continuous and always positive. Coming from large Φ, it increases and has a maximum at $\Phi = 0$. This is quite remarkable since the longitudinal parameter remains when choosing $N = 1$ field. In that case, however, the parameter shows an almost inverse behavior as it is shown in Figure 8.1 a. The transversal parameter in Figure 8.2 b jumps to negative values when approaching the origin, which does not correspond to a physical solution. Therefore, it is not surprising that the resulting

optimized effective potential in Figure 8.3 b becomes complex and, thus, non-physical itself near the origin. But coming from large values of Φ, the effective potential remains real until the minimum, which is the physically important region. Therefore, we have just continued the effective potential near the origin by plotting its real part. In spite of the differences regarding the variational parameter, the optimized effective potential in Figure 8.3 b has the same qualitative form as the one for $N=1$ field in Figure 8.1 b.

In contrast to the usual application of VPT [1, Ch. 5], we have applied the square-root substitutions (3.25) and (8.7) to the X-dependent frequency and the Φ-dependent mass, respectively. As the reason for this modification we gave the fact that the minima of the potential are shifted from zero. Such a generalized substitution (8.7) takes phase transitions into account. In the ordered phase, we can distinguish between longitudinal and transversal directions due to symmetry breakdown. Hence, we have two masses (7.21) and (7.22) and two variational parameters (8.12), each corresponding to the respective direction. In the $O(N)$-symmetric normal phase, longitudinal and transversal directions are equal and indeed, both masses (7.21) and (7.22) coincide and one single variational parameter remains.

8.4. Renormalization Invariance

We turn our attention once more to the renormalization invariance. Both results (5.21) and (6.46) represent two possible renormalized effective potentials for $N=1$. Since the only term they differ in does not depend on the mass, it is not affected by the square-root substitution (8.7) and vanishes consequently in the first derivative (8.10). For this reason, the optimized variational parameter $\mathcal{M}^{(\mathrm{opt})}$ is independent of the chosen renormalization. However, when we insert $\mathcal{M}^{(\mathrm{opt})}$ into the effective potential, different optimized potentials arise: (8.6) is specified to the renormalization (5.21) and differs from the one we would obtain for (6.46). Therefore, actual numerical values, for instance for the ground-state energy, have no significance. This consideration also holds, of course, for calculations with more than one field and two variational parameters.

8.5. Verification of Goldstone Theorem

In this section, we briefly check whether the Goldstone theorem is still preserved after renormalizing and resumming the effective potential. In accordance with (1.7), we have to verify that transversal masses, i.e., transversal curvatures, are zero at the minimum Φ_0 of the effective potential. To this end, we calculate the second derivatives of (7.55) and (8.14) with respect to the background field Φ and extract the transversal contribution by applying the transversal projection operator (7.10). In both cases, the effective potential is rotationally symmetric and the minimum is determined by the first partial derivative of the form

$$\left.\frac{\partial V_{\mathrm{eff}}(\Phi)}{\partial \Phi_i}\right|_{\Phi=\Phi_0} = \frac{\Phi_i}{\Phi}\left.\frac{\partial V_{\mathrm{eff}}(\Phi)}{\partial \Phi}\right|_{\Phi=\Phi_0} \stackrel{!}{=} 0 \quad \stackrel{\Phi_i\neq 0}{\longrightarrow} \quad \left.\frac{\partial V_{\mathrm{eff}}(\Phi)}{\partial \Phi}\right|_{\Phi=\Phi_0} = 0\,. \tag{8.17}$$

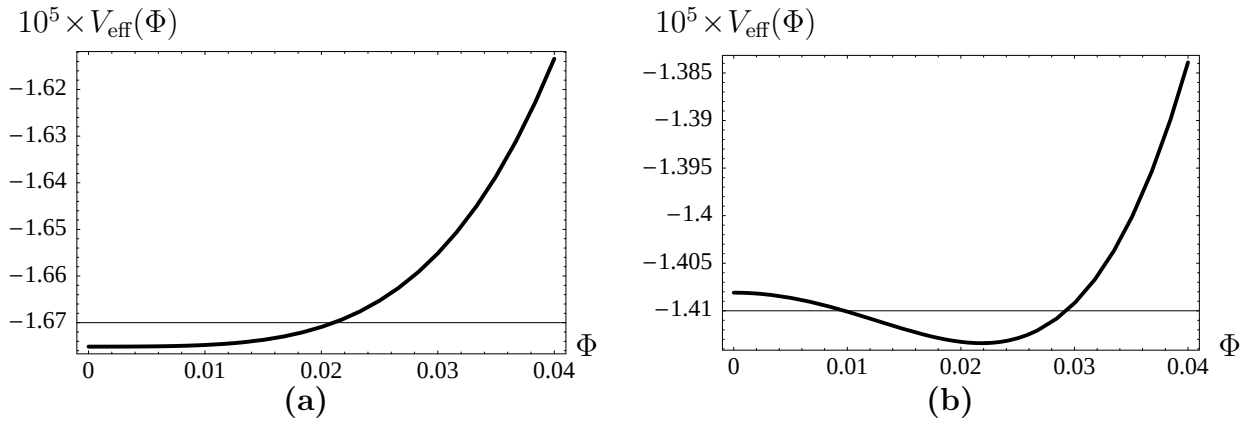

Figure 8.4.: Phase transition between the normal phase **(a)** for $m^2 = 0.0071$ and the ordered phase **(b)** for $m^2 = 0.0065$ of the effective potential (8.11) in second loop order without variational resummation ($N = 2$).

Here, we applied that we consider the ordered phase where the field expectation is nonzero. In terms of the projection operators (7.10), the second derivative of the effective potential reads

$$\frac{\partial^2 V_{\text{eff}}(\Phi)}{\partial\Phi_i\,\partial\Phi_j} \;=\; P^L_{ij}\,\frac{\partial^2 V_{\text{eff}}(\Phi)}{\partial\Phi^2} \;+\; P^T_{ij}\,\frac{1}{\Phi}\,\frac{\partial V_{\text{eff}}(\Phi)}{\partial\Phi}\,. \tag{8.18}$$

Due to (2.73), the longitudinal term in (8.18) vanishes when we apply the transversal projection operator (7.10). With regard to (2.71), (8.17), and (8.18), we verify the Goldstone theorem

$$P^T_{ij}\,\frac{\partial^2 V_{\text{eff}}(\Phi)}{\partial\Phi_i\,\partial\Phi_j}\bigg|_{\Phi=\Phi_0} \;=\; (N-1)\,\frac{\partial V_{\text{eff}}(\Phi)}{\partial\,\Phi}\bigg|_{\Phi=\Phi_0} \;=\; 0\,. \tag{8.19}$$

This calculation is valid for both (7.55) and (8.14). Thus, the Goldstone theorem is still preserved after renormalization and resummation.

8.6. Landau Expansion of Effective Potential

As already mentioned in the introduction, we can use the Landau expansion to investigate the order of the phase transition. Although we already know that the transition from the anharmonic potential to the mexican hat is continuous due to symmetry breakdown, we shall confirm this matter of fact by means of the Landau expansion and investigate the actual transition point m_c^2. Moreover, we discuss the importance of the sunset term (7.54) in connection with phase transitions.

We start with the effective potential (8.11), i.e., with $N = 2$ fields and without variational parameters. Figure 8.4 shows that there is, indeed, a transition from the normal to the

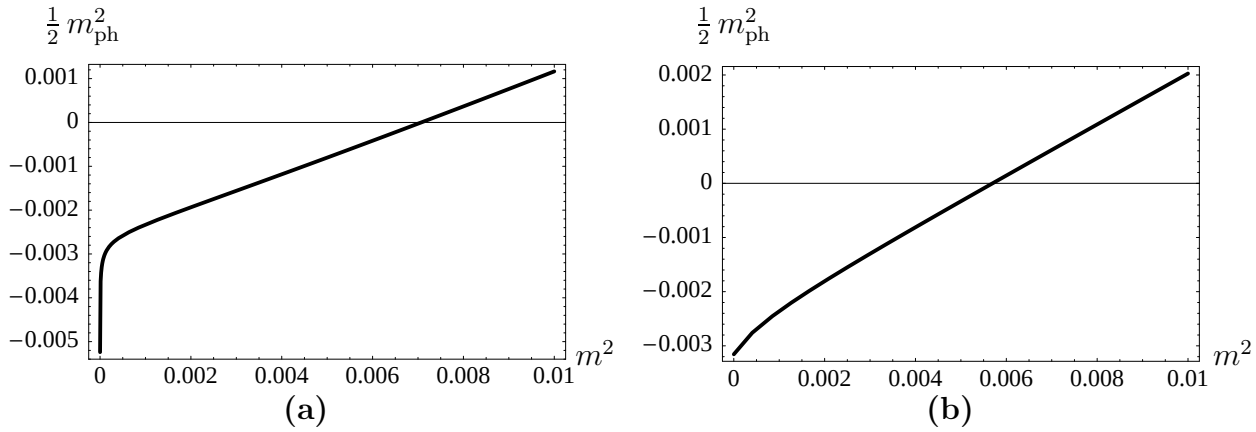

Figure 8.5.: Change of sign of the physical mass term for the effective potential in second loop order ($N=2$) without **(a)** and with **(b)** variational resummation. The roots occur at $m_c^2=0.00707$ and $m_c^2=0.00570$, respectively, indicating a continuous phase transition from the normal ($m^2_{\rm ph}>0$) to the ordered phase ($m^2_{\rm ph}<0$).

ordered phase. We read off from Figure 8.4 that the transition point lies in the interval $0.0065 < m_c^2 < 0.0071$ for natural units $\hbar = g = 1$. At a first instance, this result is quite astonishing since the potential itself is clearly separated into two phases at $m^2 = 0$, see Figure 1.3 a. The coefficient of Φ^2 in the effective potential, denoted as physical mass $m^2_{\rm ph}/2$ or $A/2$ with respect to (1.28), reads in accordance with (7.55)

$$\begin{aligned} m^2_{\rm ph} &= 2\,\frac{\partial\, V_{\rm eff}(\Phi)}{\partial\,\Phi^2}\bigg|_{\Phi=0} = m^2 - \frac{4\,\hbar\, g\, m}{24\,\pi} + \frac{\hbar^2 g^2}{72\,\pi^2} \\ &\quad - \frac{\hbar^2 g^2}{192\,\pi^2}\left[1-\gamma-\ln m^2 + \ln\frac{4\pi}{9} + \left(1-\gamma+\ln\frac{4\pi}{9} - 2\ln m\right)\right]. \end{aligned} \tag{8.20}$$

The root m_c^2 of (8.20) is numerically calculated to be $m_c^2=0.00707$ for natural units, which can also be read off from Figure 8.5 a. In accordance with (1.28) and (7.55), we also determine the coefficient B of Φ^4 at the critical point as follows:

$$B = 24\,\frac{\partial^2\, V_{\rm eff}(\Phi)}{\partial\left(\Phi^2\right)^2}\bigg|_{\Phi=0,m^2=m_c^2} = 12\,g + \frac{49\,g^3}{864\,\pi^2\,m_c^2} - \frac{5\,g^2}{12\,\pi\,m_c}\,. \tag{8.21}$$

This coefficient is positive for all values of the coupling constant g as demanded in order to guarantee stability.

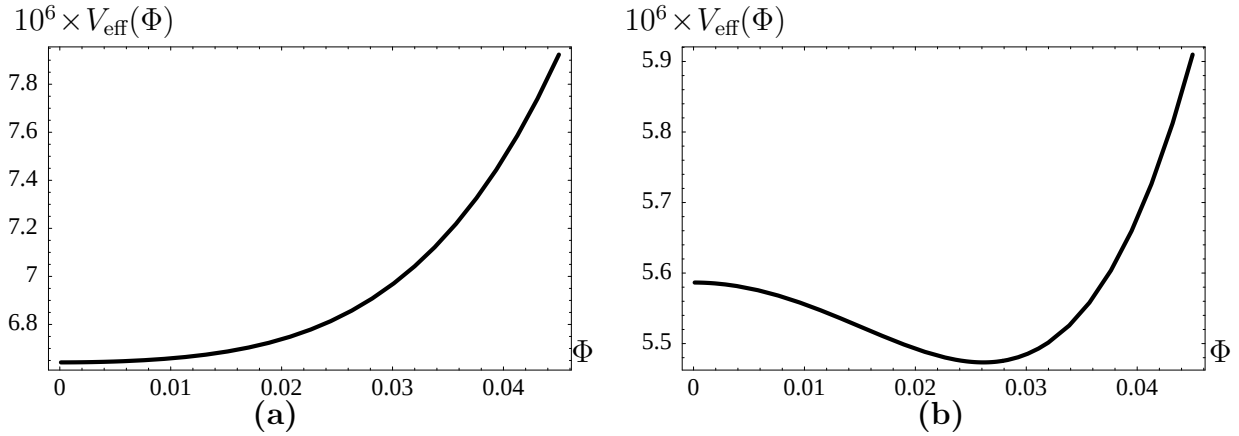

Figure 8.6.: Phase transition of the effective potential (8.14) in second loop order ($N=2$) after variational resummation between the normal phase **(a)** with $m^2=0.006$ and the ordered phase **(b)** for $m^2=0.005$.

8.7. Landau Expansion and Variational Perturbation Theory

When applying VPT, it is of crucial importance that the character of the phase transition remains conserved. In order to check this demand, we perform a Landau expansion of the effective potential (8.14) in second loop order after variational resummation. Afterwards, we study the resulting order of the phase transition. It is an interesting question whether the sunset term is indispensable or if it merely shifts the transition point. Therefore, we calculate a further Landau expansion of the effective potential without sunset term and investigate again the resulting order of the phase transition.

Starting from the effective potential (8.14) in full second loop order, both parameters $\mathcal{M}_L$ and $\mathcal{M}_T$ have to be expanded in powers of Φ^2:

$$\mathcal{M}_L = A_L + B_L\,\Phi^2 + C_L\,\Phi^4 + \cdots\,, \tag{8.22}$$
$$\mathcal{M}_T = A_T + B_T\,\Phi^2 + C_T\,\Phi^4 + \cdots\,. \tag{8.23}$$

Inserting this ansatz into the derivatives (8.15) and (8.16) and expanding them in powers of Φ^2 yields equations of the form

$$\frac{\partial\, V_{\text{eff}}(\Phi,\mathcal{M}_L,\mathcal{M}_T)}{\partial \mathcal{M}_L} = K_L^{(0)} + K_L^{(1)}\,\Phi^2 + K_L^{(2)}\,\Phi^4 + \cdots \stackrel{!}{=} 0\,, \tag{8.24}$$
$$\frac{\partial\, V_{\text{eff}}(\Phi,\mathcal{M}_L,\mathcal{M}_T)}{\partial \mathcal{M}_T} = K_T^{(0)} + K_T^{(1)}\,\Phi^2 + K_T^{(2)}\,\Phi^4 + \cdots \stackrel{!}{=} 0\,. \tag{8.25}$$

All six coefficients in (8.22) and (8.23) are numerically determined from (8.24) and (8.25) in a recursive way analogously to Section 8.1. Finally, we reinsert the coefficients (8.22) and

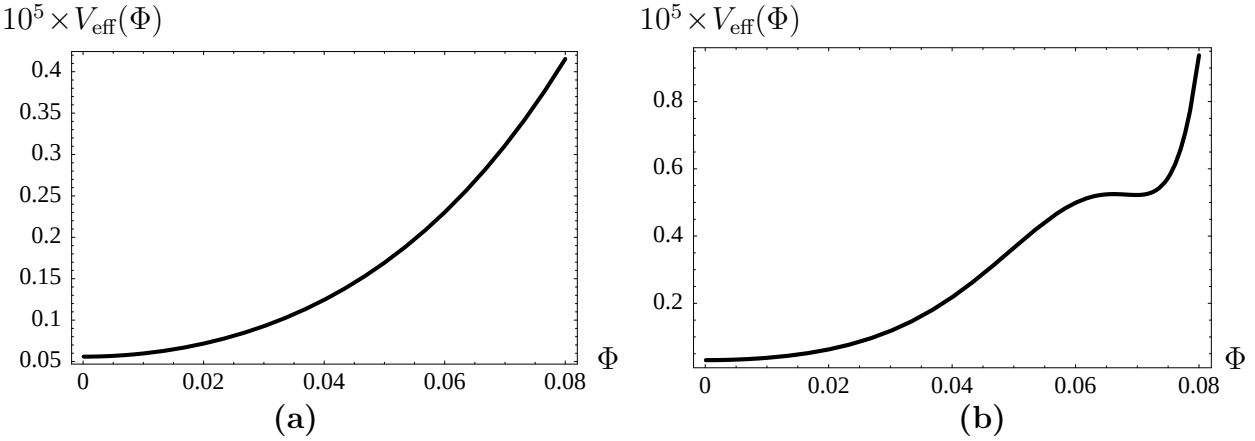

Figure 8.7.: The effective potential in second loop order ($N=2$) without sunset after variational resummation shows no continuous phase transition. We have chosen $m^2=0.005$ **(a)** and $m^2=0$ **(b)**. For m^2 being negative, the effective potential becomes even unstable.

(8.23) into (8.14). The resulting effective potential is plotted in Figure 8.6: the postulated transition of second order is clearly visible and can be located at $m_c^2=0.00570$ by numerical methods or graphically as it is done in Figure 8.5 b. However, the transition point is slightly shifted compared to the calculations without variational parameters where it was found from (8.20) at $m_c^2=0.00707$.

Now, we investigate the importance of the sunset term. Therefore, we neglect this term when performing the Landau expansion and and check subsequently, whether the transition remains continuous. We start again from (8.14) but omit the sunset terms $\sim g^2$. Thus, we have

$$\begin{aligned} V_{\text{eff}}(\Phi,\mathcal{M}_L,\mathcal{M}_T) &= \frac{1}{2}m^2\Phi^2+\frac{g}{24}\Phi^4-\frac{\hbar}{8\pi}\Big[m_L^2(\Phi)\mathcal{M}_L+m_T^2(\Phi)\mathcal{M}_T\Big]+\frac{\hbar}{24\pi}\Big[\mathcal{M}_L^3+\mathcal{M}_T^3\Big] \\ &\quad +\frac{\hbar^2}{8}\,\frac{g}{16\pi^2}\left[\mathcal{M}_L^2+\,\mathcal{M}_T^2+\frac{2}{3}\,\mathcal{M}_L\,\mathcal{M}_T\right]. \end{aligned} \tag{8.26}$$

Now we derive the Landau expansion in exactly the same manner as before. The solutions of the effective potential, however, turn out to be unstable for small masses and yield no actual physical result. Even close to the transition point when taking the sunset into account, no symmetry breaking can be observed. Figure 8.7 depicts a typical situation when coming from the normal phase. Thus, we conclude that the sunset term is of essential importance since it is responsible for conserving the character of the phase transition when applying VPT.

8.8. Field Expectation and Shift of Critical Point

In Ref. [39], the critical temperature shift for a homogeneous Bose-Einstein condensate has been calculated up to five loops as well as the perturbation expansion for the field expectation

value

$$\Phi^2 \;=\; \int \frac{d^3k}{(2\pi)^3}\;\frac{1}{\mathbf{k}^2+m^2}\,. \tag{8.27}$$

We check our calculations by further evaluating (8.27) for the shifted physical mass (8.20) instead of the bare mass m^2. The integral (8.27) has been calculated in (5.5), thus it remains to expand the result in g, yielding

$$\Phi^2 = -\frac{m}{4\pi} + \frac{(N+2)\,g}{12(4\pi)^2} - \frac{(N+2)\,g^2}{36(4\pi)^3\,m}\,\frac{1}{8}\left[-2+4\,\gamma+N+8\ln m - 4\ln\frac{4\pi}{9}\right] + \mathcal{O}(g^3). \tag{8.28}$$

The result coincides with the expansion in Ref. [39] only in the leading order. This is due to the fact that we started our calculations from the effective potential rather than from the effective action. Hence, we miss the contributions in the propagator that result from the renormalization of the wave function. These terms are of second and higher order with respect to g and therefore lead to deviations of the second-order term in (8.28) from the result in Ref. [39]. Moreover, we have an additional term linear in g since (8.28) is not expressed in terms of the physical mass following from (8.20). If we invert (8.20) and replace the bare mass m^2 by m_c^2 in (8.28), the first-order term vanishes.

In the introduction, we have mentioned that the order parameter is usually chosen to be zero in one phase and non-zero in the other. This matter of fact shall be verified here for the background Φ after variational resummation. To this end, we have plotted the minimum of the effective potential (8.14) as a function of the mass m^2. The result in Figure 8.8 a reproduces exactly the typical behavior of an order parameter. The transition point is equal to the one calculated in Figure 8.5 a.

We record the fact that the Landau expansion with and without resummation confirms the continuous transition even though at an other point than expected from the classical point of view. Indeed, quantum fluctuations shift the critical point as we shall now investigate in detail. The quadratic coefficient of the bare ϕ^4-potential (1.1) goes, of course, to zero for vanishing mass. Thus, the phase transition takes place at $m^2 = 0$. Taking quantum corrections into account, the quadratic coefficients equals (8.20), pointing out that quantum fluctuations induce corrections that do not vanish for small masses m^2. In fact, these corrections diverge to minus infinity due to the logarithmic term. This can also be read off from Figure 8.5. The bare mass m^2 is therefore shifted to a physical mass m^2_{ph} which determines the critical point. Since the leading correction is negative, the phase transition proceeds at $m^2_{\mathrm{ph}}=0$ but $m^2>0$. This result is an artifact of renormalization. Normally, adding a quartic term ϕ^4 means actually increasing the curvature, i.e., the effective coefficient of ϕ^2. Thus, we expect the original ϕ^2-coefficient to become smaller in order to yield a critical value. Regarding renormalization, it becomes the other way round: the trace-log term which yields the first-order correction is, of course, divergent. After dimensional regularization, the finite contribution in (7.55) is negative

$$\frac{1}{2}\,\mathrm{Tr}\ln G^{-1} \quad \overset{\text{dim. reg.}}{\Longrightarrow} \quad -\frac{\hbar}{12\pi}\Big[m_L^3(\Phi) + (N-1)\,m_T^3(\Phi)\Big]\,. \tag{8.29}$$

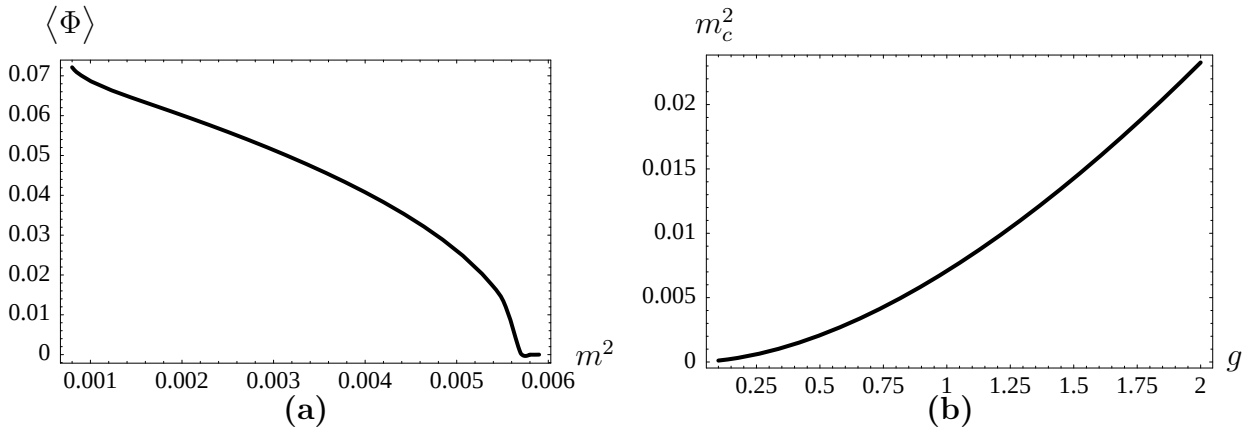

Figure 8.8.: The field expectation **(*a*)** of the effective potential (8.14) for $g = 1$ ($N = 2$) as a function of the mass shows the typical behavior of an order parameter. It is zero in the normal and non-zero in the ordered phase. The transition point at m_c^2 is shifted **(*b*)** with increasing coupling strength g.

Therefore, the mass term is shifted contrary to our intuition. The resulting transition point m_c^2 as a function of the coupling strength g is plotted in Figure 8.8 b. As it is shown in Figure 8.5, the transition point is slightly shifted to a smaller critical mass m_c^2 after resummation. It is impossible to attach a physical importance to this fact since it is likewise affected by renormalization.

Thus, we conclude that, at least, our qualitative finding $m_c^2 > 0$ is in accordance with the positive shift for a homogeneous Bose-Einstein condensate in the literature. There, both an analytical VPT calculation up to five [39] and seven [40] loops agree well with high precision Monte Carlo simulations [41–43].

8.9. Large-N Limit

The large-N limit allows the calculation of the effective potential without resummation. It is based on the so-called *Hubbard-Stratonovich transformation*

$$\sqrt{\frac{\pi}{\lambda}}\, e^{\mu^2/4\lambda} \;=\; \int_{-\infty}^{\infty} d\sigma\, e^{-\lambda\sigma^2 - \mu\sigma} \tag{8.30}$$

with a scalar field σ. In order to derive the effective potential of the mexican hat (1.1) by means of a Hubbard-Stratonovich transformation we start from the partition function

$$\mathcal{Z} \;=\; \left[\prod_{n=1}^{N} \int d\phi_n\right] e^{-\mathcal{A}[\boldsymbol{\phi}]} \tag{8.31}$$

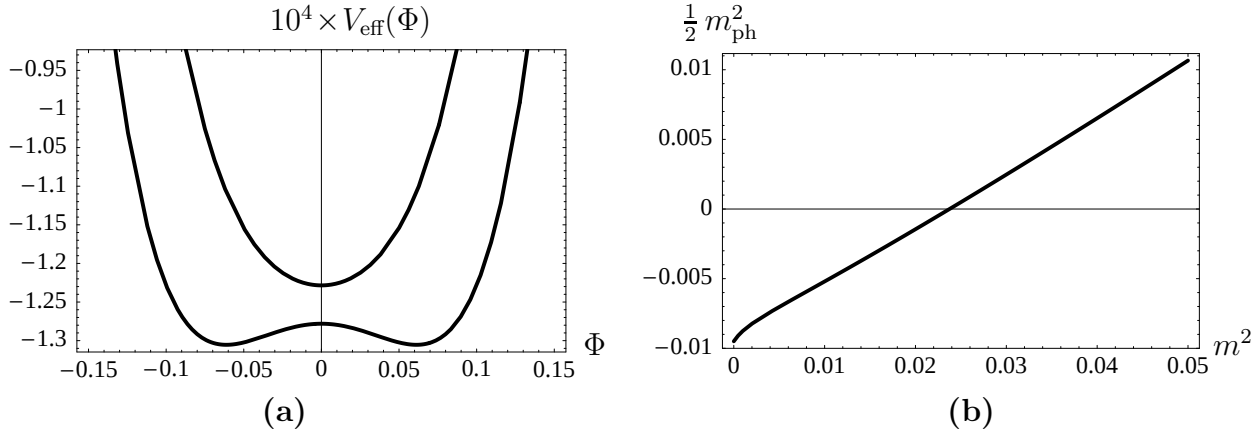

Figure 8.9.: Phase transition **(a)** of the effective potential (8.44) from the normal ($m^2 = 0.03$) to the ordered phase ($m^2 = 0.02$) in the large-N limit. The actual transition point **(b)** is determined to be $m^2 = 0.02375$. The physical mass $m^2_{\text{ph}}/2$ denotes the coefficient of Φ^2 in the effective potential.

with the action

$$\mathcal{A}[\boldsymbol{\phi}] \;=\; \int d^D x \sum_{n=1}^{N} \frac{1}{2}\, \phi_n(\mathbf{x}) \left[-\Delta + m^2\right] \phi_n(\mathbf{x}) \;+\; \frac{g}{24} \int d^D x \left[\boldsymbol{\phi}^2(\mathbf{x})\right]^2 . \tag{8.32}$$

The Hubbard-Stratonovich transformation enables us to express the interaction part of the potential with a functional integral over an additional field $\sigma(\mathbf{x})$. A functional version of (8.30) yields

$$\sqrt{\frac{\pi}{a}}\, \exp\!\left\{ -\frac{b^2}{4a} \int d^D x \big[\boldsymbol{\phi}^2(\mathbf{x})\big]^2 \right\} = \int \mathcal{D}\sigma\, \exp\!\left\{ -\int d^D x \left[a\, \sigma^2(\mathbf{x}) + \imath\, b\, \sigma(\mathbf{x})\, \boldsymbol{\phi}^2(\mathbf{x}) \right] \right\}. \tag{8.33}$$

Note, that from three possible contractions of ϕ^4 in (1.35), merely the Hartree term is taken into account. Due to (1.36), the Hubbard-Stratonovich transformation is therefore only exact in the limit $N \to \infty$.

In order to apply the Hubbard-Stratonovich transformation (8.33) to the partition function (8.31) with the action (8.32), we define the constants a and b by

$$b \;=\; \frac{1}{2}\,, \qquad a \;=\; -\frac{3}{2\, g}\,. \tag{8.34}$$

Furthermore, the overall factor on the left-hand side of (8.33) is absorbed into the functional integration measure $\mathcal{D}\sigma$. Now, the ansatz (8.33) can directly be applied to (8.31) and (8.32), yielding

$$\begin{aligned} \mathcal{Z} \;\; &= \;\; \int \mathcal{D}\sigma\, \exp\!\left\{ -\frac{3}{2\, g} \int d^D x\, \sigma^2(\mathbf{x}) \right\} \left[\prod_{n=1}^{N} \int d\phi_n \right] \\ &\quad \times \exp\!\left\{ -\int d^D x \sum_{n=1}^{N} \frac{1}{2}\, \phi_n(\mathbf{x}) \Big[-\Delta + m^2 + \imath\, \sigma(\mathbf{x}) \Big] \phi_n(\mathbf{x}) \right\}. \end{aligned} \tag{8.35}$$

Analogously to all previous calculations of the effective potential, we apply the background method, but this time for both the $\boldsymbol{\phi}$- and the σ-field

$$\phi_n(\mathbf{x}) \;=\; \Phi_n \,+\, \delta\,\phi_n(\mathbf{x})\,, \tag{8.36}$$

$$\sigma(\mathbf{x}) \;=\; -\imath\,\Sigma \,+\, \delta\,\sigma(\mathbf{x})\,. \tag{8.37}$$

The complex ansatz (8.37) compensates for (8.33) since altogether we have to obtain a real result. As explained in Section 2.4, terms linear in $\delta\phi$ vanish. Furthermore, we omit all fluctuations $\delta\sigma$ at any order. We introduce a new coupling constant $\tilde{g}=gN$ and consider the limit $N\to\infty$. This is completely analogous to the saddle point approximation in Section 2.3. Inserting (8.36) and (8.37) into (8.35) leads to the partition function

$$\begin{aligned}\mathcal{Z} \;&=\; \exp\biggl\{\frac{3\,N\,\mathrm{v}}{2\,\tilde{g}}\,\Sigma^2\biggr\}\,\exp\biggl\{-\mathrm{v}\sum_{n=1}^{N}\frac{1}{2}\,\Phi_n\Bigl[m^2+\Sigma\Bigr]\,\Phi_n\biggr\}\\ &\qquad\times\exp\biggl\{-\frac{N}{2}\,\mathrm{Tr}\ln\Bigl[-\Delta+m^2+\Sigma\Bigr]\biggr\}\\ &=:\;\exp\Bigl\{-V_{\mathrm{eff}}(\boldsymbol{\Phi},\Sigma)\Bigr\}\,.\end{aligned} \tag{8.38}$$

Thus, the effective potential divided by the volume v reads

$$V_{\mathrm{eff}}(\boldsymbol{\Phi},\Sigma) \;=\; -\,\frac{3N}{2\,\tilde{g}}\,\Sigma^2 \,+\, \frac{1}{2}\,\bigl(m^2+\Sigma\bigr)\,\boldsymbol{\Phi}^2 \,+\, \frac{N}{2}\int\frac{d^Dk}{(2\pi)^D}\ln\bigl(\mathbf{k}^2\,+\,m^2\,+\,\Sigma\bigr)\,. \tag{8.39}$$

We define

$$\lambda \;:=\; m^2 \,+\, \Sigma \tag{8.40}$$

to be a kind of *effective mass* corresponding to the variational parameter in the previous sections. The remaining integral in (8.39) is calculated applying (4.24) and we obtain

$$V_{\mathrm{eff}}(\boldsymbol{\Phi},\lambda) \;=\; -\,\frac{3N}{2\,\tilde{g}}\,\lambda^2 \,-\, \frac{3N}{2\tilde{g}}\,m^4 \,+\, \frac{3N}{\tilde{g}}\,m^2\,\lambda \,+\, \frac{1}{2}\,\lambda\,\boldsymbol{\Phi}^2 \,-\, \frac{N}{2}\,\frac{1}{(4\pi)^{D/2}}\,\Gamma\Bigl(\frac{D}{2}\Bigr)\,\lambda^{D/2}\,. \tag{8.41}$$

The effective potential (8.41) has to be optimized with respect to both the background field Φ_n and the mass λ

$$\frac{\partial\,V_{\mathrm{eff}}(\boldsymbol{\Phi},\lambda)}{\partial\,\Phi_n} \;=\; \lambda\,\Phi_n \;\stackrel{!}{=}\; 0 \qquad\Rightarrow\qquad \begin{cases}\Phi_n=0 & \text{normal phase}\,,\\ \Phi_n\neq 0\,,\;\lambda=0 & \text{ordered phase}\,,\end{cases} \tag{8.42}$$

$$\frac{\partial\,V_{\mathrm{eff}}(\boldsymbol{\Phi},\lambda)}{\partial\,\lambda} \;=\; -\frac{3N}{\tilde{g}}\lambda \,+\, \frac{3N}{\tilde{g}}\,m^2 \,+\, \frac{1}{2}\Phi_n^2 \,-\, \frac{N\,D}{(4\pi)^{D/2}}\,\Gamma\Bigl(\frac{D}{2}\Bigr)\,\lambda^{D/2-1} \;\stackrel{!}{=}\; 0\,. \tag{8.43}$$

Now we specify in $D=3$ dimensions where neither m nor $\tilde{g}$ has to be renormalized [35, Ch. 18]. The effective potential (8.41) becomes

$$V_{\mathrm{eff}}(\boldsymbol{\Phi},\lambda) \;=\; -\,\frac{3N}{2\,\tilde{g}}\,\lambda^2 \,-\, \frac{3N}{2\tilde{g}}\,m^4 \,+\, \frac{3N}{\tilde{g}}\,m^2\,\lambda \,+\, \frac{1}{2}\,\lambda\,\boldsymbol{\Phi}^2 \,-\, \frac{N}{12\pi}\,\lambda^{3/2}\,. \tag{8.44}$$

We insert the solution of (8.43) into (8.44) and plot the resulting potential in the large-N limit with constant $N/\tilde{g}=1$ for different values of m^2 in order to find a phase transition analogously to Section 8.6. Indeed, Figure 8.9 shows the transition from normal to ordered phase at $m^2=0.02375$. Analogously to the Landau expansion with and without variational resummation in Figure 8.5, we have a negative shift resulting in a transition at $m^2>0$, which confirms our previous results.

Finally, we verify explicitly that in the large-N limit, our results from variational resummation pass into the one from Hubbard-Stratonovich. We start from the effective potential (7.55) with $\hbar=1$ and take all terms up to the first loop order into account, i.e.,

$$V_{\text{eff}}(\Phi) \;=\; \frac{1}{2}\,m^2\,\Phi^2 + \frac{g}{24}\,\Phi^4 - \frac{1}{12\,\pi}\Big\{ m_L^3(\Phi) + (N-1)\,m_T^3(\Phi)\Big\}\,. \tag{8.45}$$

Since the resummed effective potential differs from the unresummed one only in the second and higher orders, (8.45) represents yet the optimized effective potential. Taking the limit $N\to\infty$ leads to

$$V_{\text{eff}}(\Phi) \;\stackrel{N\to\infty}{=}\; \frac{1}{2}\,m^2\,\Phi^2 + \frac{g}{24}\,\Phi^4 - \frac{N}{12\,\pi} m_T^3(\Phi)\,. \tag{8.46}$$

Now we start from the result (8.44) of the Hubbard-Stratonovich transformation. Resubstituting the coupling constant g and (8.40) into (8.44), we obtain

$$V_{\text{eff}}(\Phi) \;=\; -\,\frac{3}{2\,g}\,\Sigma^2 \;+\; \frac{1}{2}\,\big(m^2+\Sigma\big)\,\Phi^2 \;-\; \frac{N}{12\,\pi}\,\big(m^2+\Sigma\big)^{3/2}\,. \tag{8.47}$$

We have already remarked that the Hubbard-Stratonovich background field Σ plays the role of the variational parameter. Now we state more precisely: the parameter λ defined in (8.40) corresponds to the transversal mass $m_T^2(\Phi)$

$$\lambda \;\leftrightarrow\; m_T^2(\Phi)\,. \tag{8.48}$$

This is in accordance with the fact that for large N, the longitudinal direction can be neglected compared to the transversal one. Moreover, we identify in comparison of (7.22), (8.40), and (8.48) the Hubbard-Stratonovich background field to be $\Sigma=g\Phi^2/6$. Inserting this identity into (8.47), we obtain immediately the same result as (8.46). Thus, we conclude this chapter with the result that VPT is indeed the continuation of the Hubbard-Stratonovich transformation to an arbitrary number N of fields.

9. Summary and Outlook

In this thesis, we have considered the ϕ^4-potential (1.1) in quantum mechanics as the low-temperature limit of quantum statistics and in statistical field theory. In both cases, we have calculated the associated effective potential and applied variational perturbation theory (VPT). The reasons for doing so are different in both cases. Within quantum mechanics, it was our intention to investigate how the variational approach is, in principle, applied to the mexican-hat potential. It turned out, for instance, that due to the non-convexity of the potential, it is reasonable to apply Kleinert's square-root trick to the X-dependent frequencies $\omega(X)$ rather than to the bare frequency ω of the potential itself as it is done in the anharmonic case, see Eq. (3.25). This generalization from the procedure in Ref. [1, Ch. 5] was tested here in the more elementary context of quantum mechanics before applying it to statistical field theory.

The resummation of the effective potential has to be successful for all coupling strengths. With regard to this requirement, VPT is exceedingly appropriate since it transforms a divergent weak-coupling series into a convergent strong-coupling series [1, Ch. 5]. In order to assess the accuracy of VPT, we have calculated the ground-state energies from the optimized effective potential of the double-well. By doing so, we found that the importance of the sunset term depends on the shape of the potential: as shown in Tables A.1 and A.2, both approximations with and without sunset term yield the same result as long as the minimum of the optimized effective potential is located at $X = 0$. This is due to the fact that the sunset term goes with X^2 and vanishes therefore at $X = 0$. For small coupling constants, however, the optimized effective potential of the double-well in Figure 3.2 has its minima at $X \neq 0$. In this case, the approximations are slightly improved by taking the sunset diagram into account as shown in Figure 3.6. Moreover, this figure shows that the third loop order improves the results crucially. This finding is in accordance with the exponential convergence of VPT [6, Ch. 19] regarding the loop order, which makes the approach exceedingly powerful. Furthermore, we have verified the convergence with regard to the increasing number of dimensions $D \to \infty$ for a fixed loop order. This matter of fact is shown in Figure 3.10 and reproduces the analogy to the large-N limit in statistical field theory where the ϕ^4-theory is exactly solvable [35, Ch. 18].

In the second part of this thesis, we have treated statistical field theory, taking advantage of the experiences we gained in the previous quantum statistical part. We have derived the effective potential (7.55) in ϕ^4-theory in second loop order for an arbitrary spatial dimension D. However, we encounter singularities for $D = 3$ that typically arise in statistical field theory. For this reason, we have applied the standard rules of regularization and renormalization. Here, we have benefited from the fact that ϕ^4-theory in $D = 3$ dimensions is superrenormalizable and therefore permits us to absorb all divergencies solely by a mass

renormalization (5.20). The renormalization procedure in Chapter 5 by means of dimensional regularization and ε-expansion does not affect the rotational invariance. Thus, we can apply VPT afterwards, which is symmetry conserving itself. This order of renormalization and resummation is not self-consistent but as a consequence, the Goldstone theorem is not violated after performing both renormalization and resummation as it is shown in Section 8.5. Therefore, VPT turns out to be, indeed, a suitable procedure to extend the common Hartree-Fock-Bogoliubov theory to systems with non-vanishing field expectation. This is an important result since it affects all bosonic systems.

In contrast to VPT, the well-established Hubbard-Stratonovich transformation merely regards the Hartree term. As soon as we intend to take fluctuations into account, both Fock- and Bogoliubov-terms have to be included in the theory in order to obtain satisfying results. For this reason, the Hubbard-Stratonovich transformation is only suitable in the limit $N \to \infty$ which is dominated by the Hartree term. VPT, however, is appropriate to all values of N. We find an immediate analogy between both approaches if we identify the scalar Hubbard-Stratonovich background field Σ with a variational parameter in VPT. This connection has explicitly been verified in Section 8.9. In other words, VPT meets the claim of generalizing the Hubbard-Stratonovich transformation to arbitrary values of N without violating the Goldstone theorem.

Conserving symmetry is additionally important in connection with phase transitions. The ϕ^4-theory contains a continuous transition which has to be reproducible throughout all calculations. This matter of fact is verified by means of a Landau expansion in Chapter 8. We have obtained the continuous transition before and after variational resummation as it is shown in Figure 8.4 and 8.6, respectively. Furthermore, this calculation reveals the importance of the sunset term in statistical field theory: whereas in quantum mechanics, it is just a matter of accuracy whether we take the sunset term into account or not, the sunset turns out to be responsible for the continuous phase transition in statistical field theory, see Figures 8.6 and 8.7. In principle, we might have calculated the shift of the critical point where the phase transition takes place. In Section 8.8, we have shown, however, that the renormalization inevitably affects the point of transition in a non-physical way such that the result is not meaningful. Even VPT cannot change this lack.

There remain, of course, numerous intentions and ideas that could not be realized within the framework of this thesis. In the quantum statistical part of this thesis, we have noticed that calculating the effective potential in higher than second order requires laborious evaluations of Feynman diagrams. There exists a recursion method by C.M. Bender and T.T. Wu [44,45], that approximatively solves the time-independent Schrödinger equation. It has been extended to the time-dependent Schrödinger equation [46] as well as to the Fokker-Planck equation [47]. This method consists of a power series ansatz in the coupling constant for the energy and a twofold one in the coupling constant and the space coordinate for the wave function. The coefficients are determined recursively and in doing so, we would obtain the effective potential without explicitly evaluating the Feynman diagrams. This approach might have been suitable for our calculations. But since we were mainly interested in statistical

field theory rather than quantum mechanics, we did not pursue this idea.

Within statistical field theory, there remain more fundamental plans. It is an interesting question, how far the basic procedure of renormalization and resummation of our theory is affected when taking finite temperatures into account, for instance. Such an extension of the theory might be applied to Bose-Einstein condensates. We have drawn a first analogy in Section 8.8. Moreover, one should turn the attention to the critical exponents which are defined in the introduction. Whereas they are mostly calculated by coming from the upper phase [6, Ch. 19], our theory would yield an approach from the lower phase. We did not pay attention to this point since the second loop order is not sufficient for such applications. However, this does not imply that VPT cannot yield notable approximations in the next higher orders. Quite the contrary: due to the exponential convergence of VPT, a few higher orders are likely to lead to satisfying results.

Part III.

Appendix

A. Ground-State Energy via Shooting Method and VPT

In this appendix, we list all values for the ground-state energy E_0 of the double-well potential (3.22) and the mexican hat (3.1) in quantum mechanics that have been calculated either by means of the shooting method or of VPT. The shooting method consists of numerical integration of the Schrödinger equation (3.3): the ground-state energy E_0 is varied in such a way that the resulting wave function does not diverge. For further details, see Ref. [26], for instance. First, all results of VPT with one variational parameter are listed, i.e., solutions of the optimization equations (3.30) in second and third loop order. Values for the second loop order without sunset have merely been listed as far as they do not coincide with those of the full second loop order. All values are confronted with those obtained from the shooting method and we calculate the corresponding deviations. Note, that we have chosen natural units, i.e. $M = \hbar = 1$ and $\omega^2 = -1$.

Going to higher dimensions $D = 2,\, 3,\, 5,\, 10$, we have calculated the ground-state energy with two variational parameters. Furthermore, we apply the shooting method to the D-dimensional Schrödinger equation (3.4) and compare both results. Table A.4 shows our results for one variational parameter in $D = 2$ dimensions. All values for greater coupling constants coincide with those in Table A.5 and are therefore not repeated.

g	E_0 **(VPT)**	E_0 **(numerically)**	**deviation in per cent**
0.2	0.834367	0.617254	35.17
0.3	0.601156	0.531250	13.16
0.4	0.500018	0.470875	6.19
0.5	0.470176	0.434791	8.14
0.6	0.444508	0.414076	7.35
0.7	0.430807	0.402811	6.95
0.8	0.424383	0.397506	6.76
0.9	0.422584	0.396076	6.30
1.0	0.423829	0.397235	6.70
1.1	0.427131	0.400161	6.74
1.2	0.431849	0.404310	6.81
1.3	0.435978	0.409314	6.51
1.4	0.440770	0.414917	6.23
1.5	0.446129	0.420940	5.98
1.6	0.451891	0.427252	5.77
1.7	0.457938	0.433758	5.58
1.8	0.464182	0.440388	5.40
1.9	0.470557	0.447090	5.25
2.0	0.477014	0.453827	5.11
3.0	0.540958	0.519140	4.21
4.0	0.598905	0.577281	3.75
5.0	0.650428	0.628677	3.46
6.0	0.696634	0.674611	3.27
7.0	0.738548	0.716189	3.12
8.0	0.776964	0.754241	3.01
9.0	0.812487	0.789388	2.93
10.0	0.845577	0.822102	2.86

Table A.1.: VPT ground-state energies of the double-well potential (3.31) in second loop order. In the third column, the deviations of the VPT results from those of the shooting method are calculated.

g	E_0 **(VPT)**	E_0 **(numerically)**	**deviation in per cent**
0.2	0.687239	0.617254	11.24
0.3	0.636511	0.531250	19.81
0.4	0.549629	0.470875	16.73
0.5	0.492445	0.434791	13.26
0.6	0.460699	0.414076	11.26
0.7	0.442850	0.402811	9, 94
0.8	0.433248	0.397506	8.99
0.9	0.428832	0.396076	8.27
1.0	0.427817	0.397235	7.70
1.1	0.429103	0.400161/	7.23
1.2	0.431981	0.404310	6.84

Table A.2.: VPT ground-state energies of the double-well potential in second loop order without sunset (3.26) confronted with the results from the shooting method. For coupling constants $g > 1.2$, the VPT results are equal to those when taking the sunset into account, see Table A.1.

g	E_0 **(VPT)**	E_0 **(numerically)**	**deviation in per cent**
0.1	0.680389	0.679211	0
0.2	0.598912	0.617254	2.97
0.3	0.521212	0.531250	1.89
0.4	0.483383	0.470875	2.66
0.5	0.438392	0.434791	0.83
0.6	0.417701	0.414076	0.86
0.7	0.396135	0.402811	1.66
0.8	0.404597	0.397506	1.78
0.9	0.402255	0.396076	1.56
1.0	0.402938	0.397235	1.44
1.1	0.405094	0.400161	1.23
1.2	0.408835	0.404310	1.11
1.3	0.413518	0.409314	1.03
1.4	0.418863	0.414917	0.95
1.5	0.424673	0.420940	0.89
1.6	0.430808	0.427252	0.83
1.7	0.437164	0.433758	0.79
1.8	0.443667	0.440388	0.75
1.9	0.450259	0.447090	0.71
2.0	0.456900	0.453827	0.68
3.0	0.521645	0.519140	0.49
4.0	0.579611	0.577281	0.40
5.0	0.630905	0.628677	0.36
6.0	0.676787	0.674611	0.32
7.0	0718337.	0.716189	0.30
8.0	0.756376	0.754241	0.28
9.0	0.791520	0.789388	0.27
10.0	0.824236	0.822102	0.26

Table A.3.: VPT ground-state energies of the double-well potential (3.24) in third loop order compared to the numerical results from the shooting method.

g	E_0 **(numerically)**	E_0 **(VPT)**	**deviation in per cent**
0.2	0.601954	0.682617	13.40
0.3	0.570219	0.620170	8.76
0.4	0.568540	0.618122	8.72
0.6	0.604169	0.655796	8.55
1.0	0.709640	0.749998	5.69

Table A.4.: VPT ground-state energies of the mexican-hat potential (3.41) in second loop order ($D=2$) with one variational parameter confronted with the results from the shooting method.

g	E_0 **(VPT)**	E_0**(numerically)**	**deviation in per cent**
0.2	0.657168	0.601954	9.17
0.3	0.616803	0.570219	8.17
0.4	0.612818	0.568540	7.79
0.5	0.625360	0.582583	7.34
0.6	0.647108	0.604169	7.11
0.7	0.677789	0.629259	7.71
0.8	0.700686	0.655823	6.84
0.9	0.725073	0.682804	6.12
1.0	0.750000	0.709640	5.69
1.1	0.774946	0.736031	5.29
1.2	0.799616	0.761820	4.96
1.3	0.823849	0.786935	4.69
1.4	0.847556	0.811346	4.46
1.5	0.870695	0.835052	4.27
1.6	0.893250	0.858068	4.10
1.7	0.915222	0.880417	3.95
1.8	0.936623	0.902127	3.82
1.9	0.957469	0.923226	3.71
2.0	0.977780	0.943744	3.61
3.0	1.156140	1.122794	2.97
4.0	1.301480	1.267792	2.66
5.0	1.425000	1.390665	2.47
10.0	1.872320	1.834165	2.08

Table A.5.: VPT ground-state energies of the mexican-hat potential (3.41) in second loop order ($D=2$) calculated with two variational parameters.

g	E_0 **(VPT)**	E_0**(numerically)**	**deviation in per cent**
0.3	0.710543	0.781325	9.96
0.4	0.767765	0.825782	7.56
0.5	0.830715	0.893919	7.61
0.6	0.893799	0.950117	6.30
0.7	0.954951	1.006918	5.44
0.8	1.013471	1.062500	4.84
0.9	1.069215	1.116165	4.39
1.0	1.122261	1.167691	4.02
1.1	1.172776	1.217068	3.78
1.2	1.220952	1.264376	3.56
1.3	1.266980	1.309734	3.38
1.4	1.311041	1.353275	3.22
1.5	1.353300	1.395129	3.09
1.6	1.393906	1.435420	2.98
1.7	1.432992	1.474263	2.88
1.8	1.470679	1.511763	2.79
1.9	1.507072	1.548018	2.72
2.0	1.542268	1.583113	2.65
3.0	1.843627	1.884617	2.22
4.0	2.083052	2.125000	2.01
5.0	2.284196	2.327303	1.89
6.0	2.459095	2.503399	1.80
7.0	2.614745	2.660230	1.74
8.0	2.755596	2.802225	1.69
9.0	2.884666	2.93296	1.66
10.0	3.004101	3.052891	1.62

Table A.6.: VPT ground-state energies of the mexican-hat potential (2.133) in second loop order calculated with two variational parameters ($D=3$).

g	E_0 **(VPT)**	E_0**(numerically)**	**deviation in per cent**
0.2	0.983909	1.097802	11.58
0.3	1.175857	1.261869	7.32
0.4	1.356177	1.426616	5.19
0.5	1.520323	1.582959	4.12
0.6	1.669534	1.727660	3.48
0.7	1.805949	1.861239	3.06
0.8	1.931553	1.984962	2.77
0.9	2.047999	2.100117	2.55
1.0	2.156623	2.207840	2.38
1.1	2.258504	2.309087	3.74
1.2	2.354518	2.309087	3.74
1.3	2.445384	2.495222	2.04
1.4	2.531694	2.581334	1.92
1.5	2.613945	2.663468	1.89
1.6	2.692555	2.7402024	1.84
1.7	2.767880	2.817343	1.75
1.8	2.840225	2.889722	1.74
1.9	2.909852	2.959416	1.70
2.0	2.976993	3.026647	1.67
3.0	3.546221	3.597501	1.45
4.0	3.994104	4.047409	1.34
5.0	4.368862	4.424192	1.27
6.0	4.694088	4.751358	1.22
7.0	4.983230	5.042337	1.19
8.0	5.244741	5.305585	1.16
9.0	5.484314	5.546804	1.14
10.0	5.705981	5.770033	1.12

Table A.7.: VPT ground-state energies of the mexican-hat potential (2.133) in second loop order calculated with two variational parameters ($D=5$).

g	E_0 **(VPT)**	E_0**(numerically)**	**deviation in per cent**
0.2	2.366271	2.457481	3.86
0.3	2.996700	3.069808	2.44
0.4	3.515422	3.581415	1.88
0.5	3.957602	4.020141	1.58
0.6	4.344634	4.405337	1.40
0.7	4.690084	4.749794	1.27
0.8	5.003026	5.062228	1.18
0.9	5.289814	5.348807	1.12
1.0	5.555067	5.614047	1.06
1.1	5.802255	5.861351	1.02
1.2	6.034047	6.093351	0.98
1.3	6.252547	6.312122	0.95
1.4	6.459439	6.519331	0.93
1.5	6.656100	6.713411	0.91
1.6	6.843662	6.904278	0.89
1.7	7.023077	7.084084	0.87
1.8	7.195148	7.256558	0.85
1.9	7.360560	7.422381	0.84
2.0	7.519903	7.582140	0.83
3.0	8.850000	8.933270	0.94
4.0	9.924544	9.994836	0.71
5.0	10.809519	10.883333	0.68
6.0	11.577914	11.654947	0.67
7.0	12.261500	12.341500	0.65
8.0	12.880179	12.962925	0.64
9.0	13.447320	13.532635	0.63
10.0	13.972385	14.060116	0.63

Table A.8.: VPT ground-state energies of the mexican-hat potential (2.133) in second loop order calculated with two variational parameters ($D=10$).

B. Calculation of Propagator

In this appendix, we calculate the propagator $G(\tau_1, \tau_2)$, following Ref. [1]. First, we consider an arbitrary temperature and calculate the general form of the propagator. In a second step, we take the low-temperature limit $\beta \to \infty$ on which we focus throughout Part 1.
We start from the one-dimensional harmonic oscillator coupled to an external current. The associated generating function reads

$$\mathcal{Z}[\,j\,] \;=\; \oint \mathcal{D}x \; e^{-\mathcal{A}[x,j]/\hbar}\,, \tag{B.1}$$

with the Euclidean action

$$\mathcal{A}[x,j] \;=\; \int_0^{\hbar\beta} d\tau \left[\frac{M}{2}\,\dot{x}^2(\tau) + \frac{\omega^2}{2}\,x^2(\tau) \right] \;-\; \int_0^{\hbar\beta} d\tau \; j(\tau)\,x(\tau)\,. \tag{B.2}$$

Performing the path integral in (B.1) means integrating over all periodic paths $x(\tau)$, i.e.,

$$x(0) \;=\; x(\hbar\beta)\,. \tag{B.3}$$

Hence, these paths possess a Matsubara decomposition

$$x(\tau) \;=\; \sum_{m=-\infty}^{\infty} x_m \, e^{-\imath\,\omega_m \tau}\,, \tag{B.4}$$

with coefficients x_m and Matsubara frequencies

$$\omega_m \;=\; \frac{2\pi}{\hbar\beta}\,m, \qquad m \in \mathbb{Z}\,. \tag{B.5}$$

This is due to the fact that the functions $e^{-\imath\omega_m\tau}$ form a complete orthogonal system. In order to prove this statement, we consider *Poisson's summation formula*. It can be derived from the periodic *comb function*

$$K(x) = \sum_{m=-\infty}^{\infty} \delta(x-m)\,, \tag{B.6}$$

which has the Fourier representation

$$K(x) \;=\; \sum_{n=-\infty}^{\infty} e^{-2\pi\imath n x}\,. \tag{B.7}$$

Multiplying (B.6) and (B.7) with an arbitrary function $f(x)$ and integrating over x yields

$$\sum_{m=-\infty}^{\infty} f(m) \;=\; \sum_{n=-\infty}^{\infty} \int_{-\infty}^{\infty} dx \; f(x)\, e^{-\imath n\hbar\beta x}\,. \tag{B.8}$$

In the case of a function $f(m)=F(\omega_m)$, (B.8) reads

$$\sum_{m=-\infty}^{\infty} F(\omega_m) \;=\; \frac{\hbar\beta}{2\pi} \sum_{n=-\infty}^{\infty} \int_{-\infty}^{\infty} d\omega_m \; F(\omega_m)\, e^{-\imath n\hbar\beta\omega_m} \,. \tag{B.9}$$

Now we specify on the functions

$$x_m(\tau) \;=\; \frac{e^{-\imath\omega_m\tau}}{\sqrt{\hbar\beta}} \,. \tag{B.10}$$

These functions fulfil both the orthonormality condition

$$\int_0^{\hbar\beta} d\tau \; x_m(\tau)\, x_n^*(\tau) \;=\; \delta_{m,n} \tag{B.11}$$

and, with regard to (B.9), the completeness relation

$$\sum_{m=-\infty}^{\infty} x_m(\tau_1)\, x_m^*(\tau_2) \;=\; \delta^{(p)}(\tau_1-\tau_2) \,. \tag{B.12}$$

The periodic delta function in (B.12) is defined to be

$$\delta^{(p)}(\tau_1-\tau_2) \;=\; \sum_{n=-\infty}^{\infty} \delta\left(\tau_1-\tau_2+n\hbar\beta\right) . \tag{B.13}$$

Thus, the functions (B.10) form a complete orthonormal system, allowing us to perform the Matsubara decomposition (B.4). In order to yield a real path, the coefficients have to obey the condition

$$x_m \;=\; x_{-m}^* \,, \tag{B.14}$$

which connects coefficients with positive and negative m. As a consequence, they are completely determined by those with positive modes m. Inserting (B.4) into (B.2) yields

$$\begin{aligned} \mathcal{A}[x,j] \;\;=\;\; & \hbar\beta\,\frac{M}{2}\,\omega^2\,x_0^2 \;-\; x_0\int_0^{\hbar\beta} d\tau\; j(\tau) \;+\; \hbar\beta\, M \sum_{m=1}^{\infty} (\omega_m^2+\omega^2)\left[(\mathrm{Re}\, x_m)^2+(\mathrm{Im}\, x_m)^2\right] \\ & -2\sum_{m=1}^{\infty}\int_0^{\hbar\beta} d\tau\; j(\tau)\left[\cos(\omega_m\tau)\,\mathrm{Re}\, x_m \;+\; \sin(\omega_m\tau)\,\mathrm{Im}\, x_m\right], \end{aligned} \tag{B.15}$$

where we took (B.14) into account and separated coefficients and exponential functions into real and imaginary part. The path integral can also be replaced either by an infinite product of ordinary integrals over all Matsubara coefficients x_m or by a product of integrals over real and imaginary part of all coefficients with positive m:

$$\oint \mathcal{D}x \quad\to\quad N_0 \int_{-\infty}^{\infty} dx_0 \prod_{m=1}^{\infty} \left(N_m \int_{-\infty}^{\infty} d\,\mathrm{Re}\, x_m \int_{-\infty}^{\infty} d\,\mathrm{Im}\, x_m \right) . \tag{B.16}$$

The respective normalization constants

$$N_0 \,=\, \sqrt{\frac{M}{2\,\pi\,\hbar^2\beta}}\,, \qquad N_m \,=\, \frac{M\,\beta\,\omega_m^2}{\pi} \tag{B.17}$$

are calculated in detail in Ref. [1]. Inserting (B.15) and (B.16) into (B.1), we obtain

$$\begin{aligned}\mathcal{Z}[j] \;=\; & N_0 \int_{-\infty}^{\infty} dx_0 \,\exp\left\{-\frac{M}{2}\,\beta\,\omega^2 x_0^2 \,+\, \frac{x_0}{\hbar}\int_0^{\hbar\beta} d\tau\; j(\tau)\right\} \\ & \times \prod_{m=1}^{\infty}\left[N_m \int_{-\infty}^{\infty} d\,\mathrm{Re}\,x_m \,\exp\left\{-M\beta\,(\mathrm{Re}\,x_m)^2\,(\omega_m^2 \,+\, \omega^2) \,+\, \frac{2\,\mathrm{Re}\,x_m}{\hbar}\int_0^{\hbar\beta} d\tau\; j(\tau)\cos\left(\omega_m\tau\right)\right\}\right. \\ & \left. \times \int_{-\infty}^{\infty} d\,\mathrm{Im}\,x_m \,\exp\left\{-M\beta\,(\mathrm{Im}\,x_m)^2\,(\omega_m^2+\omega^2) + \,\frac{2\,\mathrm{Im}\,x_m}{\hbar}\int_0^{\hbar\beta} d\tau\; j(\tau)\sin(\omega_m\tau)\right\}\right]. \end{aligned} \tag{B.18}$$

These integrals are Gaussian integrals like

$$\int_{-\infty}^{\infty} dx\; e^{-a\,x^2+b\,x} \,=\, \sqrt{\frac{\pi}{a}}\; e^{\,b^2/4a}\,, \tag{B.19}$$

leading to

$$\begin{aligned}\mathcal{Z}[j] \;=\; & N_0\,\sqrt{\frac{2\pi}{M\,\beta\,\omega^2}}\left(\prod_{m=1}^{\infty}\frac{N_m\,\pi}{M\,\beta\,\left(\omega_m^2+\omega^2\right)}\right)\exp\left\{\frac{1}{2\,\hbar^2}\int_0^{\hbar\beta} d\tau_1\int_0^{\hbar\beta} d\tau_2\,\frac{1}{M\,\beta}\left[\frac{1}{\omega^2}+\right.\right. \\ & \left.\left.\sum_{m=1}^{\infty}\frac{2}{\omega_m^2+\omega^2}\left(\cos\omega_m\tau_1\,\cos\omega_m\tau_2 \,+\, \sin\omega_m\tau_1\,\sin\omega_m\tau_2\right)\right]\,j(\tau_1)\,j(\tau_2)\right\}. \end{aligned} \tag{B.20}$$

Applying trigonometric addition theorems and using the odd symmetry of Matsubara frequencies (B.5), we evaluate the sum within the exponential function:

$$\frac{1}{\omega^2} \,+\, \sum_{m=1}^{\infty}\frac{2\cos\left[\omega_m\,(\tau_1-\tau_2)\,\right]}{\omega_m^2+\omega^2} \,=\, \sum_{m=-\infty}^{\infty}\frac{e^{\imath\,\omega_m(\tau_1-\tau_2)}}{\omega_m^2+\omega^2}\,. \tag{B.21}$$

It is obvious to define the harmonic partition function without an external current to be

$$\mathcal{Z}_\omega \,=\, N_0\,\sqrt{\frac{2\pi}{M\beta\omega^2}}\,\prod_{m=1}^{\infty}\frac{\pi\,N_m}{M\,\beta\,(\omega_m^2+\omega^2)} \,=\, \frac{1}{\hbar\,\beta\,\omega}\,\prod_{m=1}^{\infty}\frac{\omega_m^2}{\omega_m^2 \,+\, \omega^2}\,. \tag{B.22}$$

Furthermore, we define the so-called *harmonic propagator* by

$$G_\omega\,(\tau_1,\tau_2) = \sum_{m=-\infty}^{\infty}\frac{e^{-\imath\,\omega_m(\tau_1-\tau_2)}}{M\,\beta\,\left(\omega_m^2+\omega^2\right)}\,. \tag{B.23}$$

In terms of the harmonic partition function (B.22) and the propagator (B.23), the generating function (B.20) factorizes into

$$\mathcal{Z}[j] \,=\, \mathcal{Z}_\omega\,\exp\left\{\frac{1}{2\hbar^2}\int_0^{\hbar\beta} d\tau_1\int_0^{\hbar\beta} d\tau_2\; G_\omega\,(\tau_1,\tau_2)\,j(\tau_1)\,j(\tau_2)\right\}. \tag{B.24}$$

Our next task is to evaluate the Matsubara series (B.23). To this end, we apply Poisson's summation formula (B.9) to (B.23), yielding

$$G_\omega(\tau_1,\tau_2) \;=\; \sum_{n=-\infty}^{\infty} g_\omega(\tau_1-\tau_2+n\hbar\beta)\,, \tag{B.25}$$

with

$$g_\omega(\tau) \;=\; \frac{\hbar}{2\,\pi\,M}\int_{-\infty}^{\infty} d\omega_m\,\frac{e^{-\imath\omega_m\tau}}{\omega_m^2+\omega^2}\,. \tag{B.26}$$

These functions can be calculated with the help of Cauchy's residue theorem. In the case of $\tau>0$, we close the curve in the lower hemisphere with a pole at $\omega_m=-\imath\,\omega$:

$$g_\omega(\tau) \;=\; \frac{\hbar}{2\pi M}\,(-2\pi\imath)\,\frac{e^{-\imath\,\tau(-\imath\omega)}}{-2\imath\,\omega} \;=\; \frac{\hbar}{2\,\omega\,M}\,e^{-\omega\tau}\,. \tag{B.27}$$

Analogously, we calculate the case $\tau<0\,$,

$$g_\omega(\tau) \;=\; \frac{\hbar}{2\pi M}\,2\pi\imath\,\frac{e^{-\imath\,\tau\imath\,\omega}}{2\imath\,\omega} \;=\; \frac{\hbar}{2\,\omega\,M}\,e^{\omega\tau}\,, \tag{B.28}$$

and combine (B.27) and (B.28) for any real value of τ to

$$g_\omega(\tau) \;=\; \frac{\hbar}{2\,\omega\,M}\,e^{-\omega|\tau|}\,. \tag{B.29}$$

After inserting (B.29) into (B.25) with respect to $\tau_1,\tau_2\in[0,\hbar\beta]$, it remains to evaluate the geometric series

$$G_\omega(\tau_1,\tau_2) \;=\; \frac{\hbar}{2\,\omega\,M}\left\{e^{-\omega|\tau_1-\tau_2|}\;+\;\sum_{n=1}^{\infty}\Big[\,e^{-\omega(\tau_1-\tau_2+n\hbar\beta)}\;+\;e^{-\omega(\tau_2-\tau_1+n\hbar\beta)}\,\Big]\right\}, \tag{B.30}$$

yielding the final result

$$G_\omega(\tau_1,\tau_2) \;=\; \frac{\hbar}{2\,\omega\,M}\,\frac{\cosh\big[\,\omega\,\big(|\tau_1-\tau_2|\;-\;\hbar\beta/2\,\big)\,\big]}{\sinh\big(\hbar\beta\omega/2\big)}\,. \tag{B.31}$$

In our calculations, we consider the low-temperature limit $T\to 0$, i.e. $\beta\to\infty$, where the propagator (B.31) simplifies to

$$\lim_{T\to 0} G_\omega(\tau_1,\tau_2) \;=\; \frac{\hbar}{2\,\omega\,M}\,e^{-\omega|\tau_1-\tau_2|}\,. \tag{B.32}$$

This follows immediately from the exponential representation of the hyperbolic functions. For further application, we continue calculating the harmonic partition function (B.22). Using (B.23), it is straightforward to show the identity

$$\frac{\partial}{\partial\,\omega}\ln\mathcal{Z}_\omega \;=\; -M\beta\omega\;G_\omega(\tau,\tau)\,. \tag{B.33}$$

Integrating (B.31) for equal arguments yields the harmonic partition function in accordance with (B.33):

$$\mathcal{Z}_\omega \;=\; \frac{1}{2\sinh\big(\hbar\beta\omega/2\big)}\,. \tag{B.34}$$

C. Functions and Integrals

In this appendix, we focus our attention on those mathematical functions that occur frequently during our calculations in quantum field theory. We summarize their definitions and most important properties as well as useful relations, following Refs. [48] and [49]. Furthermore, we shortly present some methods transforming difficult integrals into Gaussian integrals that can be solved straightforwardly.

C.1. Gamma and Beta Functions

The *Gamma function* $\Gamma(x)$ belongs to the most important and most frequently occurring functions in quantum field theory. Furthermore, it is linked to renormalization because it is a kind of *quintessence* of analytic continuation and dimensional regularization. The Gamma function has the integral representation

$$\Gamma(z) \;=\; \int_0^\infty dt\; e^{-t}\, t^{z-1}\,, \tag{C.1}$$

which is only defined if $\mathrm{Re}\, z > 0$. However, partial integration leads to the functional identity

$$z\,\Gamma(z) \;=\; \Gamma(z+1)\,. \tag{C.2}$$

Thus, the Gamma function can be extended analytically to all values of z except for negative integers which cannot be reached. This is the very property that makes the Gamma function particularly suitable in connection with dimensional regularization: many integrals are defined just for some dimensions because they diverge otherwise. If a general result for D dimensions can be found in which D is an argument of the Gamma function, than the result can be extended via an analytic continuation to dimensions in which the original integral was not defined. By applying the functional identity (C.2), it is obvious that for an integer argument n, the Gamma function yields

$$\Gamma(n) \;=\; (n-1)!\,, \qquad n \in \mathbb{N}\,. \tag{C.3}$$

There exist a so-called *doubling formula* which we cite from Ref. [48] without proof:

$$\Gamma(2x) \;=\; \frac{2^{2x-1}}{\sqrt{\pi}}\,\Gamma(x)\,\Gamma\Big(x+\frac{1}{2}\Big)\,. \tag{C.4}$$

Euler's psi function $\psi(x)$ (also called *Digamma function*) is defined to be the logarithmic derivative of $\Gamma(x)$:

$$\psi(x) \;=\; \frac{d}{dx}\ln\Gamma(x)\,. \tag{C.5}$$

Applying (C.2), we derive the functional relation

$$\psi(x+1) \;=\; \psi(x) \;+\; \frac{1}{x}\,. \tag{C.6}$$

Furthermore, Euler's constant γ is defined by

$$\gamma \;:=\; -\psi(1) \;=\; 0.577\,215\,\ldots\,. \tag{C.7}$$

The *Beta function* $B(x,y)$ is closely related to the Gamma function. It is defined by two equivalent integral representations

$$B(x,y) \;=\; \int_0^1 dt\; t^{x-1}\,(1-t)^{y-1}\,, \tag{C.8}$$

$$B(x,y) \;=\; \int_0^\infty dt\; t^{x-1}(1+t)^{-x-y}\,. \tag{C.9}$$

In terms of Gamma functions, $B(x,y)$ reads

$$B(x,y) \;=\; \frac{\Gamma(x)\,\Gamma(y)}{\Gamma(x+y)}\,, \tag{C.10}$$

which exposes a symmetry concerning both arguments:

$$B(x,y) \;=\; B(y,x)\,. \tag{C.11}$$

If the integral's upper bound in (C.8) differs from 1, we obtain the *incomplete Beta function* $B_z(x,y)$:

$$B_z(x,y) \;=\; \int_0^z dt\; t^{x-1}\,(1-t)^{y-1}\,. \tag{C.12}$$

C.2. Hypergeometric Functions

During the calculation of the sunset diagram in Appendix D and E, integrals occur that can be attributed to hypergeometric functions. Therefore, we list its relevant representations, functional relations, and special cases. The *hypergeometric function* ${}_2F_1(a,b;c;z)$ is defined by the Taylor series

$${}_2F_1(a,\,b;\,c;\,z) \;:=\; \sum_{k=0}^{\infty} \frac{(a)_k\,(b)_k}{(c)_k}\;\frac{z^k}{k!}\,, \tag{C.13}$$

with the so-called Pochhammer's symbols

$$(x)_k \;:=\; \frac{\Gamma(x+k)}{\Gamma(x)}\,. \tag{C.14}$$

Obviously, ${}_2F_1(a,b;c;z)$ is symmetric with regard to the first two arguments:

$${}_2F_1(a,b;c;z) \;=\; {}_2F_1(b,a;c;z)\,. \tag{C.15}$$

The hypergeometric function (C.13) has two subscripts, because it is obvious to extend it to a so-called *generalized hypergeometric function* with a larger number of arguments:

$$ {}_pF_q\big(\alpha_1, \alpha_2, ..., \alpha_p;\, \beta_1, \beta_2, ..., \beta_q;\, z\big) \;=\; \sum_{k=0}^{\infty} \frac{(\alpha_1)_k\,(\alpha_2)_k \,...\, (\alpha_p)_k}{(\beta_1)_k\,(\beta_2)_k \,...\, (\beta_q)_k}\; \frac{z^k}{k!}\,. \tag{C.16} $$

In our calculations, it is sufficient to concentrate on (C.13), also referred to as *Gauss' hypergeometric function*. To simplify matters, we omit both subscripts from now on. If a or b is equal to a negative integer, the hypergeometric function is defined by the sum

$$ F(-m,\, b;\, c;\, z) \;=\; \sum_{k=0}^{m} \frac{(-m)_k\,(b)_k}{(c)_k}\; \frac{z^k}{k!}\,. \tag{C.17} $$

The integral representation of the hypergeometric function reads

$$ F(a, b; c; z) \;=\; \frac{1}{B(b, c-b)} \int_0^1 dt\; t^{b-1}(1-t)^{c-b-1}(1-tz)^{-a}\,. \tag{C.18} $$

In comparison with (C.8), we state that hypergeometric functions can be regarded as a generalization of Beta functions. Whereas Beta functions have two poles at $t=0$ and $t=1$, the hypergeometric function (C.18) has an additional pole at $t=1/z$.
Moreover, the following integral occurs:

$$ \int_0^u dx\; \frac{x^{\mu-1}}{(1+\beta x)^{\nu}} \;=\; \frac{u^{\mu}}{\mu}\, F\big(\nu, \mu; 1+\mu; -\beta u\big)\,. \tag{C.19} $$

In the case of m and b being equal to $+1$, (C.17) reduces to

$$ F(-1,\, 1;\, x;\, y) \;=\; \frac{x-y}{x}\,. \tag{C.20} $$

Furthermore, there exist some special cases in which the hypergeometric function can be written in terms of other well-known functions:

$$ F(1,\, 1;\, 2;\, z) \;=\; \sum_{k=0}^{\infty} \frac{\Gamma(1+k)}{\Gamma(2+k)}\; z^k \;=\; \frac{1}{z} \sum_{k=1}^{\infty} \frac{z^k}{k} \;=\; -\,\frac{1}{z}\,\ln(1-z)\,, \tag{C.21} $$

$$ \begin{aligned} F\Big(\frac{1}{2},\, 1;\, \frac{3}{2};\, z^2\Big) \;&=\; \sum_{k=0}^{\infty} \frac{\Gamma\big(k+1/2\big)}{\Gamma\big(1/2\big)}\; \frac{\Gamma\big(3/2\big)}{\Gamma\big(k+3/2\big)}\; z^{2k} \;=\; \frac{1}{z} \sum_{k=0}^{\infty} \frac{z^{2k+1}}{2k+1} \\ &=\; \frac{1}{2z}\,\ln\frac{1+z}{1-z} \;=\; \frac{1}{z}\,\mathrm{Artanh}\,(z)\,, \end{aligned} \tag{C.22} $$

$$ F\Big(\frac{1}{2},\, \frac{1}{2};\, \frac{3}{2};\, -z\Big) \;=\; \frac{1}{\sqrt{z}}\,\mathrm{Arsinh}\,\sqrt{z}\,. \tag{C.23} $$

Another useful functional relation is

$$ \begin{aligned} F(a,\, b;\, c;\, z) \;&=\; (1-z)^{c-a-b}\, \frac{\Gamma(c)\,\Gamma(a+b-c)}{\Gamma(a)\,\Gamma(b)}\, F\big(c-a,\, c-b;\, c-a-b+1;\, 1-z\big) \\ &\quad + \frac{\Gamma(c)\,\Gamma(c-a-b)}{\Gamma(c-a)\,\Gamma(c-b)}\, F\big(a,\, b;\, a+b-c+1;\, 1-z\big)\,. \end{aligned} \tag{C.24} $$

The hypergeometric function is related to the incomplete Beta function by

$$ B_z(x, y) \;=\; \frac{z^x}{x}\, F(x, 1-y; x+1; z)\,. \tag{C.25} $$

C.3. Proper Time Representation

Feynman rules connect diagrams to integrals over combinations of propagators. *Schwinger's proper time representation* affords us to write propagators as Gaussian integrals. It is based on the identity

$$\frac{1}{a^x} \;=\; \frac{1}{\Gamma(x)} \int_0^\infty d\tau\; \tau^{x-1}\, e^{-\tau a}\,, \tag{C.26}$$

which follows immediately from (C.1). In order to show the advantages of this representation, we consider the integral

$$I_2(D) \;=\; \int \frac{d^D k}{(2\pi)^D}\; \frac{1}{\left[\mathbf{k} + 2\mathbf{kq} + m^2\right]^\gamma}\,. \tag{C.27}$$

Applying (C.26) and interchanging momentum- and τ-integral, the momentum integral reduces to a D-dimensional Gaussian integral and can easily be evaluated with the help of

$$\int \frac{d^D k}{(2\pi)^D}\; e^{-\tau \mathbf{k}^2} \;=\; \Big(\frac{1}{4\pi\,\tau}\Big)^{D/2}. \tag{C.28}$$

Thus, we obtain the intermediate result

$$I_2(D) \;=\; \frac{1}{\Gamma(\gamma)} \int_0^\infty d\tau\; \tau^{\gamma-1}\; e^{-\tau m^2}\; \frac{1}{(2\pi)^D} \Big(\frac{\pi}{\tau}\Big)^{D/2} e^{\tau \mathbf{q}^2}\,. \tag{C.29}$$

The τ-integral in (C.29) is evaluated in accordance with (C.1), yielding

$$I_2(D) \;=\; \frac{1}{(4\pi)^{D/2}}\; \frac{\Gamma\big(\gamma - D/2\big)}{\Gamma(\gamma)}\; \frac{1}{\big(m^2 - \mathbf{q}^2\big)^{\gamma - D/2}}\,. \tag{C.30}$$

Another integral similar to (C.30) reads

$$I_3(D) \;=\; \int \frac{d^D k}{(2\pi)^D}\; \frac{1}{\big(A\mathbf{k}^2 + m^2\big)^\gamma} \;=\; \frac{\Gamma\big(\gamma - D/2\big)}{(4\pi)^{D/2}\,\Gamma(\gamma)}\; \frac{\big(m^2\big)^{D/2-\gamma}}{A^{D/2}}\,. \tag{C.31}$$

Moreover, the proper time representation leads to a further representation of the logarithm: we insert (C.26) into

$$\ln a \;=\; -\,\frac{\partial}{\partial x}\Big(\frac{1}{a^x}\Big)\bigg|_{x=0}\,, \tag{C.32}$$

yielding the so-called *Schwinger representation of logarithm*:

$$\ln a \;=\; -\,\frac{\partial}{\partial x}\left\{\; \frac{1}{\Gamma(x)} \int_0^\infty d\tau\; \tau^{x-1}\, e^{-\tau a} \;\right\}\bigg|_{x=0}\,. \tag{C.33}$$

C.4. Feynman's Parametric Formula

In connection with Feynman diagrams, *Feynman's parametric integral formula*

$$\frac{1}{A^a\,B^b} \;=\; \frac{\Gamma(a+b)}{\Gamma(a)\,\Gamma(b)} \int_0^1 dx\, \frac{x^{a-1}\,(1-x)^{b-1}}{[Ax+B(1-x)]^{a+b}} \tag{C.34}$$

turns out to be highly useful. It follows from

$$\frac{1}{AB} \;=\; \frac{1}{B-A}\Big(\frac{1}{A}-\frac{1}{B}\Big) \;=\; \frac{1}{B-A}\int_A^B dz\,\frac{1}{z^2} \;=\; \int_0^1 dx\,\frac{1}{[Ax+B(1-x)]^2}\,, \tag{C.35}$$

after differentiation with respect to A and B,

$$\frac{d^{a+b-2}}{dA^{a-1}\,dB^{b-1}}\,\frac{1}{AB} \;=\; \frac{(-1)^{a+b}\,\Gamma(a)\,\Gamma(b)}{A^a\,B^b} \tag{C.36}$$

and

$$\frac{d^{a+b-2}}{dA^{a-1}\,dB^{b-1}}\,\frac{1}{[Ax+B(1-x)]^2} \;=\; \frac{(-1)^{a+b}\,\Gamma(a+b)\,x^{a-1}\,(1-x)^{b-1}}{[Ax+B(1-x)]^{a+b}}\,. \tag{C.37}$$

Although (C.36) and (C.37) are only defined for integer values of the powers a and b, (C.34) can be extrapolated analytically to arbitrary complex powers. Combinations of arbitrary powers of propagators can be rewritten by using Feynman's parametric integral formula (C.34). After interchanging momentum- and x-integral, the momentum integral can often be solved straightforwardly. Nevertheless, it remains calculating the Feynman parametric integral. To give an example, we consider

$$I_4(D) \;=\; \int \frac{d^Dk}{(2\pi)^D}\,\frac{1}{\big(\mathbf{k}^2+m_1^2\big)^a}\,\frac{1}{\big(\mathbf{k}^2+m_2^2\big)^b}\,. \tag{C.38}$$

Feynman's parametric formula (C.34) and the integral formula (C.31) yield

$$\begin{aligned} I_4(D) \;&=\; \frac{\Gamma(a+b)}{\Gamma(a)\,\Gamma(b)}\int_0^1 dx\; x^{a-1}(1-x)^{b-1}\int\frac{d^Dk}{(2\pi)^D}\,\frac{1}{\Big[\mathbf{k}^2x+m_1^2x+m_2^2(1-x)\Big]^{a+b}} \\ &=\; \frac{1}{(4\pi)^{D/2}}\,\frac{\Gamma\big(a+b-D/2\big)}{\Gamma(a)\,\Gamma(b)}\int_0^1 dx\,\frac{x^{a-1}(1-x)^{b-1}}{\Big[m_1^2x+m_2^2(1-x)\Big]^{a+b-D/2}}\,. \end{aligned} \tag{C.39}$$

Furthermore, we address ourselves two other integrals. The first one reads

$$I_5(D) \;=\; \int \frac{d^Dk_2}{(2\pi)^D}\,\frac{1}{\big[(\mathbf{k}_1+\mathbf{k}_2)^2+m_1^2\,\big]^a}\,\frac{1}{\big(\mathbf{k}_2^2+m_2^2\big)^b}\,. \tag{C.40}$$

Applying Feynman's parametric formula (C.34) to (C.40) yields with (C.30)

$$\begin{aligned} I_5(D) &= \frac{\Gamma(a+b)}{\Gamma(a)\,\Gamma(b)}\int_0^1 dx\; x^{a-1}(1-x)^{b-1}\int\frac{d^Dk_2}{(2\pi)^D}\,\frac{1}{\big[\mathbf{k}_2^2+2x\mathbf{k}_1\mathbf{k}_2+\mathbf{k}_1^2x+m_1^2x+m_2^2(1-x)\big]^{a+b}} \\ &=\; \frac{1}{(4\pi)^{D/2}}\,\frac{\Gamma\big(a+b-D/2\big)}{\Gamma(a)\Gamma(b)}\int_0^1 dx\,\frac{x^{a-1}(1-x)^{b-1}}{\Big[m_1^2\,x+m_2^2(1-x)+(x-x^2)\,\mathbf{k}_1^2\Big]^{a+b-D/2}}\,. \end{aligned} \tag{C.41}$$

Finally, we generalize (C.38) to the integral

$$I_6(D) \;=\; \int \frac{d^Dk}{(2\pi)^D}\;\frac{1}{\left(A\mathbf{k}^2+m_1^2\right)^a}\;\frac{1}{\left(\mathbf{k}^2+m_2^2\right)^b}\,, \tag{C.42}$$

that can be transformed in the same way as the former one:

$$\begin{aligned} I_6(D) \;&=\; \frac{\Gamma(a+b)}{\Gamma(a)\,\Gamma(b)}\int_0^1 dx\; x^{a-1}(1-x)^{b-1}\int\frac{d^Dk}{(2\pi)^D}\,\frac{1}{\Big[\mathbf{k}^2\,\big(1+(A-1)x\big)+m_1^2x+m_2^2(1-x)\Big]^{a+b}} \\ &=\; \frac{1}{(4\pi)^{D/2}}\frac{\Gamma\big(a+b-D/2\big)}{\Gamma(a)\,\Gamma(b)}\int_0^1 dx\,\frac{x^{a-1}(1-x)^{b-1}}{\Big[1+(A-1)x\Big]^{D/2}\Big[m_1^2x+m_2^2(1-x)\Big]^{a+b-D/2}}\,. \end{aligned} \tag{C.43}$$

D. Sunset Diagram

Thanks to all preliminaries in the previous appendix, we are now able to calculate the Feynman integral

$$I(D) \;=\; \int \frac{d^D k_1\, d^D k_2}{(2\pi)^{2D}}\, \frac{1}{\mathbf{k}_1^2 + M^2}\, \frac{1}{\mathbf{k}_2^2 + M^2}\, \frac{1}{(\mathbf{k}_1 + \mathbf{k}_2)^2 + M^2}\,, \tag{D.1}$$

which occurs when evaluating the sunset diagram $\Phi \bigcirc\!\!\!\!\!\!\bigcirc \Phi = g^2 \Phi^2 I(D)$. Furthermore, it appears in the self-energy diagram $\bigcirc\!\!\!\!\!\!\bigcirc$ if we specialize the external momentum $\mathbf{k}$ to be zero: $\bigcirc\!\!\!\!\!\!\bigcirc\,(\mathbf{k}=0) = g^2 I(D)$. We are especially interested in $D=3$ dimensions, where the integral is logarithmically divergent since its superficial degree of divergence is $\omega\,(\bigcirc\!\!\!\!\!\!\bigcirc\,) = 0$. Our intention is to calculate the integral for arbitrary dimension D and to localize the singularity for $D=3$ afterwards.

D.1. Calculation in D Dimensions

With the help of (C.40) and (C.41), the integral (D.1) can be transferred to

$$\begin{aligned} I(D) \;&=\; \int \frac{d^D k_1}{(2\pi)^D}\, \frac{1}{\mathbf{k}_1^2 + M^2} \int \frac{d^D k_2}{(2\pi)^D}\, \frac{1}{\mathbf{k}_2^2 + M^2}\, \frac{1}{(\mathbf{k}_1 + \mathbf{k}_2)^2 + M^2} \\ &=\; \frac{\Gamma\big(2 - D/2\big)}{(4\pi)^{D/2}} \int_0^1 dx_2 \int \frac{d^D k_1}{(2\pi)^D}\, \frac{1}{\mathbf{k}_1^2 + M^2}\, \frac{1}{\big[(x_2 - x_2^2)\mathbf{k}_1^2 + M^2\big]^{2-D/2}}\,. \end{aligned} \tag{D.2}$$

We continue applying (C.42) and (C.43), which enables us to perform the second momentum integral via a further Feynman parametrization

$$I(D) \;=\; \frac{\Gamma(3-D)}{(4\pi)^D}\, \frac{1}{(M^2)^{3-D}} \int_0^1 dx_1 \int_0^1 dx_2\, \frac{x_1^{1-D/2}}{\big[1 + (x_2 - x_2^2 - 1)x_1\big]^{D/2}}\,. \tag{D.3}$$

The integral with respect to x_1 is connected to a hypergeometric function due to (C.19), yielding

$$I(D) \;=\; \frac{\Gamma(3-D)}{(4\pi)^D (M^2)^{3-D}}\, \frac{1}{2 - D/2} \int_0^1 dx_2\, F\left(\frac{D}{2}, 2 - \frac{D}{2}; 3 - \frac{D}{2}; x_2^2 - x_2 + 1\right). \tag{D.4}$$

The last argument can be simplified applying (C.24), which gives us

$$\begin{aligned} I(D) &= \frac{\Gamma(3-D)}{(4\pi)^D\,(M^2)^{3-D}}\,\frac{1}{2-D/2}\int_0^1 dx_2\left\{\frac{\Gamma\big(3-D/2\big)\,\Gamma\big(1-D/2\big)}{\Gamma(3-D)\,\Gamma(1)}\right. \\ &\quad \times F\left(\frac{D}{2},2-\frac{D}{2};\frac{D}{2};x_2-x_2^2\right) + (x_2-x_2^2)^{1-D/2} \\ &\quad \left.\times\frac{\Gamma\big(3-D/2\big)\,\Gamma\big(D/2-1\big)}{\Gamma\big(D/2\big)\,\Gamma\big(2-D/2\big)}\,F\left(3-D,1;2-\frac{D}{2};x_2-x_2^2\right)\right\}. \end{aligned} \tag{D.5}$$

The remaining integral is solved straightforwardly after writing the hypergeometric function in the series representation (C.13):

$$\begin{aligned} I(D) &= \frac{(M^2)^{D-3}\,\Gamma\big(1-D/2\big)}{(4\pi)^D}\left\{\sum_{k=0}^{\infty}\frac{\Gamma\big(2-D/2+k\big)}{k!}\int_0^1 dx_2\,(x_2-x_2^2)^k\right. \\ &\quad \left.-\sum_{k=0}^{\infty}\frac{\Gamma(3-D+k)\,\Gamma(1+k)}{\Gamma\big(2-D/2+k\big)\,k!}\int_0^1 dx_2\,(x_2-x_2^2)^{k+1-D/2}\right\}. \end{aligned} \tag{D.6}$$

With these transformations, the appearing integrals correspond to Beta functions (C.8) and yield, according to (C.10),

$$\begin{aligned} I(D) &= \frac{(M^2)^{D-3}\,\Gamma\big(1-D/2\big)}{(4\pi)^D}\sum_{k=0}^{\infty}\left\{\frac{\Gamma\big(2-D/2+k\big)\,\Gamma(k+1)}{\Gamma(2+2k)}\right. \\ &\quad \left.-\frac{\Gamma(3-D+k)\,\Gamma\big(2-D/2+k\big)}{\Gamma(4-D+2k)}\right\}. \end{aligned} \tag{D.7}$$

After simplifying the Gamma functions in the denominator by the use of (C.3) and the doubling formula (C.4), the series in (D.7) is retransformed to two hypergeometric functions. Thus, our final result reads

$$\begin{aligned} I(D) &= \frac{(M^2)^{D-3}\,\Gamma\big(1-D/2\big)}{(4\pi)^D}\left\{\Gamma\left(2-\frac{D}{2}\right)\,F\left(1,2-\frac{D}{2};\frac{3}{2};\frac{1}{4}\right)\right. \\ &\quad \left.-\frac{2^{D-3}\,\sqrt{\pi}\,\Gamma(3-D)}{\Gamma\big((5-D)/2\big)}\,F\left(1,3-D;\frac{5-D}{2};\frac{1}{4}\right)\right\}. \end{aligned} \tag{D.8}$$

For $D=1$, (D.8) yields our quantum mechanical result (2.131) in one dimension

$$I(1) = \frac{1}{12}\,\frac{1}{M^4}, \tag{D.9}$$

if we take all prefactors into account, replace the mass in quantum field theory $M\to\omega_L$ and set in return the quantum mechanical mass $M=1$ in (2.131).

D.2. Divergence for $D = 3$

As mentioned above, the integral (D.8) is logarithmically divergent in $D=3$ dimensions. It is our intention to localize this divergence and to separate finite and infinite contributions. Merely the second term in (D.8) shows a divergent behavior for $D = 3$, thus we will concentrate on expanding this term in a region near $D = 3$, i.e. for $D = 3+\varepsilon$. To this end, we use the series representation (C.13) of the hypergeometric function, separate the term $k = 0$ where the divergence arises and retransform the remaining regular contribution to a hypergeometric function after a shift of the index k:

$$\begin{aligned}\frac{2^{D-3}\sqrt{\pi}\,\Gamma(3-D)}{\Gamma\big((5-D)/2\big)}\,F\left(1,3-D;\frac{5-D}{2};\frac{1}{4}\right) &= \sum_{k=0}^{\infty}\frac{\Gamma\big(2-D/2+k\big)\,\Gamma(3-D+k)}{\Gamma(4-D+2k)}\\ &= \frac{\Gamma\big(2-D/2\big)\,\Gamma(3-D)}{\Gamma(4-D)}+\sum_{k=1}^{\infty}\frac{\Gamma\big(2-D/2+k\big)\,\Gamma(3-D+k)}{\Gamma(4-D+2k)}\\ &= \frac{\Gamma\big(2-D/2\big)}{3-D}+\frac{2^{D-5}\sqrt{\pi}\,\Gamma(4-D)}{\Gamma\big((7-D)/2\big)}\,F\left(1,4-D;\frac{7-D}{2};\frac{1}{4}\right). \qquad \text{(D.10)}\end{aligned}$$

Thus, the whole integral (D.8) can be written as

$$\begin{aligned}I(D) &= \frac{(M^2)^{D-3}\,\Gamma\big(1-D/2\big)}{(4\pi)^D}\left\{\Gamma\big(2-\frac{D}{2}\big)\,F\left(1,2-\frac{D}{2};\frac{3}{2};\frac{1}{4}\right)\right.\\ &\quad\left.-\frac{2^{D-5}\sqrt{\pi}\,\Gamma(4-D)}{\Gamma\big((7-D)/2\big)}\,F\left(1,4-D;\frac{7-D}{2};\frac{1}{4}\right)-\frac{\Gamma\big(2-D/2\big)}{3-D}\right\}. \qquad \text{(D.11)}\end{aligned}$$

It remains expanding the last term for $D=3+\varepsilon$. To this end, we introduce a mass parameter μ which appears in a dimensionless ratio with the mass M in order to yield a dimensionless argument of the logarithm. It may be set to one afterwards. In connection with the effective potential, this procedure corresponds to obtaining a dimensionless coupling constant [6, Ch. 8]. Thus, the ε-expansion of the divergent term in (D.11) reads

$$\begin{aligned}-\frac{(M^2)^{D-3}\,\Gamma\big(1-D/2\big)}{(4\pi)^D}\,\frac{\Gamma\big(2-D/2\big)}{3-D} &\overset{D=3+\varepsilon}{=} -\frac{1}{32\pi^2}\,\frac{1}{\varepsilon}+\frac{1}{32\pi^2}\left\{-\ln\frac{M^2}{\mu^2}+\ln 4\pi\right.\\ &\quad\left.+\frac{1}{2}\,\psi\Big(\frac{1}{2}\Big)+\frac{1}{2}\,\psi\Big(-\frac{1}{2}\Big)\right\}+\mathcal{O}(\varepsilon), \qquad \text{(D.12)}\end{aligned}$$

where $\psi(x)$ denotes the Digamma function introduced in (C.5). With (C.6), we simplify

$$\psi\Big(\frac{1}{2}\Big)+\frac{1}{2}\,\psi\Big(-\frac{1}{2}\Big) = 1-\gamma-\ln 4. \qquad \text{(D.13)}$$

Evaluating the other regular terms in (D.11) for $D = 3$, we find hypergeometric functions (C.21) and (C.22), yielding:

$$\begin{aligned}F\Big(1,\frac{1}{2};\frac{3}{2};\frac{1}{4}\Big) &= 2\,\mathrm{Artanh}\,\frac{1}{2} = \ln 3,\\ F\Big(1,1;2;\frac{1}{4}\Big) &= 4\ln\frac{4}{3}. \qquad \text{(D.14)}\end{aligned}$$

Finally, we insert (D.12)–(D.14) into (D.11) and obtain the full ε-expansion

$$I(3+\varepsilon) \;=\; -\,\frac{1}{32\pi^2}\,\frac{1}{\varepsilon} \;+\; \frac{1}{32\pi^2}\left\{-\ln\frac{M^2}{\mu^2} \;+\; \ln\frac{4\pi}{9} \;+\; 1 \;-\; \gamma\right\} + \mathcal{O}(\varepsilon)\,. \tag{D.15}$$

D.3. Divergence for $D = 4$

In order to verify our result (D.8), we perform a further expansion for $D = 4-\varepsilon$. Both prefactors contain a Gamma function which has poles at negative integers. Thus, the integral becomes quadratically divergent. This agrees with the superficial degree of divergence which is in $D = 4$ dimensions $\omega\,(\,\Theta\,) \;=\; 2\,$. Again, we insert the mass parameter μ into the logarithm.

$$\begin{aligned} I(4-\varepsilon) = -\,\frac{M^2}{(4\pi)^D}\Bigg\{\frac{6}{\varepsilon^2} + \frac{1}{\varepsilon}\Bigg[-6\ln\frac{4\pi\mu^2}{M^2} + 7\gamma - 5 + \ln 4 + \psi\Big(\frac{1}{2}\Big) - 2\,F^{(0,1,0,0)}\Big(1,0;\frac{3}{2};\frac{1}{4}\Big) \\ - 4\,F^{(0,1,0,0)}\Big(1,-1;\frac{1}{2};\frac{1}{4}\Big) \;-\; 2\,F^{(0,0,1,0)}\Big(1,-1;\frac{1}{2};\frac{1}{4}\Big)\Bigg] \;+\; \mathcal{O}(\varepsilon^0)\Bigg\}, \end{aligned} \tag{D.16}$$

where we defined the partial derivatives

$$\begin{aligned} F^{(0,1,0,0)}(a,b;c;z) \;&:=\; \frac{\partial}{\partial\, b}\,F(a,b;c;z)\,, \\ F^{(0,0,1,0)}(a,b;c;z) \;&:=\; \frac{\partial}{\partial\, c}\,F(a,b;c;z)\,. \end{aligned} \tag{D.17}$$

The derivative in the last term of (D.16) with respect to the third argument can be calculated analytically:

$$F\Big(1,-1;x;\frac{1}{4}\Big) = \frac{4x-1}{4x} \quad\Rightarrow\quad F^{(0,0,1,0)}\Big(1,-1;x;\frac{1}{4}\Big)\bigg|_{x=\frac{1}{2}} = 1\,. \tag{D.18}$$

Inserting (D.13) and (D.18), the ε- expansion (D.16) becomes

$$\begin{aligned} I(4-\varepsilon) \;=\; -\,\frac{M^2}{(4\pi)^D}\Bigg\{\frac{6}{\varepsilon^2} \;+\; \frac{1}{\varepsilon}\Bigg[-6\ln\frac{4\pi\mu^2}{M^2} \;+\; 6\,\gamma \;-\; 7 \;-\; 2\,F^{(0,1,0,0)}\Big(1,0;\frac{3}{2};\frac{1}{4}\Big) \\ - 4\,F^{(0,1,0,0)}\Big(1,-1;\frac{1}{2};\frac{1}{4}\Big)\Bigg] \;+\; \mathcal{O}(\varepsilon^0)\Bigg\}. \end{aligned} \tag{D.19}$$

In Ref. [6, Ch. 8], the integral (D.1) has also been calculated. The authors concentrated on $D=4-\varepsilon$ from the very beginning and expanded the integrand before integrating. However, their result can be compared to (D.19). The actual coincidence of the numerical values serves as prove of our calculations which have the crucial advantage that the result (D.8) is valid for arbitrary dimensions.

E. Generalized Sunset Diagram

In the previous appendix, we calculated the integral (D.1) where all three mass terms in the denominators are equal. This integral occurs in the sunset diagram, for instance, if we consider one real field. In the case of N fields, however, longitudinal and transversal masses arise if we consider the broken symmetry phase. Thus, we have to extend our calculations to a sunset diagram with arbitrary mass terms

$$\mathcal{I}(x,y,z) \;=\; \int \frac{d^Dk_1\, d^Dk_2}{(2\pi)^{2D}}\, \frac{1}{\mathbf{k}_1^2+x}\, \frac{1}{\mathbf{k}_2^2+y}\, \frac{1}{(\mathbf{k}_1+\mathbf{k}_2)^2+z}\,. \tag{E.1}$$

For equal mass terms $x=y=z$, (E.1) reduces to the ordinary sunset integral (D.1).

E.1. Calculation for One Mass

First of all, we calculate a special case of (E.1), that is to say where $y=z=0$ without loss of generality. Then, (E.1) simplifies to

$$\mathcal{I}(x,0,0) \;=\; \int \frac{d^Dk_1\, d^Dk_2}{(2\pi)^{2D}}\, \frac{1}{\mathbf{k}_1^2+x}\, \frac{1}{\mathbf{k}_2^2}\, \frac{1}{(\mathbf{k}_1+\mathbf{k}_2)^2}\,. \tag{E.2}$$

We proceed similarly to the previous appendix where all masses were equal, yielding

$$\mathcal{I}(x,0,0) \;=\; \frac{x^{D-3}}{(4\pi)^D}\, \frac{\Gamma(3-D)}{D/2-1} \int_0^1 dx_1\, (1-x_1)^{D-3}\, F\!\left(\frac{D}{2}, \frac{D}{2}-1; \frac{D}{2}; x_1^2-x_1+1\right), \tag{E.3}$$

instead of (D.4). When we continue applying (C.24), the second term vanishes there due to the appearance of $\Gamma(0)$ in the denominator, and we obtain

$$\mathcal{I}(x,0,0) = \frac{x^{D-3}}{(4\pi)^D}\, \frac{\Gamma(3-D)}{D/2-1} \int_0^1 dx_1\, (1-x_1)^{D-3}\, (x_1-x_1^2)^{1-D/2}\, F\!\left(0,1; 2-\frac{D}{2}; x_1-x_1^2\right). \tag{E.4}$$

Consider the hypergeometric function in (E.4). In accordance with (C.13) and (C.14), it contains

$$(0)_k \;=\; \frac{\Gamma(0+k)}{\Gamma(0)} \;=\; \delta_{k,0}\,. \tag{E.5}$$

Hence, the hypergeometric function becomes

$$F\left(0,1; 2-\frac{D}{2}; x_1-x_1^2\right) \;=\; 1\,, \tag{E.6}$$

and (E.4) results in

$$\mathcal{I}(x,0,0) \;=\; \frac{x^{D-3}}{(4\pi)^D}\,\frac{\Gamma(3-D)}{D/2-1}\int_0^1 dx_1\,(1-x_1)^{D-3}\,(x_1-x_1^2)^{1-D/2}\,. \tag{E.7}$$

The integration is performed applying (C.8), and our final result reads

$$\mathcal{I}(x,0,0) \;=\; \frac{x^{D-3}}{(4\pi)^D}\,\frac{\Gamma(3-D)\,\Gamma\left(2-D/2\right)\,\Gamma^2\left(D/2-1\right)}{\Gamma\left(D/2\right)}\,. \tag{E.8}$$

The calculation procedure for three arbitrary masses in (E.1) is completely different from the previous one. We follow Ref. [50], where the integral is reduced to a system of ordinary differential equations that can be solved with the help of the so-called *method of characteristics* which we introduce shortly.

E.2. Method of Characteristics

The method of characteristics is a fundamental approach to linear and non-linear partial differential equations of first order. For our calculations, it is sufficient to restrict ourselves to a *linear partial differential equation of first order* which reads

$$X_1\,\frac{\partial\,F}{\partial x_1} \;+\; X_2\,\frac{\partial\,F}{\partial x_2} \;+\; \cdots \;+\; X_n\,\frac{\partial\,F}{\partial x_n} \;=\; G\,. \tag{E.9}$$

$F = F(x_1, x_2, \cdots, x_n)$ denotes the unknown function, $X_i = X_i(x_1, x_2, \cdots, x_n)$ with $i = 1, \cdots, n$ are given functions as well as the inhomogeneity $G{=}G(x_1, x_2, \cdots, x_n)$. In the case of $G{=}0$, the differential equation is called *homogeneous*. Then, solving (E.9) corresponds to integrating the *characteristic system*

$$\frac{dx_1}{X_1} \;=\; \frac{dx_2}{X_2} \;=\; \cdots \;=\; \frac{dx_n}{X_n} \;=:\; dt\,. \tag{E.10}$$

An inhomogeneous differential equation can be regarded as a homogeneous one if we define an additional function $H(x_1, \cdots, x_n, I) \equiv \text{const}$ so that

$$X_1\,\frac{\partial\,H}{\partial x_1} \;+\; X_2\,\frac{\partial\,H}{\partial x_2} \;+\; \cdots \;+\; X_n\,\frac{\partial\,H}{\partial x_n} \;+\; G\,\frac{\partial\,H}{\partial I} \;=\; 0\,. \tag{E.11}$$

Its characteristic system reads

$$\frac{dx_1}{X_1} \;=\; \frac{dx_2}{X_2} \;=\; \cdots \;=\; \frac{dx_n}{X_n} \;=\; \frac{dI}{G} \;:=\; dt\,. \tag{E.12}$$

E.3. Calculation in D Dimensions

Recall the integral

$$\tilde{I}(x) \;=\; \int \frac{d^Dk}{(2\pi)^D}\,\frac{1}{\mathbf{k}^2+x} \;=\; \frac{\Gamma\left(1\,-\,D/2\right)}{(4\pi)^{D/2}}\,x^{D/2-1}\,, \tag{E.13}$$

as calculated in (5.5). Its derivative reads

$$\frac{\partial\,\tilde{I}(x)}{\partial\,x} \;=\; -\,\frac{\Gamma\,(2-D/2)}{(4\pi)^{D/2}}\;x^{D/2-2}\,. \tag{E.14}$$

Furthermore, we define the following functions

$$K_1(x,y,z) \;:=\; -\,\frac{\partial\,\tilde{I}(z)}{\partial\,z}\,\Big[\,\tilde{I}(x)\;-\;\tilde{I}(y)\,\Big]\,, \tag{E.15}$$

$$K(x,y,z) \;:=\; K_1(x,y,z)\;+\;K_1(y,z,x)\;+\;K_1(z,x,y)\,, \tag{E.16}$$

where $K_1(y,z,x)$ and $K_1(z,x,y)$ arise from cyclic permutation in (E.15). For an arbitrary vector $\mathbf{v}$, we recall *Gauss' theorem*

$$\int_V \operatorname{div}\mathbf{v}\,dV \;=\; \oint_{\partial V}\mathbf{v}\,\mathbf{dS} \tag{E.17}$$

with volume V and surface ∂V. From (E.17), we conclude the identity

$$0 \;\equiv\; \int d^Dp\;d^Dq\,\frac{\partial}{\partial\,k^\mu}\;\frac{k^\mu}{(\mathbf{p}^2+x)\,(\mathbf{q}^2+y)\,[(\mathbf{p}+\mathbf{q})^2+z]}\,. \tag{E.18}$$

It results from the fact that both surface integrals in (E.17) with regard to p and q go with $\sim 1/R^4$, where R denotes the radius. For $D=3$ dimensions, the integrals vanish in the limit $R\to\infty$. With respect to (E.1), (E.15), and (E.17), we derive a differential equation for $K_1(x,y,z)$ that reads

$$K_1(x,y,z) \;=\; 2\,x\,\frac{\partial\,\mathcal{I}(x,y,z)}{\partial\,x}\;+\;(x+z-y)\,\frac{\partial\,\mathcal{I}(x,y,z)}{\partial\,y}\;+\;(D-3)\,\mathcal{I}(x,y,z)\,. \tag{E.19}$$

Appropriate cyclic permutations yield corresponding results for both other two functions in (E.16). Inserting (E.19) into (E.16), we obtain a differential equation for the function $K(x,y,z)$

$$K(x,y,z) \;=\; (y-z)\,\frac{\partial\,\mathcal{I}}{\partial\,x}\;+\;(z-x)\,\frac{\partial\,\mathcal{I}}{\partial\,y}\;+\;(x-y)\,\frac{\partial\,\mathcal{I}}{\partial\,z}\,. \tag{E.20}$$

Thus, the desired integral $\mathcal{I}(x,y,z)$ can be obtained by solving the differential equation (E.20). For reasons of simplicity, we define

$$\Gamma' \;:=\; \frac{1}{(4\pi)^D}\,\Gamma\left(2-\frac{D}{2}\right)\,\Gamma\left(1-\frac{D}{2}\right)\,. \tag{E.21}$$

When we insert (E.13) and (E.14) into (E.15), we obtain the expression

$$K_1(x,y,z) \;=\; \Gamma'\Big[x(xz)^{-\nu}\;-\;y(yz)^{-\nu}\Big] \tag{E.22}$$

with $\nu := 2-D/2$. With respect to the corresponding cyclic permutations, (E.22) transforms (E.16) to

$$K(x,y,x) \;=\; -\Gamma'\Big\{(z-x)(xz)^{-\nu}\;+\;(y-z)(yz)^{-\nu}\;+\;(x-y)(xy)^{-\nu}\Big\}\,. \tag{E.23}$$

Now we apply the method of characteristics. Starting from (E.20), the characteristic equation reads in accordance with (E.12)

$$\frac{d\mathcal{I}}{K} \;=\; \frac{dx}{y-z} \;=\; \frac{dy}{z-x} \;=\; \frac{dz}{x-y} \;=\; dt \qquad \rightarrow \qquad \mathcal{I} \;=\; \int K\,dt\,. \tag{E.24}$$

Suitable initial conditions turn out to be

$$x(t=0) \;=\; X\,, \qquad y(t=0) \;=\; Y\,, \qquad z(t=0) \;=\; 0\,. \tag{E.25}$$

Thus, (E.24) leads to the integral

$$\mathcal{I}(x,y,z) \;=\; \mathcal{I}(X,Y,0) \;+\; \int_0^t dt'\; K\Big(x(t'),y(t'),z(t')\Big)\,. \tag{E.26}$$

Recalling (E.23) and (E.24), the integral (E.26) can be written as a sum of three integrals

$$\begin{aligned}\mathcal{I}(x,y,z) \;&=\; \mathcal{I}(X,Y,0) \;-\; \Gamma'\left\{\int_0^t dt'\;(z-x)(xz)^{-\nu} \;+\; \int_0^t dt'\;(x-y)(xy)^{-\nu}\right.\\ &\qquad \left.+\; \int_0^t dt'\;(y-z)(yz)^{-\nu}\right\}\\ &=\; \mathcal{I}(X,Y,0) \;-\; \Gamma'\left\{\int_Y^y dy\,(xz)^{-\nu} + \int_0^z dz\,(xy)^{-\nu} + \int_X^x dx\,(yz)^{-\nu}\right\}. \end{aligned}\tag{E.27}$$

From the method of characteristics (E.24) and the initial conditions (E.25), we derive

$$\frac{d}{dt}\big(x+y+z\big) \;=\; 0 \qquad \Rightarrow \qquad x+y+z \;=\; X+Y \;:=\; c \;=\; \text{const}\,, \tag{E.28}$$

$$\frac{d}{dt}\big(x^2+y^2+z^2\big) \;=\; 0 \qquad \Rightarrow \qquad x^2+y^2+z^2 \;=\; X^2+Y^2 \;:=\; d^2 \;=\; \text{const}\,. \tag{E.29}$$

Furthermore, we require

$$xy \;=\; z^2 - cz + \frac{1}{2}\big(c^2-d^2\big)\,, \tag{E.30a}$$

$$yz \;=\; x^2 - cx + \frac{1}{2}\big(c^2-d^2\big)\,, \tag{E.30b}$$

$$xz \;=\; y^2 - cy + \frac{1}{2}\big(c^2-d^2\big)\,, \tag{E.30c}$$

which can be verified straightforwardly by inserting (E.28) and (E.29). The definition

$$a \;:=\; \sqrt{\frac{d^2}{2} - \frac{c^2}{4}} \;=\; \frac{1}{2}\Big(X-Y\Big) \;=\; \frac{1}{2}\sqrt{x^2+y^2+z^2-2(xy+yz+xz)} \tag{E.31}$$

transfers (E.30a)–(E.30c) to

$$xy = \Big(\frac{1}{2}\,c - z\Big)^2 - a^2\,, \tag{E.32a}$$

$$yz = \Big(x - \frac{1}{2}\,c\Big)^2 - a^2\,, \tag{E.32b}$$

$$xz = \Big(y - \frac{1}{2}\,c\Big)^2 - a^2\,. \tag{E.32c}$$

Now we start calculating the integrals (E.27) one by one. The first one reads

$$\int_X^x dx' \, (yz)^{-\nu} \;=\; \int_X^x dx' \left[\left(x' - \frac{1}{2}c \right)^2 - a^2 \right]^{-\nu} \;=\; \int_a^{x-c/2} ds \left[s^2 - a^2 \right]^{-\nu}, \tag{E.33}$$

where we substituted $s := x' - \frac{1}{2}c$ after applying (E.32b). The y-integral is solved analogously with $s := \frac{1}{2}c - y'$ and (E.32c), yielding

$$\int_Y^y dy' \, (xz)^{-\nu} \;=\; \int_Y^y dy' \left[\left(\frac{1}{2}c - y' \right)^2 - a^2 \right]^{-\nu} \;=\; \int_{c/2-y}^a ds \left[s^2 - a^2 \right]^{-\nu}. \tag{E.34}$$

With $s := \frac{1}{2}c - z'$ and (E.32a), the third integral in (E.27) results in

$$\int_0^z dz' \, (xy)^{-\nu} \;=\; \int_0^z dz' \left[\left(\frac{1}{2}c - z' \right)^2 - a^2 \right]^{-\nu} \;=\; \int_{c/2-z}^{c/2} ds \left[s^2 - a^2 \right]^{-\nu}. \tag{E.35}$$

All three integrals (E.33)–(E.35) can be solved analytically. We are left with adding them up, and $\mathcal{I}\big(x, y, z\big)$ reads

$$\mathcal{I}\big(x, y, z\big) \;=\; \mathcal{I}\big(X, Y, 0\big) \;-\; \Gamma' \left[\left(\int_a^{x-c/2} + \int_{c/2-y}^a + \int_{c/2-z}^{c/2} \right) ds \left[s^2 - a^2 \right]^{-\nu} \right]. \tag{E.36}$$

Now we have reduced $\mathcal{I}\big(x, y, z\big)$ to an integral $\mathcal{I}\big(X, Y, 0\big)$, which we simplify by applying the method of characteristics once again for two variables x and y. With $z = 0$, (E.20) and (E.22) become

$$K(x, y) \;=\; y \, \frac{\partial \mathcal{I}}{\partial x} \;-\; x \, \frac{\partial \mathcal{I}}{\partial y}, \tag{E.37}$$

$$K(x, y) \;=\; -\,\Gamma' \, (x - y) \, (xy)^{-\nu} \tag{E.38}$$

with the corresponding characteristic equation

$$\frac{dx}{y} \;=\; -\frac{dy}{x} \;=\; \frac{d\mathcal{I}}{K} \;=\; dt \qquad \Rightarrow \qquad dx = y \, dt \,, \; dy = -x \, dt \,. \tag{E.39}$$

This time, we choose the initial conditions $x(t = 0) = X - Y = 2a$ and $y(t = 0) = 0$. With respect to (E.38) and (E.39), we find

$$\begin{aligned} \mathcal{I}(x, y, 0) \;&=\; \mathcal{I}(X - Y, 0, 0) \;+\; \int_0^t dt' \, K\big(x(t'), y(t')\big) \\ &=\; \mathcal{I}(X - Y, 0, 0) \;+\; \Gamma' \left\{ \int_0^y dy \, (xy)^{-\nu} \;+\; \int_{X-Y}^x dx \, (xy)^{-\nu} \right\}. \end{aligned} \tag{E.40}$$

After replacing $xy = c^2/4 - a^2$ in accordance with (E.32a) and applying (E.31), we obtain

$$\mathcal{I}\big(X, Y, 0\big) \;=\; \mathcal{I}\big(2a, 0, 0\big) + \Gamma' \int_a^{c/2} ds \left[s^2 - a^2 \right]^{-\nu}. \tag{E.41}$$

Finally, we insert (E.41) into (E.36), yielding

$$\mathcal{I}\big(x,y,z\big) \;=\; \mathcal{I}\big(2a,0,0\big) + \Gamma'\,\Big[F\Big(\frac{c}{2}-y\Big) + F\Big(\frac{c}{2}-z\Big) - F\Big(x-\frac{c}{2}\Big)\Big]\,, \tag{E.42}$$

where we defined the function

$$F(w) = \int_a^w ds\,\Big[s^2-a^2\Big]^{-\nu}\,. \tag{E.43}$$

The integral $\mathcal{I}(x,0,0)$ has already been solved in (E.8). However, this formula is only valid for values $a^2 \geq 0$, i.e., for initial conditions $X \geq Y$. Transferring our Feynman diagrams to these calculations, a^2 turns out to be negative. Thus, we have $a \to \pm\imath b$, which affects (E.8) as follows:

$$\big(2a\big)^{D-3} \;\to\; \begin{cases} \big(2b\big)^{D-3}\,\imath^{D-3} & = \big(2b\big)^{D-3}\,e^{\imath(D-3)\pi/2} \\ \big(2b\big)^{D-3}\,\big(-\imath\big)^{D-3} & = \big(2b\big)^{D-3}\,e^{-\imath(D-3)\pi/2} \end{cases}\,. \tag{E.44}$$

Both cases are symmetrically regarded, yielding

$$\frac{1}{2}\Big[e^{\imath(D-3)\pi/2} + e^{-\imath(D-3)\pi/2}\Big] \;=\; \cos\frac{\pi}{2}(D-3) \;=\; -\sin\frac{\pi D}{2}\,. \tag{E.45}$$

We define $b^2 := -a^2$, and our final result reads

$$\mathcal{I}(x,y,z) \;=\; -\mathcal{I}(2b,0,0)\,\sin\frac{\pi D}{2} \;+\; \Gamma'\,\Big[G\Big(\frac{c}{2}-x\Big) + G\Big(\frac{c}{2}-y\Big) + G\Big(\frac{c}{2}-z\Big)\Big]\,. \tag{E.46}$$

In analogy to (E.43), we have defined the function

$$G(w) \;=\; \int_0^w ds\,(s^2+b^2)^{-\nu} \;=\; \frac{1}{2}\big(b^2\big)^{1/2-\nu}\int_0^{w^2/b^2} dv\,\frac{1}{\sqrt{v}}\,(1+v)^{-\nu}\,. \tag{E.47}$$

The latter transformation turns out to be useful, since the integral is related to those of the incomplete Beta function (C.12) and (C.25).

E.4. Divergence for $D = 3$

In this section, we specify our present general result to the sunset diagram (7.52). In comparison with (E.1), we identify

$$x = m_L^2(\Phi) \equiv m_L^2\,, \qquad y = z = m_T^2(\Phi) \equiv m_T^2\,. \tag{E.48}$$

With regard to (E.47), this corresponds to

$$b^2 \;=\; m_L^2\,m_T^2 \;-\; \frac{1}{4}\,m_L^4\,, \qquad w \;=\; m_T^2 \;-\; \frac{1}{2}\,m_L^2\,. \tag{E.49}$$

Thus, the integral (E.1) yields the result

$$\begin{aligned} \mathcal{I}(m_L^2,m_T^2,m_T^2) \;\;=\;\; & -\mathcal{I}\Big(\sqrt{4m_L^2m_T^2-m_L^2}\,,0,\,0\Big)\,\sin\frac{\pi D}{2} \\ & +\Gamma'\Big\{G\Big(m_T^2-\frac{1}{2}m_L^2\Big) \;+2\,G\Big(\frac{1}{2}m_L^2\Big)\Big\}\,. \end{aligned} \tag{E.50}$$

Analogously to the previous calculations, we have to introduce a mass parameter μ that yields a dimensionless ratio with the longitudinal and transversal mass. For reasons of clarity, we calculate the expansion without adding μ and insert it only in the final result. Now we start calculating the integrals $G(w)$ in accordance with (E.47), (C.23), and (C.25) and specialize in $D=3$ dimensions. The first one reads

$$\begin{aligned} G\left(\frac{1}{2}\,m_L^2\right) &= \left[m_L^2 m_T^2 - \frac{1}{4}m_L^4\right]^{(D-3)/2} \sqrt{\frac{m_L^2}{4m_T^2 - m_L^2}}\; F\left(\frac{1}{2}, 2-\frac{D}{2}; \frac{3}{2}; \frac{m_L^2}{m_L^2 - 4m_T^2}\right) \\ &\overset{D=3}{=} \operatorname{Arsinh}\sqrt{\frac{m_L^2}{4m_T^2 - m_L^2}}\,, \end{aligned} \tag{E.51}$$

The other integral in (7.52) contains both longitudinal and transversal mass, yielding

$$\begin{aligned} G\left(m_T^2 - \frac{1}{2}m_L^2\right) &= \left[m_L^2 m_T^2 - \frac{1}{4}m_L^4\right]^{(D-3)/2} \frac{2m_T^2 - m_L^2}{\sqrt{4m_L^2 m_T^2 - m_L^4}} \\ &\quad \times F\left(\frac{1}{2}, 2-\frac{D}{2}; \frac{3}{2}; -\frac{(2m_T^2 - m_L^2)^2}{4m_L^2 m_T^2 - m_L^4}\right) \\ &\overset{D=3}{=} \operatorname{Arsinh}\frac{2m_T^2 - m_L^2}{\sqrt{4m_L^2 m_T^2 - m_L^4}}\,. \end{aligned} \tag{E.52}$$

Furthermore, we know from (E.21) that

$$\Gamma' \overset{D=3}{=} -\frac{1}{32\,\pi^2}\,. \tag{E.53}$$

Due to (E.8), the first term in (E.50) has a pole for $D=3$. Therefore, we perform an ε-expansion analogously to the one in Section D.2. In fact, it amounts to the same as (D.15) if we substitute $\sqrt{3}M^2 \to \sqrt{4m_L^2 m_T^2 - m_L^4} \equiv \tilde{M}^2$. This substitution leads to the ε-expansion

$$-\mathcal{I}\Big(\tilde{M}^2, 0, 0\Big)\sin\frac{\pi D}{2} \overset{D=3+\varepsilon}{=} -\frac{1}{32\pi^2}\,\frac{1}{\varepsilon} + \frac{1}{32\pi^2}\Big\{-\gamma + 1 + \ln 4\pi - \ln\tilde{M}^2\Big\} + \mathcal{O}(\varepsilon)\,. \tag{E.54}$$

The substitution of $\tilde{M}^2$ emphasizes the analogy to the case of $N=1$ field where (D.15) is already the total result. For N being an arbitrary number of fields, we obtain additional finite contributions (E.51) and (E.52), leading to

$$\begin{aligned} \mathcal{I}(m_L^2, m_T^2, m_T^2) \overset{D=3+\varepsilon}{=} &-\frac{1}{32\pi^2}\frac{1}{\varepsilon} + \frac{1}{32\pi^2}\Bigg\{-\gamma + 1 + \ln 4\pi - \ln\tilde{M}^2 - 2\operatorname{Arsinh}\sqrt{\frac{m_L^2}{4m_T^2 - m_L^2}} \\ &- \operatorname{Arsinh}\frac{2m_T^2 - m_L^2}{\sqrt{4m_L^2 m_T^2 - m_L^4}}\Bigg\} + \mathcal{O}(\varepsilon)\,. \end{aligned} \tag{E.55}$$

With the help of

$$\operatorname{Arsinh} x \;=\; \ln\Big(x + \sqrt{x^2+1}\Big)\,, \tag{E.56}$$

we simplify the following expressions:

$$\text{Arsinh}\,\sqrt{\frac{m_L^2}{4m_T^2-m_L^2}} \;=\; \ln\Big(m_L+2m_T\Big) \;-\; \frac{1}{2}\ln\Big(4m_T^2-m_L^2\Big)\,, \tag{E.57}$$

$$\text{Arsinh}\,\frac{2m_T^2-m_L^2}{\sqrt{4m_L^2m_T^2-m_L^4}} = \ln\Big(4m_T^2-m_L^2\Big) - \frac{1}{2}\ln\Big(4m_L^2m_T^2-m_L^4\Big)\,. \tag{E.58}$$

Finally, we insert the mass parameter μ and (E.55) yields

$$\begin{aligned}\mathcal{I}(m_L^2,m_T^2,m_T^2) \;\overset{D=3+\varepsilon}{=}\; & \frac{1}{32\pi^2}\Bigg\{-\frac{1}{\varepsilon}-\gamma+1+\ln 4\pi+\frac{1}{2}\ln\frac{m_L^2}{\mu^2} \\ & -\ln\left(\frac{4m_T^2-m_L^2}{\mu^2}\right)-\ln\left(\frac{m_L+2m_T}{\mu}\right)\Bigg\}+\mathcal{O}(\varepsilon)\,.\end{aligned} \tag{E.59}$$

Note that for equal masses $m_L^2=m_T^2$, the result (E.59) reduces to (D.15) as required.

List of Figures

List of Tables

Bibliography

[1] H. Kleinert, *Path Integrals in Quantum Mechanics, Statistics, Polymer Physics, and Financial Markets*, Fourth Edition, World Scientific, Singapore (2006);
Internet: `http:www.physik.fu-berlin.de/~kleinert/kleiner_re.html`

[2] J. Kosterlitz and D. Thouless, *The Critical Properties of the Two Dimensional XY Model*, J. Phys. C **7**, 1046 (1973).

[3] H. Brandt, *Thermodynamik und Statistische Physik*, University Bayreuth (1996);
`hacktor.fs.uni-bayreuth.de/thermo/vdwpv/html`

[4] `www.earth.northwestern.edu/people/seth/202/new_2004/H2Ophase.html`

[5] R. B. Griffiths, *Dependence of Critical Indices on a Parameter*, Phys. Rev. Lett. **24**, 1479 (1970).

[6] H. Kleinert and V. Schulte-Frohlinde, *Critical Properties of ϕ^4-Theories*, World Scientific, Singapore (2001).

[7] B. Widom, *Surface Tension and Molecular Correlations near the Critical Point*, J. Chem. Phys. **43**, 3892 (1965).

[8] H. E. Stanley, *Introduction to Phase Transitions and Critical Phenomena*, Oxford University Press, New York (1971).

[9] R. J. Rivers, *Path Integral Methods in Quantum Field Theory*, Cambridge University Press, Cambridge (1987).

[10] J. M. Cornwall, R. Jackiw, and E. Tomboulis, *Effective Action for Composite Operators*, Phys. Rev. D **10**, 2428 (1974).

[11] L. Pitaevskii and S. Stringari, *Bose-Einstein Condensation*, Clarendon Press, Oxford (2003).

[12] L. Dolan and R. Jackiw, *Symmetry Behavior at Finite Temperature*, Phys. Rev. D **9**, 3320 (1974).

[13] J. Zinn-Justin, *Quantum Field Theory and Critical Phenomena*, Clarendon Press, Oxford (1990).

[14] H. Kleinert, *Systematic Improvement of Hartree-Fock-Bogoljubov Approximation with Exponentially Fast Convergence from Variational Perturbation Theory*, Ann. Phys. (New York) **266**, 135 (1998).

[15] J. T. Lenaghan and D. H. Rischke, *The $O(N)$ Model at Finite Temperature: Renormalization of the Gap Equations in Hartree and Large$-N$ Approximation*, J. Phys. G **26**, 431 (2000).

[16] G. Baym and G. Grindstein, *Phase Transition in the σ Model at Finite Temperatures*, Phys. Rev. D **15**, 2897 (1977).

[17] V. I. Yukalov and H. Kleinert, *Gapless Hatree-Fock-Bogoliubov Approximation for Bose Gas*, Phys. Rev. A **73**, 73063612 (2006).

[18] V. I. Yukalov and R. Graham, *Bose-Einstein-Condensated Systems in Random Potentials*, accepted in Phys. Rev. A, cond-mat/0611357

[19] R. P. Feynman, *Space-Time Approach to Non-Relativistic Quantum Mechanics*, Rev. Mod. Phys. **20**, 367 (1948).

[20] R. P. Feynman and A. R. Hibbs, *Quantum Mechanics and Path Integrals*, McGraw Hill, New York (1965).

[21] A. Pelster *Bose-Einstein Condensation*, lecture notes (in German), University Duisburg-Essen, 2004;
Internet: `http://theo-phys.uni-essen.de/tp/ags/pelster_dir/SS04/skript.pdf`

[22] B. De Witt, *Dynamical Theory of Groups and Fields*, Gordon and Breach, New York (1965).

[23] S. Coleman and E. Weinberg, *Radiative Corrections as the Origin of Spontaneous Symmetry Breaking*, Phys. Rev. D **7**, 1888 (1973).

[24] R. Jackiw, *Functional Evaluation of the Effective Potential*, Phys. Rev. D **9**, 1686 (1974).

[25] A. Pelster and H. Kleinert, *Functional Differential Equations for the Free Energy and the Effective Energy in the Broken-Symmetry Phase of ϕ^4-Theory and Their Recursive Graphical Solution*, Physica A, 370 (2003).

[26] S. Brandt, *Beyond Effective Potential Via Variational Perturbation Theory*, Diploma Theses, Free University Berlin (2004).

[27] S. Gasiorowicz, *Quantenphysik*, Oldenburg Verlag, München (2002).

[28] R. P. Feynman and H. Kleinert, *Effective Classical Partition Functions*, Phys. Rev. A **34**, 5080 (1986).

[29] J. Jaenicke and H. Kleinert, *Loop Corrections to the Effective Classical Potential*, Phys. Lett. **176**, 409 (1993).

[30] B. Hamprecht and H. Kleinert, *Dependence of Variational Perturbation Expansions on Strong-Coupling Behavior. Inapplicability of Delta-Expansion to Field Theory*, Phys. Rev. D **68**, 065001 (2003).

[31] H. Kleinert, *Systematic Corrections to Variational Calculation of Effective Potential*, Phys. Lett. A **173**, 332 (1993).

[32] W. Janke and H. Kleinert, *Resummation of Divergent Perturbation Series - An Introduction to Theory and a Guide to Practical Applications* (in preparation).

[33] P. M. Stevenson, *Optimized Perturbation Theory*, Phys. Rev. D **23**, 2916 (1981).

[34] S. F. Brandt and A. Pelster, *Large-D Expansion from Variational Perturbation Theory*, J. Math. Phys. **46**, 112105 (2005).

[35] H. Kleinert, *Particles and Quantum Fields*, lecture notes, Free University Berlin (2004); `www.physik.fu-berlin.de/ kleinert/books/qft`

[36] J. C. Collins, *Renormalization*, Cambridge University Press, Cambridge (1984).

[37] A. L. Fetter and J. D. Walecka, *Quantum Theory of Many-Particle Systems*, McGraw-Hill Book Company, New York (1971).

[38] A. Pelster and K. Glaum, *Recursive Graphical Solution of Closed Schwinger-Dyson Equations in ϕ^4-Theory – Part 1: Generation of Connected and One-Particle Irreducible Feynman Diagrams*, Physica A **335**, 455 (2004).

[39] H. Kleinert, *Five-Loop Critical Temperature Shift in Weakly Interacting Homogeneous Bose-Einstein Condensate*, Mod. Phys. Lett. B **17**, 1011 (2003).

[40] B. Kastening, *Bose-Einstein Condensation Temperature of a Homogeneous Weakly Interacting Bose Gas in Variational Perturbation Theory through Seven Loops*, Phys. Re. A **69**, 043613 (2004).

[41] V. A. Kashurnikov, N. V. Prokofev, and B. V. Svistunov, *Critical Temperature Shift in Weakly Interacting Bose Gas*, Phys. Rev. Lett. **87**, 120402 (2001).

[42] P. Arnold and G. D. Moore, *Bose-Einstein Condensation Transition Temperature of a Dilute Homogeneous Imperfect Bose Gas*, Phys. Rev. Lett. **87**, 120401 (2001).

[43] P. Arnold and G. D. Moore, *Monte Carlo Simulation of the O(2) ϕ^4 Field Theory in Three Dimensions*, Phys. Rev. E **64**, 066113 (2001).

[44] C. M. Bender and T. T. Wu, *Anharmonic Oscillator*, Phys. Rev. **184**, 1231 (1969).

[45] C. M. Bender and T. T. Wu, *Anharmonic Oscillator -II. A Study of Perturbation Theory in Large Order*, Phys. Rev. D **7**, 1620 (1973).

[46] F. Weissbach, A. Pelster, and B. Hamprecht, *High Order Variational Perturbation Theory for the Free Energy*, Phys. Rev. E **66**, 036129 (2002).

[47] J. Dreger, A. Pelster, and B. Hamprecht, *High Order Variational Perturbation Theory for Fokker-Planck Equation with Nonlinear Drift*, Jour. Phys.J **45**, 355 (2005).

[48] I. S. Gradshteyn and I. M. Ryzhik, *Table of Integrals, Series and Products*, Academic Press, New York (1965).

[49] M. Abramowitz and I. Segum *Handbook of Mathematical Functions*,Dover Publications, Inc., New York (1965).

[50] C. Ford, I. Jack, and D. R. T. Jones, *The Standard Model of Effective Potential at Two Loops*, Nucl. Phys. B **387**, 373 (1992).

Danksagung

Wenn dir ein Fels vom Herzen fällt,
so fällt er auf den Fuß dir prompt!
So ist es nun mal auf der Welt:
ein Kummer geht, ein Kummer kommt.
(Heinz Erhardt)

Zuallererst möchte ich mich vielmals bei Herrn Prof. Hagen Kleinert dafür bedanken, daß er es mir ermöglicht hat, in seiner Arbeitsgruppe meine Diplomarbeit anzufertigen. Bei allen auftretenden Problemen konnte ich mich jederzeit an ihn wenden, und er hat sich viel Zeit genommen, mir meine Fragen geduldig zu beantworten. Dadurch hat er mein physikalisches Verständnis weit über die Grenzen der Diplomarbeit hinaus bereichert und geprägt.

Eine unverzichtbare Hilfe war mir Herr PD Dr. Axel Pelster, der immer wieder seine Sonntagsruhe opfert, um sich um seine Studenten in Berlin zu kümmern. Er hat es mir durch sein überaus großes Engagement ermöglicht, die Vorhaben meiner Diplomarbeit in die Praxis umzusetzen und war stets eine Quelle der Motivation und Zuversicht.

Ein besonders großer Dank geht an Konstantin Glaum, der mich mit einzigartiger Hilfsbereitschaft bei vielen kleineren und größeren Problemen der täglichen Rechnungen unterstützt und mir mit schonungsloser Kritik bei der Korrektur der Arbeit geholfen hat.

Auch Sebastian Brandt hat mir viele Fragen beantwortet und durch seine eigene Diplomarbeit den Einstieg in das Thema erleichert. Dafür bin ich ihm sehr dankbar.

Für viel konstruktive Kritik bei der Korrektur möchte ich mich auch bei Victor Bezerra, Jürgen Dietel und Aristeu Lima bedanken.

Zum Schluß geht ein großes Dankeschön für die ausgesprochen harmonische und entspannte Arbeitsatmosphäre an meine Schreibtischnachbarn Walja Korolevski, Moritz Schütte und Parvis Soltan-Panahi sowie die übrigen Gruppenmitglieder Xiaojiang Chen, Alexander Hoffmann, Petr Jizba, Sebastian Kling, Flavio Nogueira und Steffen Röthel.